UNIVERSITY OF RIJEKA
FACULTY OF BIOTECHNOLOGY AND DRUG DEVELOPMENT

Raffaello Cimbro

ESTABLISHING HUMAN PERIPHERAL BLOOD OPTINEURIN DEFICIENCY MODELS AND EVALUATING THEIR INFLAMMATORY PROFILES AS POTENTIAL DISEASE BIOMARKERS

DOCTORAL THESIS

Rijeka, 2026

UNIVERSITY OF RIJEKA
FACULTY OF BIOTECHNOLOGY AND DRUG DEVELOPMENT

Raffaello Cimbro

ESTABLISHING HUMAN PERIPHERAL BLOOD OPTINEURIN DEFICIENCY MODELS AND EVALUATING THEIR INFLAMMATORY PROFILES AS POTENTIAL DISEASE BIOMARKERS

DOCTORAL THESIS

Supervisor: Prof. Ivana Munitić, MD, PhD
Faculty of Biotechnology and Drug Development, University of Rijeka

Rijeka, 2026

SVEUČILIŠTE U RIJECI
FAKULTET BIOTEHNOLOGIJE I RAZVOJA LIJEKOVA

Raffaello Cimbro

ESTABLISHING HUMAN PERIPHERAL BLOOD OPTINEURIN DEFICIENCY MODELS AND EVALUATING THEIR INFLAMMATORY PROFILES AS POTENTIAL DISEASE BIOMARKERS

DOCTORAL THESIS

Mentor: Prof. Ivana Munitić, MD, PhD
Faculty of Biotechnology and Drug Development, University of Rijeka

Rijeka, 2026

Supervisor: Professor Ivana Munitić, MD, PhD

Doctoral thesis was defended on XX of XX 2026 at the University of Rijeka, Faculty of Biotechnology and Drug Development, in front of Evaluation Committee:

1.
2.
3.

Scientific Support

This research was supported by the Croatian Science Foundation (CSF) grant (IP-2018-01-8563 and IP-2024-05-5814) and the support of the University of Rijeka (18-211-1369 and 23-186-3163) to Professor Ivana Munitić.

Abstract

Optineurin is a multifunctional scaffold protein that regulates various cellular processes including NF-κB and TBK1/IFN-β signaling, selective autophagy, and vesicular trafficking. Mutations in the optineurin gene (*OPTN*) are causally linked to amyotrophic lateral sclerosis (ALS) and have also been associated with several other neurodegenerative disorders, although these associations remain less well established. In ALS, available genetic and experimental evidence largely supports loss-of-function (LOF) mechanisms. Studies in murine models have demonstrated that optineurin deficiency and insufficiency impair TBK1 activation and IFN-β production in primary myeloid cells, while NF-κB signaling remains intact. However, it remains unclear whether these findings translate to human primary immune cells. In this thesis, we established siRNA-mediated optineurin silencing in human monocyte-derived dendritic cells (DCs) and macrophages to investigate its role in inflammatory signaling and various immune functions, including cytokine production, phagocytosis, and antigen presentation. We first characterized optineurin expression during myeloid differentiation, demonstrating that it is negligible in monocytes, low in immature DCs, and strongly upregulated (~3-fold) upon lipopolysaccharide (LPS)-induced maturation. In macrophages, optineurin was already expressed in resting (M0) cells and further increased upon proinflammatory (M1) but not anti-inflammatory (M2) polarization. Optineurin silencing resulted in approximately 60–70% reduction in DCs and ~50% reduction in macrophages, but did not alter the immunophenotype (CD80, CD86, CD40, CD83, HLA-DR, PD-L1, CD163) of either cell type or affect LPS-induced NF-κB signalling, assessed by p65 phosphorylation. Although upon LPS treatment a consistent trend toward reduced TBK1 phosphorylation was observed in both DCs and macrophages with reduced optineurin levels, this did not reach statistical significance. However, phosphorylated STAT1, a distal readout of the TBK1–IFN-β–IFNAR signaling cascade, was significantly reduced in optineurin-silenced macrophages at the 4-hour peak.The cytokine production (TNF-α, IL-6, IL-1β, IL-10, IL-12p70, IFN-β) was not significantly altered. Phagocytosis of bacteria particles and antigen-specific T cell activation, assessed by the CD154/CD40L assay were similarly unaffected. In conclusion, our findings show that optineurin expression is dynamically regulated during human myeloid cell differentiation and activation, yet partial optineurin reduction of approximately 50–70% was insufficient to produce major functional deficits in human myeloid

cells under basal or acute inflammatory conditions, despite subtle alterations in TBK1–STAT1 signaling. They further raise the possibility that partial LOF states, such as those associated with heterozygous *OPTN* mutations in human patients, may be insufficient on their own to produce overt innate immune dysfunction under acute inflammatory conditions, and that additional stressors such as chronic inflammation, ageing, homozygous *OPTN* LOF states, or coexisting disease-associated genetic risk factors may be required to unmask disease-relevant phenotypes, consistent with the multifactorial nature of ALS.

Key words: optineurin, amyotrophic lateral sclerosis, neuroinflammation, monocytes, macrophages, dendritic cells

Sažetak

Optineurin je multifunkcionalni organizacijski protein koji regulira različite stanične procese, uključujući prijenos signala putem NF-κB i TBK1/IFN-β puteva, selektivnu autofagiju i vezikularni transport. Mutacije u genu za optineurin (*OPTN*) uzročno su povezane s amiotrofičnom lateralnom sklerozom (ALS), a također se dovode u vezu s nekoliko drugih neurodegenerativnih poremećaja, iako su te povezanosti zasad slabije. U ALS-u, dostupni genetski i eksperimentalni dokazi u velikoj mjeri podupiru hipotezu da mutacije optineurina u ALS-u djeluju mehanizmom gubitka funkcije. Istraživanja na mišjim modelima pokazala su da deficijencija i insuficijencija optineurina narušavaju aktivaciju TBK1 i proizvodnju IFN-β u primarnim mijeloidnim stanicama, dok aktivacija NF-κB ostaje očuvana. Međutim, još uvijek nije jasno imaju li ovi nalazi translacijski značaj u ljudskim primarnim imunosnim stanicama. U ovom radu uspostavili smo utišavanje optineurina posredovano siRNA-om u dendritičnim stanicama (DC) i makrofagima, generiranim iz monocita ljudske krvi, kako bismo istražili ulogu smanjene razine optineurina u prijenosu upalnih signala i različitim imunosnim funkcijama, uključujući proizvodnju citokina, fagocitozu i prezentaciju antigena. Pritom smo najprije ispitali izražaj optineurina tijekom diferencijacije mijeloidnih stanica te pokazali da je razina optineurina vrlo niska u monocitima, niska u nezrelim DC-ima, a snažno pojačana (oko 3 puta) nakon sazrijevanja DC stanica potaknutog lipopolisaharidom (LPS-om). U makrofagima je optineurin bio prisutan već u nestimuliranim (M0) stanicama te se dodatno povećavao nakon njihove proupalne (M1), ali ne i protuupalne (M2) polarizacije. Utišavanje optineurina rezultiralo je njegovim smanjenjem od približno 60–70 % u DC-ima i oko 50 % u makrofagima, ali nije promijenilo imunofenotip (CD80, CD86, CD40, CD83, HLA-DR, PD-L1, CD163) nijedne vrste stanica niti je utjecalo na LPS-om induciran prijenos signala putem NF-κB puta, mjeren fosforilacijom p65. Iako je nakon tretmana LPS-om uočen dosljedan trend prema smanjenoj fosforilaciji TBK1 u DC-ima i makrofagima sa sniženom razinom optineurina, ta razlika nije dosegla statističku značajnost. Međutim, fosforilirani STAT1, distalni pokazatelj signalne kaskade TBK1–IFN-β–IFNAR puta, bio je značajno smanjen u makrofagima s utišanim optineurinom nakon 4 sata stimulacije. Proizvodnja citokina (TNF-α, IL-6, IL-1β, IL-10, IL-12p70, IFN-β) nije bila značajno promijenjena. Fagocitoza bakterijskih čestica i antigen-specifična aktivacija T-stanica, analizirana CD154/CD40L testom, također su ostale

nepromijenjene. Zaključno, naši rezultati pokazuju da je izražaj optineurina dinamički reguliran tijekom diferencijacije i aktivacije ljudskih mijeloidnih stanica, no da djelomično smanjenje razine optineurina od približno 50–70% nije bilo dovoljno za izazivanje većih funkcionalnih deficita u ljudskim mijeloidnim stanicama u bazalnim uvjetima ni u uvjetima akutne upale, unatoč blagim promjenama u signalizaciji TBK1–STAT1 puta. Nadalje, ti rezultati upućuju parcijalna stanja gubitka funkcije, poput onih povezanih s heterozigotnim *OPTN* mutacijama u bolesnika, sama po sebi možda nisu dovoljna za razvoj izražene disfunkcije urođene imunosti u uvjetima akutne upale te da bi dodatni stresori, poput kronične upale, starenja, homozigotnih *OPTN* mutacija ili pridruženih genetskih čimbenika rizika povezanih s bolešću, mogli biti potrebni za razotkrivanje fenotipova relevantnih za bolest, što je u skladu s multifaktorskom prirodom ALS-a.

Ključne riječi: optineurin, amiotrofična lateralna skleroza, neuroinflamacija, monociti, makrofagi, dendritične stanice

Table of Contents

1. INTRODUCTION

1.1. **Optineurin: Overview and Cellular Functions**

Optineurin is a multifunctional cytoplasmic protein that acts as an adaptor and scaffold for various cellular processes (Markovinovic et al., 2017). It was isolated and identified in 1998 in a yeast two-hybrid screening system as an interacting partner of the adenoviral protein E3-14.7K, and was therefore originally named 14.7K-interacting protein 2 (FIP-2) (Li et al., 1998). Subsequent studies uncovered additional binding partners and sequence homologies leading to optineurin being described under different names, including TFIIIA-intP (Moreland et al., 2000) as a binder of the Transcription Factor IIIA, and NEMO-related protein (NPR/NRP) (Schwamborn et al., 2000) as homologous to the NF-κB essential modulator (NEMO). The now standard name, optineurin (optic neuropathy inducing protein), reflects the association of mutations in the optineurin-encoding gene *OPTN* with normal-tension glaucoma (NTG), a subtype of primary open-angle glaucoma (POAG) (Rezaie et al., 2002).

OPTN gene is located on chromosome 10p13 in humans and comprises three non-coding exons within its 5′ UTR and 13 coding exons that produce a 64 kDa, 577-amino acid (aa) cytoplasmic protein (Slowicka et al., 2016). The biological relevance of optineurin is supported by high conservation among vertebrates, including mouse optineurin (*Optn*), which shares ~78% sequence identity with human *OPTN* and a similar 13-exon organization. Optineurin protein is expressed in all organs, with relatively highest expression in the liver, testis, heart, digestive system and brain, with median expression in the spleen and lower expression in lymph nodes (Wang et al., 2019). Optineurin expression can be further increased by inflammatory cytokines that can regulate it at the promoter level, such as TNF-α and interferons (IFNs) (Li et al., 1998; Schwamborn et al., 2000, Sudhakar et al., 2013).

Optineurin is a multidomain adaptor participating in signaling across innate immune pathways, membrane trafficking, organelle homeostasis, and selective autophagy. In immune signaling, it has been reported to act along two major axes. First, optineurin is a proposed negative regulator of nuclear factor-κB (NF-κB) activation: it can compete with NF-κB essential modulator (NEMO) for binding to K63/M1-polyubiquitinated receptor-interacting serine/threonine-protein kinase 1 (RIPK1) and recruit cylindromatosis (CYLD), a K63-specific deubiquitinase, thereby editing K63 chains and constraining canonical NF-κB signaling (Zhu et al., 2007; Nagabhushana et al., 2011). Second, optineurin functions as a regulator of TANK-binding kinase 1 (TBK1) in the interferon regulatory factor 3/7 (IRF3/IRF7)–

interferon-β (IFN-β) pathway by scaffolding TBK1 and recognizing its poly-ubiquitination, which promotes TBK1 autophosphorylation and downstream type I interferon production (Morton et al., 2008; Gleason et al., 2011; Munitic et al., 2013; Meena et al., 2016; Pourcelot et al., 2016, Betrancourt et al., 2026). Beyond immune signaling, optineurin, by supressing receptor-interacting kinase 1 (RIPK1)-dependent signaling, can prevent cell death pathways, including apoptosis and necroptosis, (Ito et al., 2016; Nakazawa et al., 2016). It also maintains Golgi complex structure and mediates post-Golgi trafficking and exocytosis, in part through interactions with myosin heavy chain VI (MYO6; myosin VI) and Ras-related protein Rab-8 (Rab8) that couple membrane compartments to actin-based motors and small GTPases (Sahlender et al., 2005; Hattula & Peränen, 2000; Del Toro et al., 2009; Tumbarello et al., 2012; Sundaramoorthy et al., 2015).

A prominent role of optineurin is its participation in selective autophagy, including mitophagy, thus regulating protein homeostasis (proteostasis) at the cellular level. It recognizes ubiquitinated cargo linked to damaged mitochondria, protein aggregates, and intracellular pathogens, and bridges this cargo to microtubule-associated protein 1 light chain 3 (MAP1LC3; LC3) on autophagosomal membranes via its LC3-interacting region (LIR) to enable enclosure and lysosomal degradation (Wild et al., 2011; Korac et al., 2013; Tumbarello et al., 2013; Lazarou et al., 2015; Wong & Holzbaur, 2014; Heo et al., 2015). Post-translational modifications tightly control this process: TBK1-mediated phosphorylation at Ser177 enhances LC3 binding and is important for xenophagic clearance of cytosolic Salmonella, while phosphorylation at Ser473 and Ser513 in the C-terminus promotes recognition of ubiquitinated mitochondria and supports mitophagy (Wild et al., 2011; Richter et al., 2016). In parallel, ubiquitination of optineurin at Lys193 by HECT domain and ankyrin repeat containing E3 ubiquitin-protein ligase 1 (HACE1) facilitates binding to sequestosome 1 (SQSTM1; p62) and sustains autophagic flux (Liu et al., 2014). More recently, optineurin was also identified as a target of ANKIB1-mediated polyubiquitination, although the target site has not been reported (Betrancourt et al., 2026). These features position optineurin at the nexus of immune signaling and proteostasis, processes central to inflammation and neurodegeneration.

1.2 **Functional Domains of Optineurin**

Optineurin is a multidomain scaffold protein comprising the following major domains: two coiled-coil domains (CC1 and CC2), a LC3-interacting region (LIR), and a C-terminal

ubiquitin-binding region that includes the ubiquitin binding in ABIN and NEMO (UBAN) and zinc finger (ZF) domains (Fig. 1). These binding motifs enable optineurin to engage proteins involved in inflammatory signaling, selective autophagy, and vesicle trafficking (Prtenjaca, 2020).

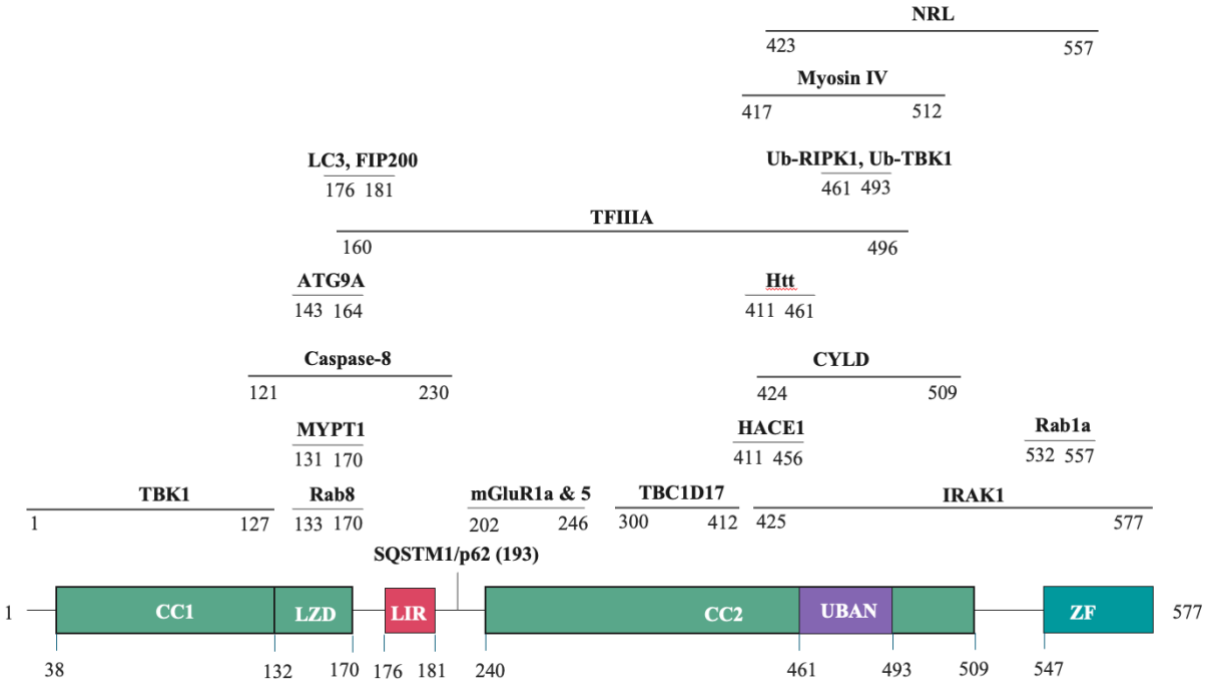

Figure 1. Optineurin motif map and major interacting proteins.

The schematic shows the principal domains along the optineurin sequence: coiled-coil 1 containing a leucine zipper (CC1 & LZD; ~38–170 aa), the LC3-interacting region (LIR; 176–181 aa), coiled-coil 2 (CC2; ~240–509 aa), the UBAN segment (~461–493 aa) and the C-terminal zinc finger (ZF; 547–577 aa). The C-terminal ubiquitin-binding region comprises UBAN plus ZF. Interaction partners listed in Table 1 are positioned over their approximate binding spans. (Adapted from Markovinovic et al., 2017; Ryan et al., 2018). Notes: due to small size, the LIR region (176–181 aa) was not drawn to scale; although the canonical core motif comprises residues 178–181, the broader functional region includes Ser177, whose phosphorylation enhances LC3 binding; SQSTM1 (p62) binds optineurin following HACE1-mediated ubiquitination at Lys193.

1.2.1. **Coil-Coiled, Leucin Zipper Domains and Oligomerization**

Coiled-coil regions comprise roughly 70% of the optineurin sequence. CC1 is located at the N-terminus (38–170 aa) and contains a specialized leucine zipper (LZ) coiled-coil subdomain that

promotes protein interaction and multimerization, while CC2 spans the mid-to-C-terminal region (238–509 aa). CC domains mediate protein–protein interactions and oligomer formation; in optineurin they support both self-oligomerization and interactions with other coiled-coil–containing partners (Minegishi et al., 2016; Truebestein and Leonard, 2016, Gao et al., 2014). CC1 includes a TBK1–binding site and supports interaction with the C-terminal coiled-coil region of TBK1; CC1 self-oligomerization further enhances TBK1 docking (Li et al., 2016). CC2 self-oligomerization promotes binding of optineurin to linear polyubiquitin chains (Nakazawa et al., 2016). This increased avidity for polyubiquitin chains is also thought to convert low-affinity interactions into high-avidity complexes that ensure stable cargo recognition. Oligomerization can also enhance TBK1 recruitment and activation by clustering multiple TBK1 molecules in close proximity, promoting its trans-autophosphorylation at Ser172 and amplifying downstream IRF3/IRF7 signaling (Li et al., 2016; Pourcelot et al., 2016).Finally, oligomerization may also facilitate formation of phase-separated signaling hubs at sites of cargo aggregation or autophagosome biogenesis, concentrating autophagy receptors, kinases, and membrane machinery into functional microdomains (Turco et al., 2021).

1.2.2 **LC3-Interacting Region (LIR)**

The LIR of optineurin is a short motif located at residues 176–181 that mediates direct binding to LC3 on autophagosomal membranes (Wild et al., 2011). This interaction is essential for selective autophagy: optineurin recognizes ubiquitinated cargo via its C-terminal ubiquitin-binding region and, through the LIR–LC3 interface, tethers that cargo to the expanding phagophore for enclosure and degradation. TBK1 phosphorylation of optineurin at Ser177, adjacent to the LIR, enhances LC3 affinity and is required for efficient clearance of targets such as cytosolic bacteria and damaged mitochondria.

1.2.3 **Ubiquitin-Binding Domains**

Optineurin’s key biological roles are closely tied to its capacity to recognize and bind ubiquitin-modified proteins. Ubiquitination is a widespread post-translational modification in which ubiquitin is attached as chains to substrates through isopeptide linkages at one of seven lysine (Lys; K) residues (K6, K11, K27, K29, K33, K48, K63) or via the N-terminal methionine (Met; M) at position 1 (M1), linked to the C-terminus of the following ubiquitin (Akutsu et al., 2016). The current literature supports the concept that K48 (and K11/K29) chains commonly target proteins for proteasomal degradation, whereas K63, M1, and K11 polyubiquitin chains, drive assembly of signaling complexes (see Sections 1.7.1 and 1.7.3 for NF-κB and TBK1

pathways) and/or guide cargo toward selective autophagy (Akutsu et al., 2016; Hu & Sun, 2016; Komander & Rape, 2012; Pohl & Dikic, 2019).

Optineurin contains a conserved ubiquitin-binding region (UBR) composed of two modules: the ubiquitin-binding region of A20-binding inhibitor of NF-κB (ABIN) proteins and NF-κB essential modulator (NEMO), termed UBAN, and a distal zinc finger (ZF). As the name implies, UBAN shares sequence and functional homology with the ubiquitin-binding domains (UBDs) of NEMO and the ABIN family (ABIN-1/2/3) (Wagner et al., 2008; Laplantine et al., 2009; Schwamborn et al., 2000; Zhu et al., 2007). Moreover, substituting NEMO's UBD with those from optineurin or ABIN-2 preserves biological function, underscoring conserved Ub-binding specificity (Laplantine et al., 2009). Functionally, unlike NEMO's UBAN, which is selective for M1, the optineurin UBAN binds both linear M1- and K63-linked chains while excluding K48-linked chains (Gleason et al., 2011; Wagner et al., 2008; Nakazawa et al., 2016). The ZF module contributes additional ubiquitin-binding affinity, enabling engagement of K63-modified substrates involved in selective autophagy and innate immune signaling (Laplantine et al., 2009). More recently, K11-linked chains assembled on innate immune signalosome components have also been implicated as ligands for optineurin (Betrancourt et al., 2026). Overall, through its dual-module UBR, optineurin engages a spectrum of ubiquitinated partners and pathways, including NF-κB and TBK1 signaling.

1.3 **Optineurin-Interacting Proteins**

In this dissertation, we focus on the subset of optineurin-interacting partners most relevant to (neuro)inflammation and phagocytosis, specifically those linking innate immune signaling (TBK1 and NF-κB), to the pathophysiological context of neurodegeneration. Figure 1 maps the major optineurin binding partners to approximate residue spans, and Table 1 summarizes their precise binding sites, associated cellular functions, and references.

Binding partner	Domain Region	Binding site (aa)	Cellular function	References
TBK1	CC1	26–103	Inflammation, autophagy	Morton et al., 2008; Wild et al., 2011; Gleason et al., 2011; F. Li et al., 2016;

				Munitic et al., 2013; Meena et al., 2016; Pourcelot et al., 2016; Richter et al., 2016; Brenner et al., 2024
Caspase 8	CC1	121–230	Apoptosis	Nakazawa et al., 2016
MYPT1	CC1	131–170	Mitosis	Kachaner et al., 2012
Rab8	CC1	133–170	Vesicle trafficking	Hattula & Peränen, 2000; Chi et al., 2010; V aibhava et al., 2012; J. Zhang et al., 2024
TFIIIA	CC1 – LIR Vicinity	160–469	Transcription	Moreland et al., 2000
LC3	LIR	176–181	Autophagy	Wild et al., 2011
p62		193 (upon ubiquitination)	Autophagy	Z. Liu et al., 2014
mGLUR1a		202–246	Excitotoxicity	Anborgh et al., 2005
HACE1	CC2	411–456	Autophagy	Z. Liu et al., 2014
Htt	CC2	411–461	Vesicle trafficking	Hattula & Peränen, 2000
Myosin VI	CC2 -UBAN	412–520	Exocytosis	Sahlender et al., 2005; Tumbarello et al., 2012; Sundaramoorthy et al., 2015
CYLD	CC2 -UBAN	424–529	Inflammation	Nagabhushana et al., 2011; Obaid et al., 2015
RIPK1	UBAN	461-493	Inflammation, necroptosis	Zhu et al., 2007; Y. Ito et al., 2016; Nakazawa et al., 2016

Table 1. Optineurin main interaction partners, domains, binding sites, and cellular functions.

Interaction partners listed in Table 1: TANK-binding kinase 1 (TBK1), cysteine-aspartic protease 8 (caspase 8), myosin phosphatase target subunit 1 (MYPT1), Ras-related protein Rab-8 (Rab8), transcription factor IIIA (TFIIIA), microtubule-associated protein 1 light chain 3 (LC3; MAP1LC3), sequestosome 1 (p62; SQSTM1), metabotropic glutamate receptor 1a (mGluR1a; GRM1), HECT domain and ankyrin repeat containing E3 ubiquitin-protein ligase 1 (HACE1), huntingtin (Htt; HTT), myosin heavy chain VI (myosin VI; MYO6), cylindromatosis (CYLD), and receptor-interacting serine/threonine-protein kinase 1 (RIPK1). The table is modified from Toth & Atkin, 2018.

1.3.1 **Cylindromatosis (CYLD) Interaction**

CYLD is a tumor suppressor with K63-specific deubiquitinase activity that counteracts NF-κB activation by removing K63-linked polyubiquitin from substrates such as RIPK1 and NEMO, thereby terminating downstream signaling (Kovalenko et al., 2003). Optineurin binds CYLD within the proximal region of coiled-coil 2 (CC2), containing the UBAN domain and spanning approximately residues 424–509, and can recruit CYLD to ubiquitinated complexes at the NF-κB signalosome to restrain excessive signaling (Nagabhushana et al., 2011; Obaid et al., 2015). Although this mechanism is supported by overexpression systems, the relative contribution of CYLD recruitment versus direct competition with NEMO for ubiquitinated RIPK1 likely varies by cell type and signaling context.

1.3.2 **Receptor-Interacting Serine/Threonine Protein Kinase 1 (RIPK1) Interaction**

RIPK1 is a central node connecting proinflammatory signaling and cell survival (Newton & Manning, 2016). Upon pattern recognition receptor (PRR, e.g., TLR 4) or tumor necrosis factor 1(TNFR1) engagement, Ub ligases assemble K63 and M1 chains on RIPK1, creating a docking platform for TAK1 and the NEMO-containing IKK complex, leading to canonical NF-κB activation (Ben-Neriah, 2002; Tokunaga & Iwai, 2012; Shih et al., 2011). Optineurin binds polyubiquitinated RIPK1 via UBAN and has been proposed to compete with NEMO and/or recruit CYLD to dampen signaling (Zhu et al., 2007; Nagabhushana et al., 2011). Beyond NF-κB, prolonged RIPK1 signaling can shift toward cell death pathways, including necroptosis, releasing damage-associated molecular patterns (DAMPs) that further amplify inflammation (Newton & Manning, 2016). The balance of optineurin's interactions with RIPK1, CYLD, and Ub chains likely influences whether proinflammatory survival signals or cell death programs predominate under specific conditions.

1.3.3 **TANK Binding Kinase 1 (TBK1) Interaction**

TBK1 is a major kinase driving interferonβ (IFNβ) production (see Section 1.7.3 for detailed pathway description) (Ahmad et al., 2016). Its activation requires autophosphorylation at Ser172 and recruitment to Ub–marked signaling complexes. Optineurin engages TBK1 through two complementary mechanisms: a constitutive interaction via the N-terminal coiledcoil 1 (CC1) region with the TBK1 C-terminus, and an inducible interaction via the

UBAN/ZF domains recognizing K63linked polyubiquitin chains on TBK1 (Tu et al., 2013). This inducible binding is promoted in the context of PRR signaling, where TRAF3 catalyzes K63 polyubiquitination of TBK1 and facilitates adaptor recruitment to optineurin (Morton et al., 2008; Tu et al., 2013; Meena et al., 2016). Beyond K63 chains, the E3 ligase ANKIB1 has recently been reported to assemble K11-linked polyubiquitin on TRIF, STING, and NEMO within TLR3-, TLR4-, and cGAS–STING-associated complexes, providing an additional ubiquitin-based docking platform that supports optineurin–TBK1 recruitment and IRF3 activation (Betrancourt et al., 2026, Nat Cell Biol). Such binding increases local TBK1 concentration, promotes dimerization and catalytic activation, and initiates IRF3/IRF7 phosphorylation cascades (Pourcelot et al., 2016).

Activated TBK1, in turn, phosphorylates optineurin at Ser177 within the LC3-interacting region (LIR), enhancing LC3 affinity and enabling xenophagic clearance of cytosolic *Salmonella enterica* (Wild et al., 2011). TBK1 also phosphorylates optineurin at Ser473 and Ser513 in the C-terminal region, which facilitates binding to ubiquitinated mitochondria and promotes autophagy-mediated degradation of damaged mitochondria (mitophagy) (Richter et al., 2016). Whether these phosphorylation events also contribute to TBK1-driven innate immune signalling in vivo remains to be determined.

1.3.4 **Additional Optineurin Interaction Partners**

Beyond the core immune signaling partners (CYLD, RIPK1, TBK1), optineurin engages a diverse network of proteins that coordinate selective autophagy, vesicular trafficking, and cellular stress responses.

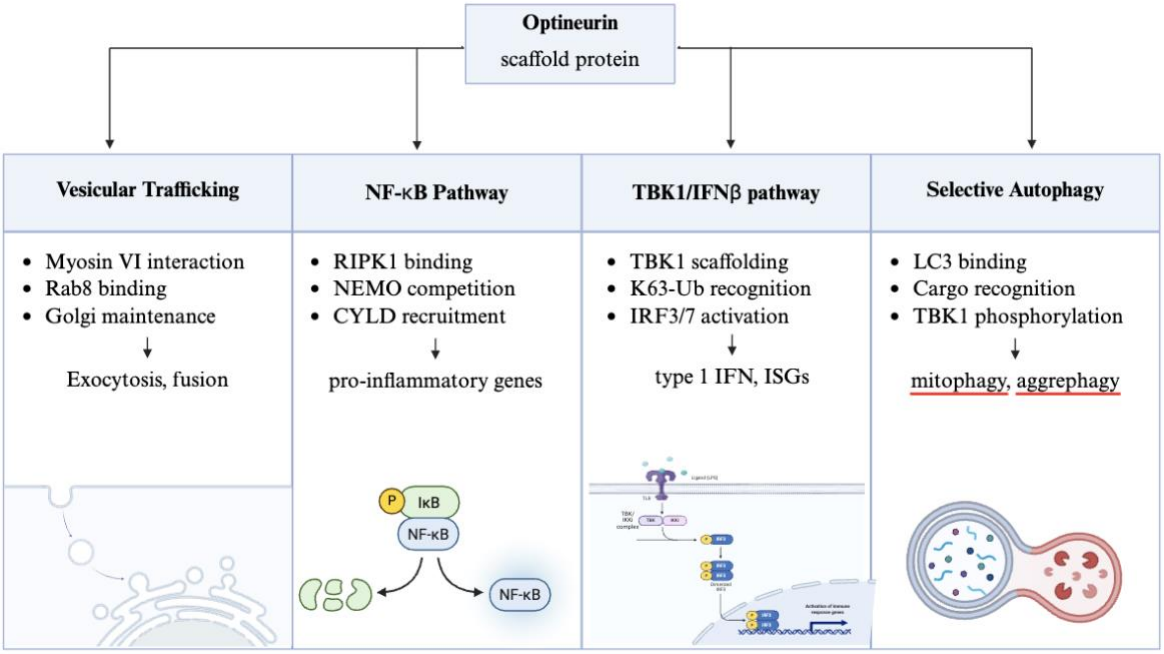

Figure 2. Optineurin functions in innate immune signaling, vesicular trafficking and selective autophagy.

Optineurin functions in multiple major cellular pathways: (1) context-dependent inhibition of NF-κB signaling via RIPK1 binding and CYLD recruitment; (2) regulation of TBK1/IFN-β signaling through bivalent TBK1 scaffolding (CC1 + UBAN/ZF recognition of K63-ubiquitinated TBK1); (3) selective autophagy via TBK1-phosphorylated optineurin (pSer177) binding LC3 to clear damaged mitochondria and protein aggregates; and (4) vesicular trafficking through myosin VI and Rab8 interactions. ALS-associated *OPTN* mutations disrupt these pathways, causing chronic neuroinflammation and proteostasis failure. Image generated with Biorender.

1.3.4.1 **Autophagy Partners**

LC3 (Microtubule-Associated Protein 1 Light Chain 3)

LC3 is the canonical marker of autophagosomal membranes and serves as the direct docking site for selective autophagy receptors. Optineurin binds LC3 through its LIR motif (residues 176–181), tethering ubiquitinated cargo—damaged mitochondria, protein aggregates, and intracellular pathogens—to expanding phagophores for lysosomal degradation (Wild et al., 2011). This interaction is dynamically regulated by TBK1-mediated phosphorylation at Ser177, which increases LC3 binding affinity approximately 10-fold and is essential for

efficient xenophagy and mitophagy (Wild et al., 2011; Rogov et al., 2013; Lazarou et al., 2015). Mutations disrupting the LIR or its phosphorylation site can abolish LC3 binding and impair clearance of TDP-43 and SOD1 aggregates, contributing to proteostasis collapse in motor neurons (Korac et al., 2013).

p62/SQSTM1 (Sequestosome 1)

p62 is a multifunctional autophagy receptor that, like optineurin, bridges ubiquitinated cargo to LC3-positive membranes via its ubiquitin binding motif and LIR motif (Bjørkøy et al., 2005; Pankiv et al., 2007). Optineurin and p62 physically interact when optineurin is ubiquitinated at Lys193 by HACE1, forming a cooperative receptor complex that enhances cargo recognition and autophagic flux (Liu et al., 2014). While the two receptors can function redundantly, they exhibit distinct substrate preferences: optineurin preferentially engages K63-linked and M1-linked ubiquitin chains playing a role in mitophagy (Lazarou et al., 2015), whereas p62 shows broader chain specificity and plays a more prominent role in aggrephagy (Komatsu et al., 2010). Both receptors co-localize within TDP-43- and SOD1-positive inclusions in ALS patient tissue, and mutations in SQSTM1 are also causally linked to ALS/FTD, underscoring convergent autophagy receptor dysfunction in disease (Fecto et al., 2011; Korac et al., 2013).

HECT Domain and Ankyrin Repeat Containing E3 Ubiquitin-Protein Ligase 1 (HACE1)

HACE1 is an E3 ubiquitin ligase that catalyzes K27-linked polyubiquitination and regulates oxidative stress responses and inflammation (Daugaard et al., 2013). HACE1 binds optineurin within CC2 (residues 411–456) and ubiquitinates it at Lys193, a modification critical for recruiting p62 and sustaining autophagic flux under cellular stress (Liu et al., 2014). This ubiquitination does not target optineurin for degradation but serves as a regulatory signal that amplifies the autophagic response to aggregated cargo. Loss of HACE1 function or prevention of Lys193 ubiquitination impairs optineurin–p62 complex formation and reduces aggregate clearance efficiency, particularly relevant in ALS where oxidative stress and proteasome dysfunction elevate the demand for selective autophagy (Liu et al., 2014).

1.3.4.2 **Vesicular Trafficking Partners**

Myosin VI (MYO6)

Myosin VI is a unique minus-end-directed actin motor essential for endocytic trafficking, autophagosome maturation, and exocytosis (Wells et al., 1999). Optineurin interacts with myosin VI through CC2 and the UBAN domain (residues 412–520), facilitating autophagosome movement along actin filaments toward lysosomes and promoting fusion events (Sahlender et al., 2005; Tumbarello et al., 2012). The ALS-associated E478G mutation disrupts this interaction, impairing autophagosome–lysosome fusion and causing accumulation of autophagosomes, ER stress, Golgi fragmentation, and cell death (Sundaramoorthy et al., 2015). In neurons, where long-distance vesicular transport is critical for synaptic function and axonal homeostasis, loss of the optineurin–myosin VI axis results in defective retrograde transport and accumulation of damaged organelles in axonal compartments (Sundaramoorthy et al., 2015).

Ras-Related Protein Rab-8a (Rab8a)

Rab8 is a small GTPase regulating post-Golgi trafficking, polarized membrane transport, and ciliogenesis (Huber et al., 1993, Knödler, A., et al., 2010; Hattula, K., et al., 2006; Dhekne, H. S., et al., 2018). Optineurin binds Rab8a through LDZ in CC1 (residues 133–170), coordinating vesicle delivery from the trans-Golgi network to the plasma membrane in polarized cells, including neurons (Zhang et al., 2024). This pathway is critical for synaptic vesicle recycling, and delivery of growth factor receptors to the cell surface, therefore maintaining axonal integrity (Chi et al., 2010; Vaibhava et al., 2012). Other studies implicate the optineurin–Rab8a axis in autophagosome biogenesis and maturation, linking membrane trafficking to selective autophagy (Ryan et al., 2018). Optineurin can also regulate Rab8a function by recruiting GTPase-activating protein TBC1D17 via its central coiled-coil domain leading to inactivation of Rab8a, thereby negatively regulating Rab8a-mediated endocytic recycling. In ALS, impaired Rab8-mediated trafficking may contribute to protein mislocalization, defective membrane homeostasis, and synaptic dysfunction (Hattula & Peränen, 2000).

Target of Myb1 (Tom1)

Tom1 is an endosomal sorting adaptor regulating trafficking of ubiquitinated membrane receptors into multivesicular bodies for lysosomal degradation (Yamakami et al., 2003). Optineurin interacts with Tom1 to coordinate delivery of ubiquitinated endosomal cargo to

autophagosomes and facilitate autophagosome–lysosome fusion (Tumbarello et al., 2012). Disruption of this interaction impairs endosomal maturation and autophagic flux, leading to accumulation of ubiquitinated proteins in endosomal compartments. These effects could be particularly problematic in neurons where efficient endosomal trafficking is essential for synaptic vesicle recycling and receptor turnover.

1.3.4.3 **Additional Regulatory Partners**

Beyond autophagy and trafficking partners, optineurin interacts with several regulatory proteins that underscore its multifunctional nature. Optineurin binds transcription factor IIIA (TFIIIA), potentially regulating ribosome biogenesis and translational control (Moreland et al., 2000). Optineurin also binds caspase-8 through CC1 (residues 121–230), potentially suppressing apoptosis under specific stress conditions (Nakazawa et al., 2016), and interacts with the mGluR1a C-terminal tail, possibly regulating receptor trafficking and protecting against excitotoxicity (Anborgh et al., 2005). While these interactions highlight optineurin's diverse cellular roles, their specific contributions to ALS pathogenesis remain incompletely understood.

1.4. **Optineurin Variants Associated with Human Diseases**

Optineurin variants and dysregulation have been implicated in multiple human diseases. In the early 2000s, variants in OPTN were linked to POAG, a neurodegenerative disease characterized by progressive loss of retinal ganglion cells that ultimately leads to blindness. The most common POAG-linked optineurin variant E50K exhibits gain-of-function, including increased aggregation propensity and enhanced binding to TBK1 (Rezaie et al., 2002; Morton et al., 2008; Minegishi et al., 2013; Li et al., 2016). Around additional 15 optineurin POAG-associated variants have been reported, with variable functional consequences, but their pathogenicity is unclear (Minegishi et al., 2016).

In 2010, the first amyotrophic lateral sclerosis (ALS) associated OPTN variants were identified, including homozygous deletion of exon 5 (Δex5; null), homozygous Q398X truncation (premature stop), and heterozygous E478G missense affecting the UBAN region (Maruyama et al., 2010). These variants co-segregated with disease, were absent in controls, and exhibited altered NF-κB regulation, subcellular localization, and neuropathological features, strongly supporting their pathogenicity. Since then, >100 OPTN variants have been

reported in ALS and/or frontotemporal dementia (FTD) patients (Markovinovic et al., 2017; Xiao et al., 2025). Notably, there is almost no overlap between variants implicated in POAG and those in ALS/FTD. In contrast to POAG where the only confirmed pathogenic variant (E50K) is thought to result in gain-of-function, in ALS/FTD, functional studies and inheritance patterns support loss-of-function and/or haploinsufficiency for most of the confirmed pathogenic *OPTN* variants, with possibly dominant-negative effects for some truncations and missense mutations that could interfere with oligomerization or Ub-chain recognition (Tümer et al., 2012; van Blitterswijk et al., 2012; Del Bo et al., 2011; Weishaupt et al., 2013; Özoğuz et al., 2015; Fifita et al., 2017). However, the pathogenicity of most *OPTN* variants potentially linked to ALS/FTD is still unclear.

Beyond neurodegeneration, polymorphisms lowering *OPTN* expression have been associated with Paget's disease of bone and Crohn's disease, consistent with optineurin's roles in inflammation and bone remodeling (Albagha et al., 2011; Obaid et al., 2015; Smith et al., 2015). Moreover, wild-type optineurin has been detected in disease-specific inclusions in senile plaques in Alzheimer's disease (AD) and in Lewy bodies in Parkinson's disease (PD), and in Creutzfeldt–Jakob's and Pick's disease; optineurin-positive aggregates have also been observed in sporadic inclusion body myositis (IBM) and oculopharyngeal muscular dystrophy (OPMD) (Osawa et al., 2011; Yamashita et al., 2013).

Together, these findings support a broad involvement of optineurin in human disease, spanning neurodegeneration, inflammation, and protein homeostasis. Given that loss-of-function mechanisms are thought to predominate in ALS-associated *OPTN* pathology (Maruyama et al., 2010; Markovinovic et al., 2017), this dissertation focuses on the cellular consequences of optineurin deficiency.

1.5. **Amyotrophic Lateral Sclerosis: Clinical Manifestation and Current Therapies**

ALS, also referred to Lou Gehrig's disease, is a progressive neurodegenerative disorder affecting upper and lower motor neurons in the brain and spinal cord with a prevalence of 6 cases per 100,000 individuals and an average onset between 58 and 60 years (Talbott et al., 2016). Clinically, ALS typically presents as spinal-onset disease, with limb weakness and fasciculations in ~65% of cases, or as bulbar-onset disease (~35%) with dysarthria and dysphagia; over time, both forms converge on similar manifestations, including spasticity,

muscle weakness and atrophy, and ultimately paralysis (Hardiman et al., 2017; Brown & Al-Chalabi, 2017; Es et al., 2017; Masrori & Van Damme, 2020). Respiratory failure due to diaphragmatic and intercostal involvement is the usual cause of death. The average age of onset is ~58–60 years with a life expectancy averaging 3 to 5 years and incidence ~2–3 per 100,000 in European ancestry populations and a male predominance of ~1.2–1.5:1 (Es et al., 2017; Hardiman et al., 2017). Cognitive and behavioral features are increasingly recognized: up to 50% of ALS patients exhibit some degree of cognitive impairment, and ~15% develop frontotemporal dementia (FTD); conversely, ~15% of FTD patients develop ALS, aligning with the concept of an ALS/FTD spectrum (Ringholz et al., 2005; Lomen-Hoerth et al., 2002; Ling et al., 2013; Pottier et al., 2018).

Therapy remains limited and mostly symptomatic. Riluzole, thought to modulate glutamatergic transmission, extends survival modestly (initially estimated at 2–3 months, with more recent real-world estimates of 6–19 months) (Andrews et al., 2020). Edaravone, an antioxidant drug approved in the USA, Canada and Japan, slows disease progression in a subset of patients, with a questionable effect on survival due to a small cohort of patients (Abe et al., 2017; Al-Chalabi et al., 2017). More recently, Tofersen, an antisense oligonucleotide reducing misfolded SOD1 protein levels in *SOD1*-linked ALS by targeting superoxide dismutase 1 (SOD1) mRNA, has shown on a limited number of patients promising results with delayed disease progression (Mead et al., 2022, Miller et al., 2025). Symptom-targeted interventions include agents to reduce hypersalivation, respiratory insufficiency, pain, muscle cramps and depression (Hardiman et al., 2017). Despite progress, robust disease-modifying therapies remain an unmet need.

1.5.1. **Etiopathological Risk Factors In ALS**

The etiopathogenesis of ALS is generally considered multifactorial, requiring concomitant genetic and environmental hits (Al-Chalabi et al., 2014). ALS is genetically heterogeneous, with mutations identified in over 40 genes that influence diverse cellular systems including RNA metabolism, protein homeostasis, autophagy, nucleocytoplasmic transport, vesicular trafficking, and innate immunity (Mead et al., 2022; Hardiman et al., 2017; Akçimen et al., 2023). Major genes with mutations associated to ALS include *C9ORF72* (hexanucleotide repeat expansion), *SOD1*, *TARDBP* (encoding TDP-43), and *FUS*. Approximately 10% of ALS are familial (fALS), while the remaining ~90% are sporadic (sALS) (Andersen & Al-Chalabi, 2011; Renton et al., 2014). Notably, fALS and sALS are clinically indistinguishable and often

share mutations in the same genes, suggesting shared pathogenic mechanisms underlying motor neuron loss (Hardiman et al., 2017; Renton et al., 2014). In fALS, gene frequency and penetrance may vary by ancestry; for example, *C9ORF72* expansions are highly prevalent in Europeans but less common in some Asian cohorts, where SOD1 mutations are comparatively more frequent (Zou et al., 2017).

Protein aggregation and proteostasis dysfunction are central to ALS pathobiology. The first ALS-linked mutation was discovered in the gene encoding superoxide dismutase 1 (SOD1), an enzyme that clears reactive oxygen species (H. X. Deng et al., 1993; Rosen et al., 1993). Although early hypotheses speculated that SOD1 mutations caused oxidative stress via loss of enzymatic function, transgenic SOD1G93A models and biochemical studies established toxic gain-of-function aggregation as a key driver of neurodegeneration, with misfolded SOD1 forming neurotoxic inclusions (Rosen et al., 1993; Gurney et al., 1994; Bruijn et al., 1998; Watanabe et al., 2001). It is now established that aggregation of TDP-43, FUS, and C9ORF72-related dipeptide repeats are present in both neurons and glia in ALS (Arai et al., 2006; Neumann et al., 2006; Kwiatkowski et al., 2009; DeJesus-Hernandez et al., 2011). In particular, TDP-43 is a central hallmark in ALS with more than 95% of patients displaying hyperphosphorylated and ubiquitinated TDP-43 aggregates, while aggregation of SOD1, FUS, and C9ORF72-related dipeptide repeats is observed in genetically defined ALS subgroups. TDP-43 aggregation is also present in about 50% of the patients with FTD. The nuclear protein TDP-43, by binding both mRNA and DNA, plays a central role in mRNA splicing, stability and translation as well as gene transcription in neural development and function. TDP-43 protein structure, and cellular and environmental processes act as the main drivers of TDP-43 aggregation in pathological conditions, while mutations the TDP-43 gene (*TARDBP*) are rare (Ling et al., 2013; Coan & Mitchell, 2015).

TDP-43 contains a prion-like C-terminal domain with high aggregation and phase-separation propensity. Post-translational modifications and proteolytic cleavage in pathological settings can lead to the generation toxic C-terminal fragments (TDP-35 and TDP-25) further promoting TDP-43 generation of insoluble protein complexes and mislocalization within the cell (Prasad et al., 2019; Jo et al., 2020; Neumann et al., 2006; Braak et al., 2010; Gitler & Shorter, 2011).

Impairments in protein degradation systems play a prominent role in promoting TDP-43 aggregation and dysregulation. Soluble TDP-43 is preferentially degraded by the ubiquitin–proteasome system (UPS), whereas aggregated TDP-43 is primarily cleared via autophagy; age-related declines in lysosomal function and autophagic flux compromise both pathways

(Scotter et al., 2014; Pohl & Dikic, 2019; Ivashkiv & Donlin, 2014). Mutations affecting autophagy adaptors and modulators, including optineurin (*OPTN*), sequestosome 1 (*p62/SQSTM1*), TANK-binding kinase 1 (*TBK1*), cylindromatosis (*CYLD*), and ubiquilin-2 (*UBQLN2*), can disrupt cargo recognition, LC3 engagement, and ubiquitin-chain editing, collectively converging on TDP-43 accumulation (Dobson-Stone et al., 2020; Fecto et al., 2011; Freischmidt et al., 2017; Maruyama et al., 2010; Freischmidt et al., 2015; Deng et al., 2011). *C9ORF72* repeat expansions further complicate the picture by generating dipeptide repeat proteins, abnormal RNA species, and nucleocytoplasmic transport defects, together with anomalies in autophagy initiation and lysosomal function, thereby amplifying proteostasis stress (DeJesus-Hernandez et al., 2011; Sullivan et al., 2016; Mead et al., 2022). In this regard, proteostasis stress and neuroinflammation are bidirectionally linked: aggregated proteins can act as DAMPs that activate microglia, while inflammatory signaling can exacerbate misfolding and aggregation, as shown by lipopolysaccharide (LPS)-induced TDP-43 mislocalization and aggregation in glia and spinal neurons (Correia et al., 2015; Zhao et al., 2015).

Additional mechanisms implicated in ALS include defects in RNA metabolism (transcription, splicing, transport, translation), excitotoxicity driven by excess glutamate and NMDA receptor activation, oxidative stress, mitochondrial dysfunction, endoplasmic reticulum (ER) stress, and cytoskeletal/axonal transport disruptions (Rossi et al., 2016; Ferraiuolo et al., 2011; Polymenidou et al., 2012).

Environmental factors, such as smoking, chemical exposures, strenuous physical activity, and air pollutants, have been implicated as potential triggers for ALS, but their overall impact remains debated. In contrast, aging consistently emerges as the dominant risk factor, aligning with well-documented, age-related declines in proteostasis and immune regulation (Talbott et al., 2016; Hou et al., 2019; López-Otín et al., 2023; Wilson et al., 2023). Aging drives broad cellular changes, including genomic instability, immune inflammation, impaired protein homeostasis, cellular senescence, and mitochondrial dysfunction (López-Otín et al., 2023), all of which are associated with neurodegenerative pathologies (Wilson et al., 2023).

Overall, aging is firmly established as the most significant risk factor which, in conjunction with a permissive genetic milieu, can trigger the onset of ALS leading to protein aggregation and neurodegeneration. Neuroinflammation (detailed in Section 1.6) is intertwined with these processes and is detectable pre-symptomatically in ALS models, supporting a contributory role in disease initiation and progression (Hall et al., 1998; Komine & Yamanaka, 2015).

1.6 **Neuroinflammation in Amyotrophic Lateral Sclerosis**

Neuroinflammation is a cardinal feature of amyotrophic lateral sclerosis (ALS), characterized by activation of glial cells and infiltration of peripheral immune cells in affected regions of the motor cortex, brainstem, and spinal cord (McGeer et al., 1991; Kawamata et al., 1992; McCauley & Baloh, 2019). Although motor neurons are the primary cells lost in ALS, extensive evidence demonstrates that neurodegeneration arises from both cell-autonomous and non-cell-autonomous mechanisms driven by surrounding glia and infiltrating immune cells (Philips & Robberecht, 2011; Boillée et al., 2006). This section examines the cellular and molecular basis of neuroinflammation in ALS, with particular emphasis on the roles of resident microglia and peripheral myeloid cells, macrophages and dendritic cells, that interface with the central nervous system to shape disease initiation and progression.

1.6.1 Glial Cells and Neuroinflammation: The Central Role of Microglia

Glial cells (microglia, astrocytes, oligodendrocytes, and ependymal cells) are indispensable for CNS homeostasis, neuronal signaling, and orchestration of neuroinflammatory responses that can either protect tissue or precipitate injury (Prinz & Priller, 2014). Among these populations, microglia serve as the resident macrophages of the brain and spinal cord and function as the primary innate immune sentinels within the CNS parenchyma.

1.6.1.1 Microglial Origin and Maintenance

Unlike most tissue macrophages, which are maintained locally at steady state but can derive from bone marrow monocytes during inflammatory conditions, microglia originate from yolk sac hematopoietic progenitors that colonize the CNS during early embryogenesis and are largely maintained independently of circulating monocytes under homeostatic conditions (Ginhoux et al., 2010). Thus, under physiological conditions, circulating monocytes do not replace microglia; instead, microglial populations are sustained by local proliferation and self-renewal throughout life, dependent on CSF1R signaling (Ginhoux et al., 2010; Wang et al., 2012). Microglia colonize the CNS before neurons and other glial cells and exhibit distinct spatiotemporal distribution that implicates them in neurodevelopmental processes including neurogenesis, synaptic pruning, and circuit refinement (Tong & Vidyadaran, 2016; Li & Barres, 2018).

1.6.1.2 Microglial Surveillance and Activation

At rest, microglia display a highly ramified morphology with small soma and long, motile processes used to continuously survey the parenchyma and identify danger signals (Nimmerjahn et al., 2005). Upon exposure to threats such as pathogens, aggregated proteins, or tissue injury, microglia transition to an activated, amoeboid phenotype characterized by soma enlargement, process retraction, upregulation of pattern-recognition receptors (PRRs), and secretion of pro-inflammatory mediators including TNF-α, IL-1β, IL-6, reactive oxygen species (ROS), and nitric oxide (NO). Microglia express a broad repertoire of PRRs—including TLR (such as TLR2/4), NOD-like receptors (NLRs), cyclic GMP–AMP synthase (cGAS), and RIG-I-like receptors—that engage canonical inflammatory signaling cascades, notably NF-κB and TBK1-dependent pathways (see Sections 1.7.1 and 1.7.3) (Bsibsi et al., 2002; Kawai & Akira, 2010; Li & Wu, 2021).

1.6.1.3 Microglial Polarization: M1/M2 Framework and Functional Heterogeneity

Microglial activation encompasses a spectrum of phenotypic states historically framed between classically activated (M1-like) and alternatively activated (M2-like), by analogy to macrophage nomenclature (Tang & Le, 2016). Although this dichotomy oversimplifies the *in vivo* biological variability and continuum of immune responses, as documented in multiple studies characterizing disease-associated microglia (DAM) and microglial neurodegenerative phenotype (MGnD) (Guo et al., 2022; Paolicelli et al., 2022), the framework remains useful for describing divergent functional programs:

- **M1-like microglia** are induced by microbial stimuli (LPS, IFN-γ) and characterized by robust NF-κB activation and production of pro-inflammatory cytokines (TNF-α, IL-1β, IL-6), ROS, and NO via inducible nitric oxide synthase (iNOS) (Murray & Wynn, 2011; Tang & Le, 2016). M1-like microglia heighten antimicrobial responses but can exert neurotoxic effects if sustained.
- **M2-like microglia** are skewed by anti-inflammatory cues (IL-10, IL-4, TGF-β) and promote tissue protection and repair through secretion of neurotrophic factors (IGF-1, BDNF) and expression of enzymes (such as arginase 1, Arg1) that support matrix remodeling and resolution of inflammation (Cherry et al., 2014; Tang & Le, 2016). Mechanisms include competitive metabolism of arginine via Arg1 to limit NO synthesis and enhanced phagocytic clearance via scavenger receptor upregulation.

In acute CNS insults, an effective transition from early M1-like responses (damage control) to M2-like programs (resolution and repair) is essential to restore homeostasis (Philips & Robberecht, 2011). However, chronic injury disrupts this switch. Persistent exposure to damage-associated molecular patterns (DAMPs), such as extracellular ATP, HMGB1, and aggregated proteins released by dying neurons, maintains microglia in a dysregulated state with reduced phagocytic efficiency (Murray & Wynn, 2011). This failure to resolve inflammation fosters a feedforward loop: impaired debris clearance sustains PRR stimulation, amplifies cytokine production, and exacerbates neuronal stress, thereby perpetuating chronic neuroinflammation characteristic of neurodegenerative diseases including ALS (Philips & Robberecht, 2011; Béland et al., 2020).

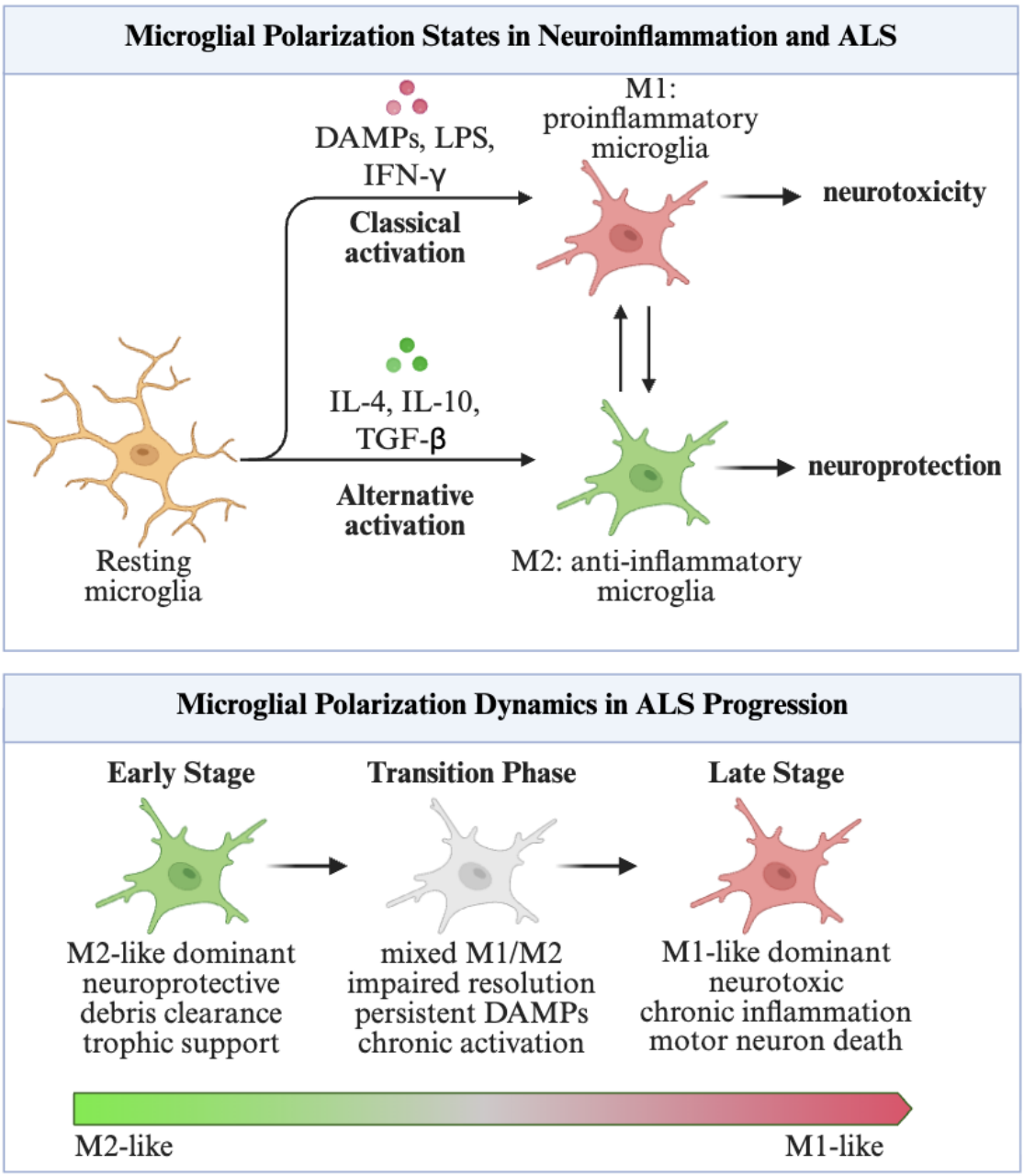

Figure 3. Microglial polarization states and temporal dynamics in ALS.

(Top) Three functional states of microglia: **(Left)** Resting microglia display a ramified morphology with small soma and long, motile processes that continuously survey the CNS parenchyma for homeostatic maintenance. **(Middle)** M1-like (classically activated) microglia adopt an amoeboid morphology with enlarged soma and retracted processes. Stimulated by LPS, IFN-γ, and DAMPs, M1-like microglia produce pro-inflammatory mediators (TNF-α, IL-1β, IL-6, ROS, NO) that exert neurotoxic effects. **(Right)** M2-like (alternatively activated) microglia also display amoeboid morphology but are induced by anti-inflammatory cues (IL-10, IL-4, TGF-β) and secrete neuroprotective factors (IGF-1, BDNF) and express Arg1 to

support tissue repair and resolution. **(Bottom)** Temporal dynamics of microglial polarization in ALS progression. In early stages, M2-like microglia predominate, providing neuroprotective support and debris clearance. During disease progression, impaired resolution and persistent DAMP exposure drive a transition toward M1-like states. In late stages, M1-like microglia dominate, sustaining chronic neuroinflammation and contributing to motor neuron death. The gradient bar illustrates the progressive shift from M2-like (green) to M1-like (red) phenotypes over disease course. Image generated with Biorender.

1.6.1.4 Microglia in ALS Pathogenesis

In ALS, activated microglia and reactive astrocytes are consistently observed in affected CNS regions (McGeer et al., 1991; Kawamata et al., 1992). Evidence from mutant SOD1 animal models demonstrates that while motor neurons harbor the primary genetic lesion, glial cells actively contribute to disease progression. Restricting mutant SOD1 expression to motor neurons alone is insufficient to cause disease, whereas chimeric mice with increasing proportions of wild-type glial cells show delayed progression and extended survival (Gong et al., 2000; Clement et al., 2003). Transgenic $SOD1^{G37R}$ mice with a conditional deletion of the transgene in microglia or astrocytes show slower disease progression without affecting onset, whereas transgene deletion from motor neurons delays onset, highlighting stage- and cell-type-specific contributions (Boillée et al., 2006; Yamanaka et al., 2008). SOD1(G93A) microglia exhibit heightened oxidative stress and increased motor neuron toxicity (Beers et al., 2006; Liao et al., 2012), and longitudinal profiling reveals that microglia initially display an M2-like, neuroprotective program that shifts toward an M1-like, neurotoxic state as damage accumulates (Beers et al., 2011).

1.6.1.5 Broader Glial Network and Neurodegenerative Cascades

Microglia act in concert with other glial populations during neuroinflammation. Astrocytes increase GFAP expression and adopt reactive phenotypes with age and injury, integrate microglial cytokine cues, and contribute to the inflammatory milieu through their own cytokine production and alterations in glutamate handling that can promote excitotoxicity (Olmos & Lladó, 2014; Gudkov et al., 2023). Oligodendrocytes and their precursors are sensitive to cytokines and oxidative stress and can amplify signals leading to demyelination. While activated microglia can produce neuroprotective mediators during resolution phases, sustained pro-inflammatory signaling is neurotoxic, contributing to synaptic dysfunction, mitochondrial

injury, and excitotoxic pathways that culminate in neuronal death (von Bernhardi et al., 2015; Mattson & Arumugam, 2018).

1.6.2 **Peripheral Immune Cells in ALS: Macrophages, Dendritic Cells, and Systemic Inflammation**

It is increasingly recognized that immune disbalance in ALS is not solely restricted to intrinsic CNS processes. Peripheral immune cells, particularly monocytes, macrophages, and dendritic cells (DC), dynamically interface with the neurovascular unit, meningeal compartments, and cervical lymph nodes, coupling systemic immune tone to CNS homeostasis and disease trajectories (Prinz & Priller, 2014; Ransohoff & Brown, 2012; Louveau et al., 2015). Accumulating evidence indicates that peripheral myeloid cells contribute to ALS pathogenesis through multiple mechanisms: direct infiltration into the CNS, amplification of systemic inflammatory signals that cross the BBB, modulation of adaptive immune responses, and impaired clearance of cellular debris and protein aggregates.

1.6.2.1 ***Peripheral Immune Alterations in ALS Patients and Models***

Multiple peripheral immune lineages show pathological changes in ALS. In blood, monocytes from ALS patients exhibit pro-inflammatory polarization, including increased MHC class II expression and elevated transcripts for IL-1β, IL-8, and CXCL10 (Zhang et al., 2005; Zhao et al., 2017). Similarly, monocytes from SOD1(G93A) mice display elevated TNF-α and IL-1β production (Butovsky et al., 2012). At neuromuscular junctions in mutant SOD1 models, activated macrophages, mast cells, and neutrophils accumulate and hinder reinnervation through degranulation and phagocytosis of degenerating axons (Chiu et al., 2009; Graber et al., 2010; Lincecum et al., 2010; Trias et al., 2018). Dendritic cell transcripts are detectable in ALS spinal cord, and DC numbers and chemokine outputs (CCL2, IL-8) are reported to be altered in patient tissues (Henkel et al., 2004; Rusconi et al., 2017). Natural killer (NK) cells infiltrate the CNS in ALS and can promote motor neuron death and M1-like microglial polarization (Garofalo et al., 2020).

Adaptive immune responses are similarly dysregulated. T helper cell polarization shifts over the disease course: TH2 and regulatory T cells (Tregs) dominate early stages and restrain microglial activation (see Section 1.6.1.3 for microglial polarization states), whereas TH1 and TH17 responses rise later and are associated with pro-inflammatory milieus in patients and

models (Beers et al., 2011; Henkel et al., 2013; Saresella et al., 2013; Béland et al., 2020). Treg dysfunction and reduced numbers correlate with faster progression and shorter survival (Henkel et al., 2013; Beers et al., 2017). $CD8^+$ T cells can directly injure motor neurons via granzymes, FasL, and IFN-γ in vitro, though T cell deficiency has not consistently extended survival in SOD1 models (Coque et al., 2019). Systemic cytokine patterns align with these observations: higher circulating TNF-α, IFN-γ, IL-6, CCL2, and IL-8 associate with more rapid progression, whereas IL-4 and IL-10 relate to symptomatic improvement (Béland et al., 2020; De Marchi et al., 2021, 2023).

1.6.2.2 ***Mechanisms of Peripheral Myeloid Cell Contribution to Neuroinflammation***

Peripheral macrophages and dendritic cells contribute to ALS pathogenesis through several interconnected mechanisms. Monocyte recruitment and CNS infiltration occur when perivascular, meningeal, and choroid plexus macrophages respond to systemic inflammation or aging-related endothelial activation. Chemokine gradients, particularly the CCL2–CCR2 axis, recruit circulating monocytes that differentiate into macrophages in CNS-adjacent niches and can infiltrate the parenchyma (Mildner et al., 2007; Shechter et al., 2009; Saederup et al., 2010). This influx amplifies local cytokine networks and perpetuates microglial activation (Ajami et al., 2011). In ALS models, blocking monocyte recruitment via CCR2 inhibition modulates disease progression, supporting a potential pathogenic role for infiltrating myeloid cells (Butovsky et al., 2012). It has also been shown that monocytes in ALS are functionally altered, showing a pro-inflammatory phenotype that can also contribute to establishing a neuroinflammatory environment.

Cytokine and danger-signal amplification occurs as peripheral macrophages sense pathogen- and damage-associated molecular patterns via TLRs, NLRs, and cGAS–STING pathways, producing TNF-α, IL-1β, IL-6, type I interferons, and ROS and reactive nitrogen species (NOS) (Kawai & Akira, 2010; Chen et al., 2016). NLRP3 inflammasome activation propagates pyroptotic signaling and DAMP release, intensifying neuroinflammatory tone both peripherally and within the CNS (Heneka et al., 2013; Ising et al., 2019). Systemic cytokines can cross a compromised BBB or signal through circumventricular organs to modulate CNS inflammation. Conversely, defective phagocytosis and debris clearance undermines inflammation resolution. Aging diminishes phagocytic and efferocytic capacity in macrophages while elevating oxidative stress (Mahmoudi et al., 2019; Moss et al., 2023), and inefficient clearance of apoptotic cells, myelin debris, and protein aggregates sustains cytokine

production and exposes neurons to toxic lipids, iron, and aggregated proteins (Neumann et al., 2009; Green et al., 2016).

Antigen presentation and T cell priming by dendritic cells shapes adaptive immune responses that feed back into the CNS. DCs at CNS borders and in cervical lymph nodes acquire CNS-derived antigens and present them to T cells, shaping TH1/TH17 versus Treg polarization based on co-stimulatory molecules and cytokine milieu (Guermonprez et al., 2002; Segal, 2019). Pro-inflammatory T cell responses augment microglial activation and BBB dysfunction (Ransohoff et al., 2003), while age and chronic inflammation erode tolerogenic DC function, skewing toward pro-inflammatory and autoimmune responses (Maldonado & von Andrian, 2010, Michaelis et al., Nature 2025).

These convergent mechanisms, including sustained cytokine production, defective debris clearance, and maladaptive T cell priming, establish a chronic inflammatory milieu that destabilizes the BBB, perturbs synaptic homeostasis, and heightens neuronal vulnerability to proteostatic stress and excitotoxicity (Mattson & Arumugam, 2018; Gate et al., 2020). In ALS, peripheral myeloid signatures correlate with disease severity and progression (Zhao et al., 2017; Keren-Shaul et al., 2017).

1.6.3 **Aging, Inflammaging, and Immunosenescence: The Permissive Context for Neurodegeneration**

Aging is the principal risk factor for ALS and other neurodegenerative diseases, entailing systemic remodeling of the immune system that creates a permissive environment for chronic neuroinflammation and proteostasis failure (López-Otín et al., 2023; Wilson et al., 2023). This age-related immune dysregulation manifests as two interconnected phenomena: inflammaging and immunosenescence.

Inflammaging describes the age-associated state of chronic, low-grade inflammation characterized by elevated circulating pro-inflammatory mediators (TNF-α, IL-6, C-reactive protein) and diminished capacity to resolve inflammatory responses (Franceschi et al., 2000, 2018; López-Otín et al., 2013). This state arises from impaired resolution of inflammatory challenges (tissue injury and infections), accumulation of senescent cells that secrete pro-inflammatory factors via the senescence-associated secretory phenotype (SASP), and persistent activation of innate immune pathways (Franceschi et al., 2018; Li et al., 2023). The resulting

chronic inflammatory milieu impairs tissue regeneration, promotes metabolic dysfunction, and increases vulnerability to age-related pathologies including neurodegeneration.

Immunosenescence encompasses quantitative and qualitative changes across innate and adaptive immunity (Mittelbrunn & Kroemer, 2021). Among innate immune populations, myeloid-derived cells, including macrophages, dendritic cells, and microglia, are central to inflammaging due to their prominent cytokine and chemokine production. With age, macrophages exhibit reduced phagocytic capacity, altered cytokine secretion profiles, and increased generation of reactive oxygen species (Moss et al., 2023). Neutrophils and dendritic cells show age-associated reductions in phagocytosis and antigen presentation efficiency (Wenisch et al., 2000; Agrawal & Gupta, 2011). Monocytes from older individuals display heightened basal inflammatory gene expression and altered responses to TLR stimulation. Specifically, aged monocytes exhibit elevated constitutive expression of pro-inflammatory genes including *TNFA*, *IL6*, and *IL1B*, a phenomenon driven in part by age-related epigenetic reprogramming, including changes in DNA methylation patterns and histone modifications, that results in a more permissive chromatin state at inflammatory gene loci (Saare et al., 2020; Gowers et al., 2011). Functionally, monocytes from elderly individuals show a paradoxical phenotype: while basal inflammatory tone is elevated, TLR-stimulated responses are often dysregulated, with some studies reporting increased TNF-α production but decreased type I interferon (IFN-α/β) output upon TLR stimulation, suggesting a selective impairment of the TBK1/IRF3 axis relative to the NF-κB pathway (Panda et al., 2010; Nyugen et al., 2010; van Duin et al., 2007). This age-related reduction in type I interferon responses is particularly relevant to optineurin biology, given optineurin's role in scaffolding TBK1 for IFN-β production. Additionally, decreased surface expression of specific TLRs, particularly TLR1, has been linked to diminished cytokine production in aged monocytes (van Duin et al., 2007). Monocyte-derived macrophages and dendritic cells from older donors also show impaired phagocytic capacity, reduced antigen processing efficiency, and altered metabolic programming — with a shift from oxidative phosphorylation toward glycolysis — that collectively compromise their ability to mount effective immune responses while paradoxically sustaining low-grade inflammation (Hearps et al., 2012; Mahbub et al., 2012). Furthermore, aged monocytes can acquire features of "trained immunity" through epigenetic and metabolic reprogramming, where prior inflammatory exposure leads to enhanced pro-inflammatory responses upon subsequent stimulation, contributing to the self-perpetuating nature of inflammaging (Netea et al., 2016; Bekkering et al., 2021). In the adaptive immune

compartment, the naïve T cell pool contracts while memory T cells expand, reducing the capacity to respond to new antigens (Mittelbrunn & Kroemer, 2021).There is enrichment of pro-inflammatory $CD4^+$ T cell subsets, including Th1 (producing TNF-α and IFN-γ) and Th17 (producing IL-17A), which collectively amplify systemic inflammation. Cytotoxic $CD8^+$ T cells similarly skew toward increased IFN-γ production in older individuals (Pulko et al., 2016). Regulatory T cell numbers may increase but their suppressive function often declines, and B cell repertoire diversity decreases with reduced antibody response efficacy.

Aging-related immune dysregulation extends to the central nervous system. Microglia in aged brains adopt a primed or activated morphology with enlarged soma, shortened processes, elevated expression of pro-inflammatory markers (CD68, MHC-II, complement components), and reduced phagocytic function (von Bernhardi et al., 2015). This primed state renders aged microglia hyper-responsive to subsequent inflammatory stimuli, leading to baseline cytokine secretion, exaggerated cytokine production upon stimulation and prolonged activation. Astrocytes also display altered phenotypes in aging, with increased GFAP expression, morphological changes, and a more pro-inflammatory transcriptional profile (Gudkov et al., 2023). The resulting inflammatory microenvironment is neurotoxic, contributing to synaptic loss, neuronal injury, and impaired neurogenesis (Mattson & Arumugam, 2018).

In the context of ALS, inflammaging and immunosenescence create a milieu in which multiple pathological processes converge. Reduced autophagy and lysosomal capacity lead to accumulation of damaged mitochondria and protein aggregates (including TDP-43 and SOD1), overwhelming cellular proteostasis machinery. Chronic activation of innate immune pathways (NF-κB, inflammasomes) in both peripheral macrophages and CNS microglia sustains pro-inflammatory cytokine production and impairs the transition to resolution/repair programs. Defective phagocytosis and efferocytosis by aged macrophages and microglia result in persistent DAMP exposure, further amplifying inflammation. Altered adaptive immunity with skewing toward Th1/Th17 responses and Treg dysfunction fails to restrain neuroinflammation and may actively promote neuronal injury. Together, these age-related changes position the immune system to respond maladaptively to genetic or environmental insults, tipping the balance toward chronic neuroinflammation and neurodegeneration (López-Otín et al., 2023; Wilson et al., 2023).

1.7 **Molecular Pathways in Neuroinflammation: NF-κB and TBK1/IFN-β Signaling**

The innate immune response in neuroinflammation is orchestrated by multiple signaling pathways activated downstream of pattern-recognition receptors (PRRs), including NF-κB, TBK1/IRF3/IRF7, MAPK (p38, JNK, ERK), and JAK/STAT (Li et al, 2021; Oh et al., 2025). Among these, the NF-κB pathway, which drives pro-inflammatory cytokine production, and the TBK1/IRF3/IRF7 pathway, which induces type I interferon responses, are particularly central to neuroinflammation and are both tightly regulated by ubiquitin-dependent mechanisms. Optineurin, through its ubiquitin-binding and scaffolding functions, my act as an adaptor for both pathways and thereby influence the balance between inflammation and resolution in myeloid cells and glia. This section focuses on NF-κB and TBK1/IFN-β signaling given their direct regulation by optineurin and their established roles in ALS pathogenesis, providing an overview of these pathways, their regulation, and their contributions to neuroinflammation.

1.7.1 **The NF-κB Signaling Pathway**

The NF-κB signaling pathway orchestrates key aspects of immune and stress responses, as well as cell survival and proliferation (Sen & Smale, 2010; Liu et al., 2017; Guo et al., 2024). NF-κB can be activated via canonical and non-canonical signaling cascades; the canonical pathway is triggered by PRRs (e.g., TLRs), cytokine receptors (e.g., TNFR1, IL-1R), and lymphocyte antigen receptors and is the primary pathway relevant to neuroinflammation and optineurin function.

Prototypically, upon TLR engagement by lipopolysaccharide (LPS), the receptor recruits adaptor proteins TRIF and TRAM to its cytoplasmic domain. These adaptors recruit E3 ubiquitin ligases such as TRAF6 and the linear ubiquitin chain assembly complex (LUBAC), which assemble K63-linked and M1-linked (linear) polyubiquitin chains on receptor-interacting serine/threonine-protein kinase 1 (RIPK1) (Shih et al., 2011; Tokunaga & Iwai, 2012). These ubiquitin scaffolds serve as docking platforms for the transforming growth factor-β-activated kinase 1 (TAK1) complex and the IκB kinase (IKK) complex. The latter consists of catalytic subunits IKKα and IKKβ and the regulatory subunit NEMO (IKKγ). TAK1-mediated phosphorylation activates IKKβ, which in turn phosphorylates IκBα at Ser32 and Ser36, leading to K48-linked ubiquitination and proteasomal degradation of IκBα (Alkalay et

al., 1995; Zandi et al., 1997; Chen et al., 1996). IκBα acts as a primary cellular inhibitor of NF-κB by sequestering it in the cytoplasm, preventing its translocation to the nucleus. Thus, proteasomal degradation of IκBα and simultaneous phosphorylation of p65, frees up NF-κB dimers (commonly referred as p65:p50) to translocate to the nucleus and induce transcription of various pro-inflammatory genes including *TNF*, *IL1B*, *IL6*, and *NFKBIA* (encoding IκBα) (Ghosh & Hayden, 2012).

NF-κB signaling is constrained by multiple feedback loops. Newly synthesized IκBα re-enters the nucleus, binds NF-κB dimers, and exports them back to the cytoplasm, terminating transcription (Sun et al., 1993; Arenzana-Seisdedos et al., 1997). Deubiquitinases (DUBs) such as A20 (TNFAIP3) and CYLD edit K63-linked ubiquitin chains on RIPK1 and other substrates, disassembling signaling complexes and terminating NF-κB activation (Wertz et al., 2004; Kovalenko et al., 2003). NEMO-related proteins, including optineurin and the ABIN family, can compete with NEMO for binding to ubiquitinated substrates or recruit DUBs to signaling complexes, providing additional layers of regulation (Zhu et al., 2007; Verhelst et al., 2012).

1.7.2 **NF-κB in Neuroinflammation and ALS**

NF-κB exerts cell-type-specific roles in the CNS. Neurons display relatively high basal NF-κB activity that supports synaptic function, plasticity, and survival (Bhakar et al., 2002; Kaltschmidt et al., 2005). In glia, NF-κB activation is typically inducible and contributes to inflammatory responses. Persistent NF-κB activation in microglia (see Section 1.6.1 for microglial roles in ALS) is neurotoxic, in part via TNF-driven amplification loops and modulation of astrocyte glutamate handling, TNF-α promotes glutamate exocytosis and inhibits uptake by astrocytes, favoring excitotoxicity (Olmos & Lladó, 2014).

Abnormal NF-κB activation (e.g., increased p65 nuclear localization) has been reported in ALS tissues, especially in glia (Swarup et al., 2011; Sako et al., 2012; Nakazawa et al., 2016). Functionally, microglia-specific NF-κB inhibition rescues motor neuron survival *in vitro* and delays disease progression *in vivo*, whereas constitutive microglial NF-κB activation recapitulates ALS-like pathology (Frakes et al., 2014). Astrocyte-specific NF-κB inhibition shows limited efficacy, highlighting microglia as a key driver of NF-κB-mediated neurotoxicity (Crosio et al., 2011; Frakes et al., 2014). Notably, TDP-43 interacts with NF-κB pathways: overexpressed TDP-43 can enhance p65 activity and increase pro-inflammatory cytokine expression, and TDP-43 colocalizes with p65 in human ALS tissue (Swarup et al.,

2011). Moreover, LPS-driven activation of NF-κB promotes TDP-43 mislocalization and aggregation in glia and spinal motor neurons (Correia et al., 2015; Zhao et al., 2015).

1.7.3 **The TBK1/IFN-β Signaling Pathway**

Whereas NF-κB signaling is broadly activated downstream of multiple PRRs, selected PRR pathways in parallel engage TBK1 and IκB kinase ε (IKKε) to activate IRF3/IRF7, and elicit type I interferon (IFN-α/β) responses (Fitzgerald et al., 2003; Takeuchi et al., 2004). TBK1 activation occurs downstream of TRIF-dependent TLR3 and TLR4 signaling, as well as RIG-I-like receptor and cGAS–STING pathways. Upon PRR engagement, the adaptor proteins TRIF, TRAM, MAVS, and STING recruit TNF receptor-associated factor 3 (TRAF3), an E3 ubiquitin ligase that catalyzes K63-linked polyubiquitination of TBK1 at multiple sites (Tu et al., 2013; Helgason et al., 2013). These K63-linked ubiquitin chains serve as docking sites for TBK1 itself and for adaptor proteins that facilitate TBK1 dimerization and trans-autophosphorylation at Ser172 within the kinase activation loop, a critical event for TBK1 catalytic activity (Helgason et al., 2013, Paul et al., 2025). Recent work additionally identified a role for the E3 ubiquitin ligase ANKIB1-mediated K11-linked ubiquitination in promoting TBK1 activation downstream of TLR3, TLR4, and cGAS–STING signaling through recruitment of optineurin-containing signaling complexes (Betrancourt et al., 2026). Activated TBK1 phosphorylates IRF3 and IRF7 at multiple serine residues in their C-terminal regulatory domains, promoting their dimerization, nuclear translocation, and binding to interferon-stimulated response elements (ISREs) to induce transcription of *IFNB1* and other interferon-stimulated genes (ISGs) (Lin et al., 1999; Sharma et al., 2003; Honda et al., 2005). TBK1 also phosphorylates AKT at Thr308 and Ser473, linking innate immune activation to PI3K–AKT pathways that control cell growth, survival, and metabolism (Xie et al., 2011).

Secreted IFN-β binds to the type I interferon receptor (IFNAR1/IFNAR2) on target cells in an autocrine and paracrine manner, activating Janus kinase 1 (JAK1) and tyrosine kinase 2 (TYK2) to phosphorylate signal transducer and activator of transcription 1 and 2 (STAT1/STAT2). Phosphorylated STAT1/STAT2 heterodimerize and associate with IRF9 to form the interferon-stimulated gene factor 3 (ISGF3) transcriptional complex, which translocates to the nucleus and binds ISREs to induce a broad program of ISGs (Platanias, 2005; Rauch et al., 2013). Among these ISGs, IRF7 itself function as a transcription factor that amplifies IFN-β production by binding to interferon regulatory factor binding sites (IRFBSs)

on *IFNB1* and other interferon genes, generating a positive feedback loop that underpins both antiviral defenses and broader immunomodulation (Ning et al., 2011).

IFN-β exerts context-dependent pro-inflammatory and anti-inflammatory effects. It upregulates genes with antimicrobial, antiviral, and immunoregulatory functions, including NOS2 (iNOS) and chemokines such as CXCL10, CCL2 (MCP-1), and CCL5 (RANTES), thereby orchestrating leukocyte recruitment and shaping the inflammatory milieu (Gao et al., 1998; Trinchieri, 2010; Ivashkiv & Donlin, 2014; Rauch et al., 2013). Conversely, IFN-β restrains certain pro-inflammatory circuits by increasing IL10 expression and limiting neutrophil-attracting chemokines (e.g., CXCL1/CXCL2), and can suppress TNF-mediated NF-κB activation (González-Navajas et al., 2012; Manna et al., 2000; Rauch et al., 2013). These bidirectional effects are dose-, timing-, and context-dependent and are particularly relevant in the CNS, where excessive inflammation is detrimental, yet robust damage and pathogen clearance is necessary.

1.7.4 **TBK1/IFN-β in Neuroinflammation and ALS**

TBK1/IFN-β signaling exerts complex, context-dependent influences on neuroinflammation. In microglia, IFN-β can upregulate classical pro-inflammatory mediators (TNF-α, IL-1β, IL-6, NO) under strong TLR stimulation (Kawanokuchi et al., 2004; Jin et al., 2007), yet it also induces IL-10 and other anti-inflammatory factors, demonstrating immunomodulatory capacity (Lobo-Silva et al., 2017). IFN-β promotes M1→M2 microglial transitions (see Section 1.6.1.3) via IRF7, facilitating the resolution phase and tissue repair (Cohen et al., 2014). Functionally, IFN-β reduces microglial activation, protects neurons from axonal damage and death, and protects astrocytes against TNF-induced apoptosis (di Penta et al., 2013; Barca et al., 2008). In vivo, loss of neuronal IFN-β signaling ($Ifnb^{-/-}$ or $Ifnar^{-/-}$) leads to Parkinson-like neurodegeneration and Lewy body formation; IFN-β supplementation can protect dopaminergic neurons in familial PD models (Ejlerskov et al., 2015). However, sustained or excessive activation of the TBK1–IFN axis has also been implicated in chronic neuroinflammation and neurodegeneration. In ALS, activation of ISG programs and cGAS–STING signaling has been observed in both mouse models and patient CNS tissue, while recent studies demonstrated that stronger IFN signatures correlate with disease severity and that pharmacological STING inhibition can delay disease progression in SOD1 mice (Gerbino et al., 2020; McCauley et al., 2020; Yu et al., 2020; Carletta et al., 2026). These data indicate that

intact TBK1–IFN-β pathways are important for CNS homeostasis, and that their dysregulation may tip the balance toward chronic inflammation and neurodegeneration.

TBK1 loss-of-function mutations have been reported in ALS and FTD and are associated with reduced IRF3 phosphorylation and diminished binding to optineurin (Freischmidt et al., 2015; de Majo et al., 2018; Brenner et al., 2024). TBK1 haploinsufficiency can produce stage-dependent effects on disease—detrimental early, potentially beneficial later via reduced microgliosis—highlighting the nuanced role of IFN-β signaling in neuroinflammation (Brenner et al., 2019). The convergence of OPTN and TBK1 mutations in ALS/FTD suggests that disruption of the optineurin–TBK1–IFN-β axis may contribute to disease onset or progression by skewing glial responses, compromising antiviral defenses, and impairing autophagic clearance of damaged mitochondria and protein aggregates.

1.8 **Optineurin in Immune Signaling and Neuroinflammation**

Optineurin's ubiquitin-binding and scaffolding functions position it at the intersection of NF-κB and TBK1/IFN-β pathways, potentially allowing it to play a role in integrating signals across innate immune regulation, selective autophagy, and cell survival. This section examines optineurin's roles in these pathways and discusses the implications of optineurin deficiency for neuroinflammation and ALS pathogenesis.

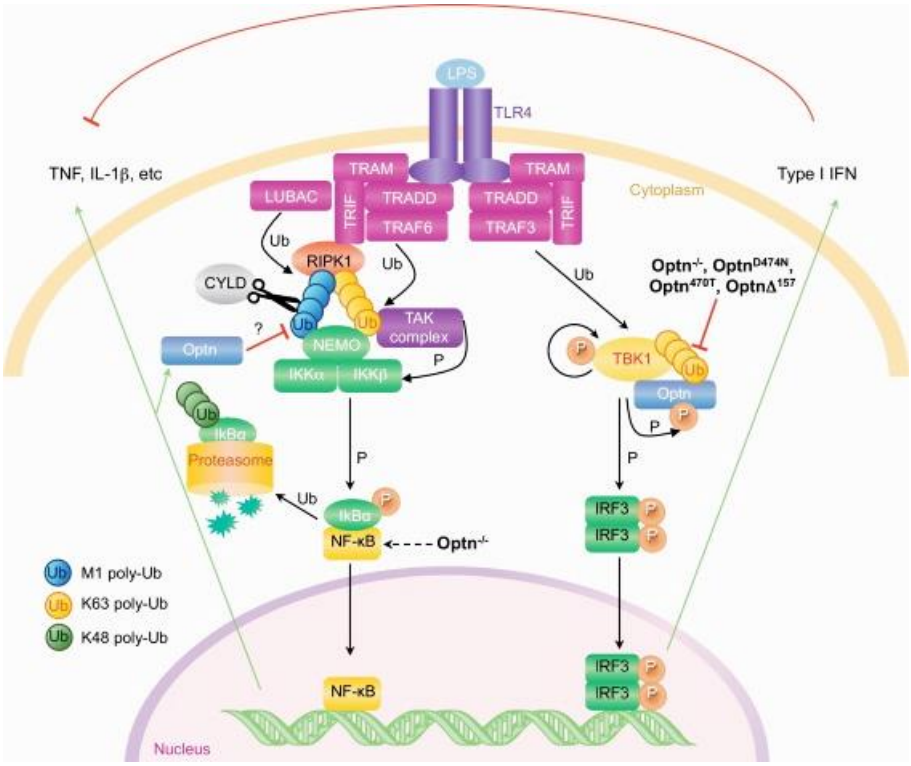

Figure 4. NF-κB and TBK1/IFN-β signaling pathways in innate immune responses.

Left: TLR4, used as prototypical example for PRRs, engagement triggers TRAF6/LUBAC-mediated K63/M1-ubiquitination of RIPK1, recruiting TAK1 and the IKK complex (NEMO). IKKβ phosphorylates IκBα, leading to its degradation and nuclear translocation of p65/p50 NF-κB dimers, which induce pro-inflammatory gene transcription (*TNF*, *IL1B*, *IL6*). Optineurin can compete with NEMO for RIPK1 binding and recruits CYLD, providing context-dependent inhibition. **Right:** TLR4 engagement triggers TRAF3-mediated K63-ubiquitination of TBK1. Optineurin can serve as ancillary scaffold, among other adaptors, for TBK1 via bivalent interactions (CC1 + UBAN/ZF), promoting TBK1 dimerization and autophosphorylation at Ser172. Activated TBK1 phosphorylates IRF3/7, leading to nuclear translocation and *IFNB1*/ISG transcription. IFN-β signals through IFNAR/JAK/STAT, inducing ISGs including *IRF7*, which amplifies IFN-β production (positive feedback, dashed arrow). This image was taken from our review article: "Optineurin in amyotrophic lateral sclerosis: Multifunctional adaptor protein at the crossroads of different neuroprotective mechanisms" (Markovinovic et al., 2017).

1.8.1 Optineurin Regulation of NF-κB Signaling: Context-Dependent Inhibition

Optineurin's UBAN/ZF region shares structural and functional homology with NEMO and the ABIN family by binding polyubiquitin chains, leading to the hypothesis that it influences NF-κB signaling (Schwamborn et al., 2000; Wagner et al., 2008; Laplantine et al., 2009). Early studies in cell lines supported an inhibitory role: optineurin overexpression suppressed TNF-induced NF-κB activation, while optineurin silencing enhanced it (Zhu et al., 2007; Sudhakar et al., 2009). Mechanistically, optineurin was proposed to compete with NEMO for binding to K63-ubiquitinated RIPK1 and/or to recruit the deubiquitinase CYLD to hydrolyze K63 chains, thereby disassembling the signaling complex (Zhu et al., 2007; Nagabhushana et al., 2011). The optineurin variants found in ALS patients (e.g., E478G, Q398X) and certain engineered ubiquitin-binding-deficient variants often demonstrated inhibitory activity in these overexpression systems (Maruyama et al., 2010; Akizuki et al., 2013; Nakazawa et al., 2016).

However, extensive analysis of primary murine cells suggested that optineurin is not required for acute NF-κB activation by TLR or TNF-α stimulation. Bone marrow-derived macrophages (BMDMs), bone marrow-derived dendritic cells (BMDCs), and mouse embryonic fibroblasts (MEFs) showed comparable IκBα degradation, p65 nuclear translocation, and target gene

induction in wild-type versus optineurin-deficient or -insufficient settings (Gleason et al., 2011; Munitic et al., 2013; Slowicka et al., 2016). These findings indicate that under physiological conditions with endogenous expression levels, optineurin is dispensable for the initial wave of NF-κB activation in response to canonical inflammatory stimuli. Exceptions to this pattern have been observed in specific contexts: during RANKL-driven osteoclastogenesis, osteoclast precursors derived from $Optn^{D477N/D477N}$ mice, which express a ubiquitin-binding-deficient optineurin variant, exhibited sustained NF-κB hyperactivation, suggesting that optineurin may restrain prolonged or oscillatory NF-κB signaling in certain differentiation programs (Obaid et al., 2015). Additionally, optineurin-deficient ($Optn^{-/-}$) microglia and spinal cord tissue showed slightly elevated basal TNF-α levels and enhanced necroptosis, a form of regulated necrotic cell death driven by RIPK1/RIPK3/MLKL signaling (Ito et al., 2016; Nakazawa et al., 2016), suggesting that optineurin may suppress RIPK1-dependent cell death pathways that secondarily amplify NF-κB activation through DAMP release and autocrine/paracrine TNF-α signaling. These data collectively suggest that optineurin's inhibitory effect on NF-κB signaling is context-dependent and may become evident primarily under prolonged or necroptotic signaling conditions rather than in early acute responses.

1.8.2 **Optineurin as a Regulator of TBK1/IFN-β Signaling**

Evidence from most primary cell models supports optineurin as a positive regulator of TBK1–IRF3–IFN-β signaling through interaction with TBK1 and recognition of K63-linked ubiquitin chains. Impaired TBK1 activation and IFN-β production following TLR stimulation were observed in cells from $Optn^{-/-}$ mice, as well as in various insufficiency models with disrupted ubiquitin-binding, including the ubiquitin-binding-deficient $Optn^{D477N}$ mice (corresponding to human E478G variant) and the truncated $Optn^{470T}$ mice lacking the UBR (Gleason et al., 2011; Munitic et al., 2013; Pourcelot et al., 2016; Slowicka et al., 2016; Markovinovic et al., 2018). Optineurin binds TBK1 in part directly via its N-terminal CC1 region, which interacts with the CC1 of TBK1 (Morton et al., 2008; Li et al., 2016), explaining why similar defects were also observed following deletion of the TBK1-binding region in the $Optn^{\Delta 157}$ model (Meena et al., 2016). Upon inflammatory stimulation (see Section 1.7.3 for TBK1 pathway details), TRAF3 catalyzes K63-linked polyubiquitination of TBK1, and optineurin engages these K63-polyubiquitinated TBK1 molecules via its C-terminal UBAN/ZF region (Gleason et al., 2011; Meena et al., 2016; Pourcelot et al., 2016). This bivalent interaction—constitutive binding via

CC1 and inducible binding via UBAN/ZF—increases local TBK1 concentration in signalosomes and facilitates TBK1 dimerization and trans-autophosphorylation at Ser172, the critical activating event for TBK1 catalytic activity (Helgason et al., 2013; Li et al., 2016). Recent mechanistic work in HEK293T-based reconstitution systems further suggested that ANKIB1-mediated K11-linked ubiquitination promotes recruitment of optineurin-containing signalosomes required for optimal TBK1 activation downstream of TLR3, TLR4, and cGAS–STING signaling (Betrancourt et al., 2026). In this study, optineurin itself was also ubiquitinated, predominantly with K63-linked ubiquitin chains and to a lesser extent K11-linked chains, suggesting that optineurin functions both as a reader of polyubiquitin signals and as a polyubiquitinated partner in TBK1 signalosomes. Activated TBK1 phosphorylates IRF3, and IRF7 during the later amplification phase, promoting their nuclear translocation and induction of IFN-β transcription (Lin et al., 1999; Sharma et al., 2003). In turn, TBK1 phosphorylates optineurin at Ser177 (adjacent to the LIR), enhancing LC3 binding affinity ~10-fold and might promote optineurin binding to ubiquitinated mitochondria and supporting mitophagy (Wild et al., 2011; Richter et al., 2016). However, it remains unclear whether Ser177 phosphorylation directly regulates optineurin function in PRR-driven TBK1/IRF3 pathway.

Notably, several studies using overexpression systems, transformed cell lines, and selected human cell models have instead suggested inhibitory roles for optineurin in TBK1 signaling. Optineurin overexpression suppressed Sendai virus- and dsRNA-induced IFN-β production and IRF3 activation, whereas siRNA-mediated optineurin depletion enhanced antiviral signaling and reduced viral replication (Mankouri et al., 2010). Similarly, HEK293 reporter assays demonstrated that overexpression of full-length optineurin suppressed poly(I:C)-induced IRF3 reporter expression, whereas ubiquitin-binding-deficient mutants failed to do so (Munitic et al., 2013). More recent studies in retinal pigment epithelium cells, patient-derived fibroblasts carrying E478G or Q398X OPTN mutations, and HEK293T-/MEF-based STING signaling systems likewise reported enhanced TBK1/IRF3 activation following optineurin disruption or loss (O'Loughlin et al., 2020; Fukushi et al., 2023; Kaveti et al., 2026). These findings contrast with the majority of primary myeloid-cell studies and likely reflect differences in stimuli (viral vs. TLR/STING), cell type, expression systems, and timing or magnitude of signaling responses.

1.8.3 Optineurin Deficiency in ALS: a Translational Perspective

The fact that both *OPTN* and *TBK1* mutations have been found in ALS and FTD patients underscores the importance of the TBK1-optineurin axis in disease pathogenesis (Maruyama et al., 2010; Freischmidt et al., 2015; Cirulli et al., 2015). ALS-associated *OPTN* mutations with confirmed pathogenicity (E478G and Q398X) impair both ubiquitin recognition and/or self-oligomerization, functions essential for TBK1 scaffolding, selective autophagy, and vesicular trafficking (Markovinovic et al., 2017). *TBK1* loss-of-function mutations similarly reduce IRF3 phosphorylation and optineurin binding, whereas the ALS-associated TBK1 p.E696K variant selectively abolishes optineurin binding while preserving kinase activity and interaction with other known TBK1 partners, strongly supporting the importance of the TBK1–OPTN interaction itself in ALS pathogenesis (de Majo et al., 2018; Brenner et al., 2024).

Based on findings from mouse models, optineurin deficiency impairs TBK1 activation and IFN-β production, disrupts selective autophagy and mitophagy, and enhances necroptosis under specific conditions (Gleason et al., 2011; Munitic et al., 2013; Korac et al., 2013; Lazarou et al., 2015; Ito et al., 2016). In parallel, context-dependent dysregulation of NF-κB may occur under chronic or necroptotic signaling conditions, where loss of optineurin's inhibitory checkpoint could sustain pro-inflammatory cytokine production (Obaid et al., 2015; Nakazawa et al., 2016). Together, these findings suggest that optineurin insufficiency may disturb the balance between inflammatory signaling, autophagic clearance, and proteostasis, particularly in the context of aging-associated inflammaging and declining autophagic capacity.

Given the emerging contribution of peripheral innate immune dysfunction to ALS pathogenesis, these mechanisms are of particular interest in human myeloid cells. However, they have not been tested in human primary immune cells, particularly professional antigen-presenting cells such as dendritic cells and macrophages that shape systemic immunity and interface with the CNS. This thesis addresses these critical gaps by establishing optineurin-deficient human monocyte-derived dendritic cells and macrophages and systematically characterizing their functional consequences.

2. THESIS AIMS AND HYPHOTESES

Thesis Aims and Hypotheses

While optineurin's molecular functions have been extensively characterized in murine models, its role in human primary immune cells remains poorly understood. Optineurin-deficient mice ($Optn^{-/-}$, $Optn^{470T}$) exhibit diminished TBK1 activation and reduced IFN-β production in primary macrophages and dendritic cells (Gleason et al., 2011; Munitic et al., 2013; Slowicka et al., 2016). However, these mice do not develop spontaneous motor neuron degeneration or ALS-like symptoms (Gleason et al., 2011; Munitic et al., 2013; Slowicka 2016; Ito et al., 2016; Mohovic et al., 2023), contrasting with human *OPTN* mutations that are causally linked to ALS. Mouse and human immune systems differ substantially in TLR expression patterns, cytokine profiles, and inflammatory responses as human monocytes and macrophages express higher TLR4 levels and produce different cytokine kinetics than mouse cells (Mestas & Hughes, 2004). Moreover, human and mouse optineurin are not fully conserved, and regulatory mechanisms may differ between species.

The overarching goal of this thesis is to investigate how optineurin deficiency impacts the maturation and functional abilities of human DCs and macrophages, with a focus on their roles in inflammatory signaling, cytokine production, phagocytosis, and antigen processing and presentation. By establishing human primary cell models of silenced optineurin, this work aims to bridge the gap between mouse model insights and human disease mechanisms, providing a foundation for understanding optineurin's role in peripheral immune dysfunction in ALS.

Human monocyte-derived dendritic cells and macrophages represent relevant translational models for these studies as increasing evidence implicates peripheral innate immune dysfunction in pathogenesis of neurodegeneration.

Aim 1: Characterize optineurin expression during human myeloid cell differentiation. We aimed to evaluate the expression pattern of optineurin in human peripheral blood-isolated monocytes, as well as in monocyte-derived DCs and macrophages at different stages of differentiation and activation. Given that *OPTN* expression is regulated by inflammatory factors (Schwamborn et al., 2000; Sudhakar et al., 2009; Sudhakar et al., 2009; Munitic et al., 2013), we hypothesized that distinct expression profiles may emerge across subpopulations, potentially reflecting functional specialization.

Aim 2: Evaluate the effect of optineurin deficiency on TBK1 pathway activation and type I interferon production. Based on insights from murine research demonstrating that optineurin's ubiquitin-binding region is required for optimal TBK1 scaffolding and activation (Gleason et al., 2011; Munitic et al., 2013; Pourcelot et al., 2016), we hypothesized that siRNA-mediated optineurin deficiency in human DCs and macrophages would lead to compromised activation of the TBK1 signaling pathway. This would be expected to result in decreased phosphorylation of TBK1, reduced production of type I interferons such as IFN-β.

Aim 3: Evaluate the effect of optineurin deficiency on NF-κB pathway activation and immunophenotype. Given optineurin's proposed role as a context-dependent negative regulator of NF-κB signaling through competition with NEMO for ubiquitinated RIPK1 binding and CYLD recruitment (Zhu et al., 2007; Nagabhushana et al., 2011), we hypothesized that optineurin deficiency may alter NF-κB pathway activation in human DCs and macrophages. Specifically, disruption of NF-κB regulation could affect the expression of co-stimulatory molecules (CD80, CD86, CD40), MHC class II molecules (HLA-DR) and proinflammatory cytokines (including but not limited to TNF-α and IL-6) on DCs.

Aim 4: Evaluate the effect of optineurin deficiency on phagocytosis and antigen presentation. Phagocytosis is a critical function of DCs and macrophages, enabling antigen uptake, processing, and presentation to initiate adaptive immune responses. Optineurin has been implicated in vesicular trafficking and immune signaling pathways that may influence phagosome maturation and antigen presentation (Sahlender et al., 2005; Tumbarello et al., 2012). We thus hypothesized that optineurin deficiency would impair phagocytic efficiency in human DCs and macrophages, leading to suboptimal antigen uptake, processing, and presentation.

3. MATERIALS AND METHODS

3.1 Material

3.1.1 Human sample processing and PBMC/monocyte/CD4+ T cell isolation

- PBS (1X), pH 7.4 (Gibco, Thermo Fisher Scientific, 10010023).
- Ficoll-Paque PREMIUM 1.073 (GE Healthcare, GE17-5446-52).
- CD14 MicroBeads, human (Miltenyi Biotec, 130-050-201).
- CD4+ T Cell Isolation Kit, human (Miltenyi Biotec, 130-096-533).
- MS Columns (Miltenyi Biotec, 130-042-201); LS Columns (Miltenyi Biotec, 130-042-401).
- StemPro Accutase (Gibco; A1110501).
- Trypan Blue (Gibco, Thermo Fisher Scientific, 15250061)
- Millicell disposable Neubauer haemocytometer (Merk, MDH-2N1-50PK).

3.1.2 Cell culture media, supplements, cytokines, and activators

3.1.2.1. Basal media and supplements

- RPMI 1640; Gibco (Thermo Fisher Scientific, 11875-093)
- FBS, heat-inactivated; Gibco (Thermo Fisher Scientific, 16000-044)
- Penicillin–Streptomycin (100 U/mL / 100 μg/mL); Gibco (Thermo Fisher Scientific, 15070-063)
- L-glutamine (200 mM stock; used at 2 mM); Gibco (Thermo Fisher Scientific, 25030-081)

61522561188

3.1.2.2. Dendritic cell (moDC) differentiation

- moDC Differentiation Medium (Miltenyi Biotec, 130-094-812).
- Recombinant human TNF-α (Thermo Fisher, 300-01A; 20UG)
- Recombinant human IFN-γ (Thermo Fisher, 300-02; 20UG)

3.1.2.3. Macrophage differentiation and activation

- Recombinant human M-CSF (Thermo Fisher, 300-25; 50 µg).
- LPS (E. coli O111:B4; Thermo Fisher, 00-4976-93).
- Recombinant human IL-4 (Thermo Fisher, 200-4; 20 µg).

3.1.2.5. DC/T-cell antigen reagents and CD40 blocking

- Anti-human CD40 blocking antibody, clone G28.5 (BioLegend, 334302)
- Cytomegalovirus, Epstein-Barr Virus, Influenza virus and Clostridium tetani peptide pool (CEFT): 1 µg/mL (GenScript, RP30950).
- Tetanus toxoid (TT): 15 µg/mL (GenScript, RP19980).

3.1.3. Transfection and gene silencing

- ON-TARGETplus Human OPTN (10133) siRNA SMARTpool (Horizon Discovery/Dharmacon; L-016269-00-0020).
- ON-TARGETplus Non-targeting Control siRNA (Horizon Discovery/Dharmacon, D-001810-01-20).
- HiPerFect Transfection Reagent (Qiagen, 301705; 1 mL).

3.1.4. Protein extraction, quantification, and Western blot reagents

3.1.4.1. Lysis and quantification

- RIPA Buffer, 250 mL (Thermo Fisher Scientific, 89901)
- Halt Protease and Phosphatase Inhibitor Cocktail (100X) (Thermo Fisher Scientific, 78442)
- Pierce BCA Protein Assay Kit (Thermo Fisher Scientific, A55865)

3.1.4.2. SDS-PAGE and immunoblotting

- NuPAGE™ LDS Sample Buffer (4X) (Thermo Fisher, NP0007)
- NuPAGE Bis-Tris Mini Gels 4–12%, 12-well (Thermo Fisher, NP0322BOX)
- 10X Tris/Tricine/SDS running buffer (Bio-Rad, 1610744)
- NuPAGE™ MES SDS Running Buffer (20X) (ThermoFisher, NP000202)

- TBS with Tween™ (TBST), 20X Solution, Molecular Biology Grade, Ultrapure (ThermoFisher, J77500.K2)
- Blocker BSA (ThermoFisher, 37520)
- SuperBlock Blocking Buffer (ThermoFisher, 37535)
- iBlot Transfer stacks, nitrocellulose: (Thermo Fisher, IB23001)
- HRP-conjugated secondary antibodies anti-rabbit IgG-HRP (Jackson ImmunoResearch, 111-035-003)
- Chemiluminescent substrates:
  SuperSignal West Dura Extended Duration Substrate (Thermo Scientific, 34076)
  SuperSignal West Femto Maximum Sensitivity Substrate (Thermo Scientific, 34094)

3.1.4.3 ProteinSimple Wes and Jess capillary Western reagents

- Jess/Wes Separation Module, 12–230 kDa (ProteinSimple, SM-W004)
- Total Protein Detection Module (ProteinSimple, DM-TP01)
- Anti-Rabbit Detection Module (ProteinSimple, DM-001)

3.1.5. Primary antibodies for Western blot and ProteinSimple

Target	Supplier	Catalog	Dilution	Notes
Vinculin	Cell Signaling Technology	13901	1:50 Jess/Wes	Loading control; ~120 kDa
Phospho-TBK1 (Ser172)	Cell Signaling Technology	5483	1:50 Jess/Wes	~84–85 kDa
Phospho-p65 (Ser536)	Cell Signaling Technology	3033	1:50 Jess/Wes	~65–66 kDa
Phospho-IRF3 (Ser396)	Cell Signaling Technology	29047 or 4947	1:50 Jess/Wes	Not in ProteinSimple DB

Phospo-Stat1	Cell Signaling Technology	9167	1:50 Jess/Wes	~85 kDa
OPTN (C-term)	Cayman Chemical	100000	1:1000 WB	~66–74 kDa
OPTN (N-term)	Cayman Chemical	100002	1:1000 WB	~66–74 kDa
OPTN	ThermoFisher	711879	1:50 Jess/Wes	~66–74 kDa
TDP-43	Cell Signaling Technology	3448	1:50 Jess/Wes	~43–45 kDa

Table 2. Primary antibodies for Western blot and ProteinSimple

3.1.6. Flow cytometry reagents

- FACS flow buffer: 2% heat-inactivated FBS and 0.05% sodium azide in 1X PBS.
- CellTrace CFSE (ThermoFisher; C34570)

3.1.6.1. Antibodies and viability dyes

Marker	Fluorochrome	Supplier	Catalog	Dilution
CD14 (Panel 1)	BUV395	BD Biosciences	563561	1:40
CD14 (Panel 2)	PE	BD Biosciences	561707	1:100
CD80 (Panel 1)	BUV661	BD Biosciences	741647	1:40
CD80 (Panel 2)	FITC	BD Biosciences	560926	1:50
CD11c (Panel 1)	BUV805	BD Biosciences	742005	1:80

CD11c (Panel 2)	PerCP-Cy5.5	BD Biosciences	570297	1:50
CD86 (Panel 1)	BV711	BD Biosciences	563158	1:40
CD86 (Panel 2)	BUV395	BD Biosciences	740305	1:50
HLA-DR (Panel 1)	BV570	BioLegend	307637	1:160
HLA-DR (Panel 2)	BV510	BioLegend	307646	1:200
CD40 (Panel 1)	FITC	BioLegend	334305	1:40
CD40 (Panel 2)	BV605	BioLegend	334335	1:100
CD83 (Panel 1)	BV421	BioLegend	305323	1:80
CD83 (Panel 2)	PE-Cy7	BioLegend	305325	1:100
PD-L1 (CD274) (Panel 1)	APC	BD Biosciences	563741	1:80
PD-L1 (CD274) (Panel 2)	PE-CF594	BD Biosciences	568985	1:100
CD163 (Panel 1)	PE-CF594	BD Biosciences	562670	1:40
CD3 (Panel 3)	BV510	BD Biosciences	563109	1:50
CD4 (Panel 3)	Pacific Blue	BD Biosciences	558116	1:200

CD154 (Panel 3)	PE	BD Biosciences	561720	1:50
CD69 (Panel 3)	APC	BD Biosciences	560711	1:100
Live/Dead Blue	Amine-reactive	Thermo Fisher	L23105	1:1000

Table 3. Antibodies and viability dyes

- Fc block: Human TruStain FcX (BioLegend, 422302).
- Compensation beads: UltraComp eBeads (Invitrogen, 01-3333-42)

3.1.7. Phagocytosis and functional assay reagents

- pHrodo E. coli BioParticles (Thermo Fisher, P35366).
- Matrigel (Corning, 354234).

3.1.8. ELISA and multiplex immunoassays

- MSD/ELISA wash buffer: 0.05% Tween-20 in 1X PBS.
- MSD V-PLEX Proinflammatory Panel 1 Plus (human) (Meso Scale Diagnostics, K15049D-1).
- Abcam Human Interferon beta SimpleStep ELISA Kit (Abcam, ab278127).

3.1.9. Cells and biological materials

- Human monocytes: cryovials for each donor.
- PBMCs: Prepared as per Section 3.2.1 using Ficoll-Paque PREMIUM 1.073 (GE17-5446-52).
- moDCs/macrophages/microglia-like cells: Generated per Section 3.2.2.

3.1.10. Instruments and software

- Flow cytometers: BD LSRFortessa / BD FACSAria III/ BD FACS Symphony A5; BD FACSDiva software (Waters Corporation).
- Capillary Western: Jess or Wes (ProteinSimple); Compass for Simple Western software.
- Data analysis: FCS Express (Dotmatics – version 7), GraphPad Prism (Dotmatics – version 10), ImageJ (NIH).
- Plate quantification reader: EnVision Xcite (Revvity).
- MESO QuickPlex SQ 120MM (Meso Scale Discovery)

3.2 Methods

3.2.1. Human Sample Collection and Processing

3.2.1.1. Ethical Approval and Donor Consent

Experiments performed in the United States, including samples procured via Scientists.com and analyses at Johns Hopkins, were approved by the IRB and conducted in accordance with HIPAA. Written informed consent was obtained from donors where required under the applicable ethics approvals and procurement procedures. Experiments performed in Croatia were approved by the Ethics Committee of the Faculty of Biotechnology and Drug Development, University of Rijeka.

3.2.1.2. Isolation of Peripheral Blood Mononuclear Cells

Peripheral blood mononuclear cells (PBMC) were obtained from healthy volunteer buffy coats or fresh blood samples through density gradient centrifugation (50 mL). Blood samples were diluted 1:1 with sterile PBS before being carefully layered onto Ficoll-Paque PREMIUM 1.073 (GE Healthcare, 17-5446-52) at a 3:1 ratio of diluted blood to Ficoll. Centrifugation was performed at 400 × g for 30 min at room temperature with the brake off to maintain interface integrity. The mononuclear cell layer at the plasma-Ficoll interface was collected carefully, washed twice with PBS at 300 × g for 10 min, and resuspended in the appropriate culture medium. Cell viability was determined by Trypan Blue (Gibco, 15250061) exclusion, and cell concentration was determined using a Millicell disposable Neubauer haemocytometer (Merck, MDH-2N1-50PK).

3.2.1.3. Monocyte Purification

Monocytes were enriched from freshly isolated PBMCs by positive magnetic selection using anti-CD14 MicroBeads (Miltenyi Biotec, 130-050-201) according to the manufacturer's instructions. Labeled cells were passed through MS or LS Columns (Miltenyi Biotec) mounted on a magnetic separator, and CD14+ cells were collected for downstream assays. Monocyte purity was routinely assessed by flow cytometry using CD14 staining and typically exceeded 95% (see below; Fig. 6B).

3.2.2. Cell Culture Systems

3.2.2.1. Generation and Maturation of Monocyte-Derived Dendritic Cells

Purified monocytes were cultured at 0.5-1.0 × 10^6 cells/mL and differentiated into immature DC using the monocyte to DC (moDC) Differentiation Medium (Miltenyi Biotec, 130-094-812; containing GM-CSF and IL-4; hereafter referred to as complete medium) in T75 flasks under humidified conditions at 37°C and 5% CO_2. On day 3, fresh differentiation medium was added according to the manufacturer's recommendations. Immature moDCs were generated by day 5-7.

To induce maturation, immature DCs were stimulated for 24 h with LPS (Escherichia coli O111:B4) at 100 ng/mL or TNF-α at 50 ng/mL or IFN-γ at 25 ng/mL. Maturation status was confirmed by light microscopy and/or flow cytometric analysis of CD83, CD86, HLA-DR,

CD80, and CD40 expression relative to immature controls. For a subset of experiments, LPS was added for 4 h and then removed from the cell culture.

3.2.2.2. Development and Activation of Monocyte-Derived Macrophages

Isolated monocytes were cultured at 0.5-1.0 × 10^6 cells/mL in RPMI 1640 supplemented with 10% heat-inactivated FBS, 1% Penicillin-Streptomycin, 2 mM L-glutamine, and 50 ng/mL recombinant human M-CSF for 5-7 days at 37°C and 5% CO_2 *(complete media)*. Fresh cytokine-containing medium was added or replaced every 3 days. Differentiated macrophages (MØ) were identified by *light microscopy by* their adherent morphology and by expression of CD14, HLA-DR, CD80, CD83, CD86, CD40, PDL-1 and CD163, assessed by flow cytometry (*see below,* Fig. 12).
M1-like polarization/activation was elicited by 100 ng/mL LPS (Escherichia coli O111:B4; Thermo Fisher Scientific, 00-4976-93) for 24 h before experimentalanalysis (Fig. 12B), and M2-like polarization by IL-4 20 ng/mL (Thermo Fisher, 200-4) for 24 h before experimental analysis.

3.2.3. Gene Silencing Methodology

3.2.3.1. OPTN Knockdown via siRNA

OPTN expression was silenced using ON-TARGETplus Human OPTN (10133) siRNA SMARTpool (Horizon Discovery/Dharmacon, L-016269-00-0020). ON-TARGETplus Non-targeting Control siRNA (Horizon Discovery/Dharmacon, D-001810-01-20) was used as a negative control. All cultures and transfections were performed under antibiotic-free conditions during the transfection step to minimize toxicity. Fresh primary human CD14+ monocytes, isolated from PBMCs by CD14-positive magnetic selection, were first differentiated into macrophages or moDCs for 5-7 days, as described above.
siRNA stocks were prepared according to the manufacturer's instructions. Transfections were performed at a final siRNA concentration of 200 nM using a 20 µM working stock. This corresponded to 15 µL siRNA of working stock per well in 6-well plates or 3.75 µL siRNA per well in 24-well plates. siRNA-lipid complexes were prepared in warm serum-free RPMI 1640 and incubated for 15-20 min at room temperature before addition to cells.
For DCs, cells were resuspended in warm complete medium at 1.5 × 10^6 cells in 1 mL per well for 6-well plates or 3 × 10^5 cells in 250 µL per well for 24-well plates. For each 6-well, the transfection mixture contained 470 µL serum-free RPMI, 15 µL HiPerFect, and 15 µL of

20 µM siRNA (total complex volume 500 µL). For each 24-well, the mixture contained 117.5 µL serum-free RPMI, 3.75 µL HiPerFect, and 3.75 µL siRNA (total complex volume 125 µL). Complexes were first added to the well, followed by the cell suspension without vigorous pipetting. Plates were gently swirled and incubated for 4 h at 37°C and 5% CO_2. Transfection was then stopped by adding complete medium.

For macrophages, transfection was performed on days 5-7 of differentiation. Wells were gently washed twice with warm medium to remove non-adherent cells, and fresh medium was added (1 mL/well in 6-well plates or 250 µL/well in 24-well plates). For each 6-well, the transfection mixture contained 440 µL serum-free RPMI, 45 µL HiPerFect, and 15 µL of 20 µM siRNA (final volume 500 µL). For each 24-well, the mixture contained 110.25 µL serum-free RPMI, 11 µL HiPerFect, and 3.75 µL siRNA (final volume 125 µL). After 15-20 min incubation at room temperature, complexes were added dropwise to adherent cells. After 6 h, complete RPMI containing M-CSF was added at 2.0 mL/well (6-well) or 0.5 mL/well (24-well) to a final concentration of 10 ng/mL, and cells were allowed to recover overnight.

OPTN knockdown was assessed 48-72 h post-transfection by Western blot and ProteinSimple capillary Western. Functional experiments were performed only after confirming ≥60% silencing relative to the non-targeting siRNA control.

3.2.4. T Cell Activation Protocols

3.2.4.1. CD4+ T Cell Purification

CD4+ T cell isolation from PBMCs was performed by CD4+ T Cell Isolation Kit (Miltenyi Biotec, Germany) according to manufacturer ‘s guidelines. PBMCs were first incubated with biotinylated antibody cocktail, followed by anti-biotin beads, which allowed CD4+ T cell isolation upon LS/MS column separation on magnetic apparatus. Flow cytometric verification routinely confirmed CD4+ T cell purity exceeding 95%.

3.2.4.2. Antigen-Specific CD4+ T Cell Activation Using CD154 as Readout

CD4+ T cells were co-cultured with autologous DCs serving as antigen-presenting cells in 96-well plates at a DC:T-cell 1:5 ratio (2 × 10^5 CD4+ T cells/well per 96-well plate). To prevent CD154 internalization, cells were preincubated with anti-human CD40 blocking antibody (clone G28.5) at 1 µg/mL for 15 min. Cells were then stimulated for 18 h with a peptide poll combination of Cytomegalovirus, Epstein-Barr Virus, Influenza virus and Clostridium tetani (CEFT - 1 µg/mL) or Tetanus Toxoid (TT - 15 µg/mL).

After stimulation, cells were washed with PBS and stained with Live/Dead Fixable Blue Dead Cell Stain Kit together with the following antibodies: BV510-conjugated anti-CD3, Pacific Blue-conjugated anti-CD4, PE-conjugated anti-CD154 (also known as CD40L), APC-conjugated anti-CD69.

3.2.5. Flow Cytometric Analysis

3.2.5.1. Cell Preparation and Surface Marker Staining

DC and macrophages were harvested from culture plates by gentle pipetting and scraping. Cells were then washed once with PBS and transferred to 96-well V-bottom plate for staining and centrifuguged at 300-400 g for 3 minutes at room temperature before supernatant aspiration. Cell viability was assessed using LIVE/DEAD Blue Cell Stain Kit according to the manufacturer's instructions. Cells were incubated with Human TruStain FcX Fc blocking reagent diluted in FACS buffer for 10 min at 4°C, followed by staining with fluorochrome-conjugated antibodies against surface markers for 20 min at room temperature protected from light. Antibody concentrations were determined by prior titration experiments. Cells were then washed twice with FACS buffer by centrifugation at 300–400 × g for 5 min. Compensation was performed with single-stained cells and/or compensation beads (BioLegend UltraComp Beads) for each panel fluorochrome.

3.2.6. Phagocytosis Assay

Phagocytic capacity of DCs and macrophages was assessed using pHrodo Red *E. coli* BioParticles™ Conjugate (Thermo Fisher, P35366). Cells were harvested and plated at 10,000 cells per well in 96-well plates. pHrodo E. coli BioParticles were added at 10 μg per sample in a final volume of 100 μL. Cells were incubated at 37°C for either 30 minutes or 3 hours to allow phagocytosis. Parallel samples incubated at 4°C served as negative controls to distinguish active phagocytosis from passive particle association, as pHrodo fluorescence requires both internalization and phagolysosomal acidification, which are energy-dependent processes inhibited at 4°C. Following incubation, cells were acquired directly by flow cytometry without washing. Phagocytosis was quantified as the percentage of pHrodo-positive cells using FCS Express software, with the 4°C condition used to set the fluorescence threshold for positive events.

3.2.7. Western Blot Methodology

3.2.7.1. Protein Extraction from Cultured Cells, Quantification and Separation via SDS-PAGE

At the end of each treatment, cells were washed twice with ice-cold PBS and lysed in RIPA Buffer (Thermo Fisher Scientific, 89901) supplemented with 1X Halt Protease and Phosphatase Inhibitor Cocktail (Thermo Fisher Scientific, 78442). For adherent cells, lysis was performed directly in the culture vessel using 80-150 µL buffer depending on well size. Suspension cells such as DCs were first collected by centrifugation at 300 × g for 3 min, washed twice with ice-cold PBS, and lysed in 70-110 µL of supplemented RIPA buffer.

Lysates were incubated on ice for 15 min with periodic vortexing, then clarified by centrifugation at 14,000 × g for 15 min at 4°C. Supernatants were transferred to fresh tubes, and protein concentration was determined using the Pierce BCA Protein Assay Kit (Thermo Fisher Scientific, A55865) according to the manufacturer's instructions. Protein concentrations were calculated from the BSA standard curve using 4-parameter logistic (4PL) fitting in GraphPad Prism. Protein samples underwent normalization to equal concentrations via RIPA buffer dilution, mixing with 4X Laemmli sample buffer for standard Westen Blot, and 95°C denaturation for 5 minutes. Samples underwent ice cooling before immediate use or -20°C storage until analysis. Proteins were separated by SDS-PAGE using NuPAGE™ Bis-Tris Mini Protein Gels (4-12%, 1.0 mm; Thermo Fisher Scientific) in a compatible mini gel electrophoresis apparatus according to the manufacturer's instructions.

3.2.7.2. Membrane Transfer Process and Immunodetection Procedure

Proteins separated by SDS-PAGE were transferred to a PVDF membrane using the iBlot Dry Blotting System with the 7-min transfer program, according to the manufacturer's instructions. Briefly, following electrophoresis, the gel was carefully equilibrated and assembled with the appropriate iBlot transfer stack and membrane, ensuring removal of air bubbles between the gel and membrane. The transfer sandwich was placed in the iBlot device and run using the standard 7-min transfer setting. After transfer, membranes were briefly rinsed in TBS or PBS and either processed immediately for blocking and antibody incubation.

Post-transfer, membranes received brief TBS-T rinsing before blocking solution incubation 5% (w/v) BSA in TBS-T for 1 hour at RT with gentle agitation. Membranes were incubated

overnight at 4°C with primary antibodies diluted in antibody probing solution (5% BSA in TBS-T for phospho-proteins; 5% milk in TBS-T for total proteins) with gentle agitation. Subsequently, membranes were washed three 10-minute TBS-T. For phosphorylated protein detection, additional 1-hour RT blocking with 5% BSA in TBS-T was performed before secondary antibody incubation. Membranes then were incubated with HRP-conjugated secondary antibodies anti-rabbit IgG-HRP (1:5000-1:10000) diluted in blocking solution for 1 hour at RT with gentle agitation. After secondary antibody incubation, membranes were washed agin three times for 10-minute in TBS-T. Proteins were detected by ECL Western Blotting DURA Detection Reagent (Peroxidase/Luminol substrate; Roche, Switzerland) or, for low-abundance or phosphorylated protein, by SuperSignal West Femto Maximum Sensitivity Substrate (Thermo Scientific, USA). ChemiDoc™ MP Imaging System (Bio-Rad, USA) captured chemiluminescent signals. Multiple exposure time collection ensured signals remained within linear detection range.

ImageJ software (National Institutes of Health, USA) was used to quantify band intensities. Each lane yielded background-subtracted integrated density values. Total protein values underwent normalization to loading control proteins (β-actin). Normalized values expressed as fold change relative to control.

3.2.8. Automated Capillary Western Blot Analysis Using Protein Simple Technology

As an alternative approach to traditional Western blotting, protein quantification was also performed using the automated capillary-based immunoassay system (Jess or Wes, Protein Simple, Bio-Techne, USA). This technology enables precise protein quantification through automated capillary electrophoresis followed by chemiluminescence immunodetection.

Cell lysates prepared as described in section 3.2.5.1.1 were diluted to 0.5-0.85 mg/mL in 0.1X sample buffer provided in the kit. Samples were mixed with fluorescent molecular weight markers and heated at 95°C for 5 minutes for denaturation. The automated capillary system separated proteins by size through capillary electrophoresis, immobilized them to the capillary wall using proprietary photoactivated capture chemistry, performed immunoprobing with primary antibodies followed by HRP-conjugated anti-rabbit secondary detection antibody. Chemiluminescence was captured by a CCD camera, with signal intensity quantified as peak area or peak height.

Data analysis was performed using Compass for Simple Western software (version 6, Protein Simple, Bio-Techne, USA). Protein expression levels were calculated as the ratio of target protein signal to vinculin housekeeping gene protein signal, and results were expressed as fold change relative to control condition. The system's automated nature provides enhanced reproducibility with coefficients of variation typically <10% for replicate samples, and the digital detection eliminates issues associated with film saturation in traditional Western blotting.

3.2.9. Multiplex Cytokine Quantification

3.2.9.1. Sample Collection and Preparation

Cell culture supernatants were collected at specified timepoints followed by centrifugation at 300 g for 5 minutes for removing cellular debris and transferred to fresh tubes. Supernatants underwent immediate aliquoting with -80°C storage until analysis to minimize freeze-thaw cycle and prevented protein degradation.

3.2.9.2. V-PLEX Multiplex Immunoassays

Cytokine and chemokine levels in supernatants were measured using the MSD V-PLEX Proinflammatory Panel 1 Human Kit (Meso Scale Diagnostics, USA) according to the manufacturer's instructions, detecting IL-1β, IL-6, IL-10, IL-12p70, and TNF-α.Briefly, capture antibody pre-coated MSD 96-well plates underwent blocking with Diluent 2 and kit-provided blocking solution for 1 hour at RT with 700 rpm shaking. Post-blocking, 25 µL of calibrator standards (kit-provided) or samples were loaded in wells in duplicates. Sample dilution 1:2, 1:3 and 1:10 were tested to ensured that values were within assay dynamic range. Sealed plates underwent 2-hour RT incubation with 700 rpm shaking.

Post-incubation, plates were washes three times with PBS containing 0.05% Tween-20 (MSD Wash Buffer) using automated plate washer or manual washing. SULFO-TAG-conjugated detection antibody addition, 25 µL per well, preceded 2-hour RT incubation with 700 rpm shaking. Plates underwent three washes before 150 µL MSD Read Buffer T addition per well.

Immediate plate reading on MESO QuickPlex SQ 120MM (Meso Scale Diagnostics, USA) measured electrochemiluminescence signals. Calibration curves using 4-parameter logistic (4-PL) curve fitting in MSD Discovery Workbench software calculated analyte concentrations. Each analyte's lower limit of detection (LLOD) and lower limit of

quantification (LLOQ) underwent determination. LLOD-below samples received unassigned value, while upper limit-exceeding samples underwent dilution.

3.2.9.3. SimpleStep ELISA for IFN-β detection

IFN-β levels in cell culture supernatants were quantified using the Human Interferon Beta in vitro SimpleStep ELISA Kit (Abcam, ab278127) according to the manufacturer's instructions. Briefly, reagents, standards, and cell culture supernatant were prepared as recommended by the manufacturer. Then, 50 µL of standards or cell culture supernatant were added to the appropriate wells, followed by 50 µL of antibody cocktail. The plate was incubated for 1 hour at room temperature with 300 rpm shaking and then washed three times with 350 µL of 1X Wash Buffer PT to remove unbound material. Next, 100 µL of TMB Development Solution was added to each well and incubated for 10 minutes for color development. The reaction was stopped by adding 100 µL of Stop Solution, and absorbance was measured at 450 nm using a microplate reader. IFN-β concentrations in the cell culture supernatants were calculated from a standard curve generated using the kit standards. GraphPad Prism software with 4-PL curve fitting performed data analysis. Results are shown as pg/mL for supernatants.

3.2.10 Text Editing

ChatGPT (OpenAI; version 5) and Claude (Anthropic; version 4.5) were used for the purpose of language editing and assistance with text formulation. After using these tools, the content was reviewed, edited, and revised as needed.

3.2.11. Statistical Analysis

Minimum three independent biological replicates were performed in all experiments unless otherwise stated. Data are presented as mean ± SEM. GraphPad Prism software version 10 (GraphPad Software, USA) was used for graphical representation and statistical analyses. Statistical comparisons were performed using a paired Student's t-test for two-group comparison, one-way ANOVA for multiple comparisons, or two-way ANOVA with Tukey's post-hoc test for experiments involving two independent variables. A p value < 0.05 was considered statistically significant. Significance levels appear as: *$p < 0.05$; **$p < 0.01$; ***$p < 0.001$; ****$p < 0.0001$.

4. RESULTS

4.1. Establishment and validation of the human monocyte-derived dendritic cell model

4.1.1. Experimental strategy for investigating optineurin function in human dendritic cells

To investigate the role of optineurin in human dendritic cells, we designed an experimental workflow encompassing monocyte isolation, DC differentiation and maturation, optineurin silencing, and functional characterization (Fig. 5).

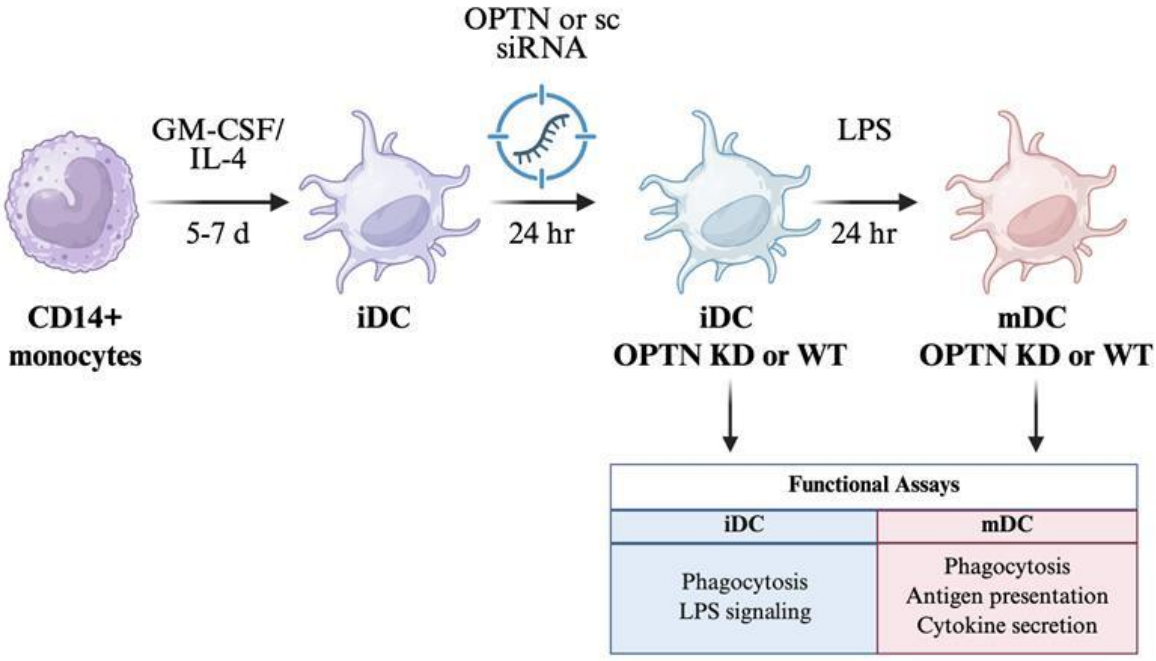

Figure 5. Workflow for optineurin silencing in human monocyte-derived dendritic cells.

Schematic overview of the experimental workflow used to assess the effects optineurin silencing during human monocyte-derived dendritic cell differentiation, maturation, and functional analyses. CD14+ human monocytes were positively selected from PBMCs, differentiated into immature dendritic cells (iDCs) using GM-CSF and IL-4, and analyzed either under immature conditions or following LPS-induced maturation into mature dendritic cells (mDCs). Cells were transfected with scrambled siRNA (sc siRNA) or optineurin siRNA (OPTN siRNA). Image was generated with Biorender.

CD14+ monocytes were isolated from healthy donor peripheral blood mononuclear cells (PBMCs) by magnetic bead positive selection, routinely achieving purity >95% as confirmed by flow cytometry (see below, Fig. 6 B). Isolated monocytes were subsequently cultured in the presence of GM-CSF and IL-4 for 5–7 days to generate immature DCs (iDCs). Maturation was induced by stimulation with LPS (100 ng/mL) for 24 hours to obtain mature DCs (mDCs). This differentiation protocol, described in detail in the Methods section,

recapitulates the physiological transition from circulating monocytes to functionally competent antigen-presenting cells and enables analysis of both immature and LPS-activated states.

4.1.2. Validation of dendritic cell differentiation and maturation by light microscopy and flow cytometry

To confirm successful differentiation at each stage, we performed morphological assessment by light microscopy and immunophenotyping by multicolor flow cytometry. Freshly isolated CD14+ monocytes displayed characteristic small, round, non-adherent morphology with high CD14 expression (Fig. 6A and B). Monocytes were also positive for CD11c, HLA-DR, and CD86, with lower but detectable expression of CD80 and CD83 in approximately 50% of cells. In contrast, CD40 and PD-L1 staining was similar to lymphocytes used as an internal biological control, indicating little or no expression (Fig. 6B). Upon culture with GM-CSF and IL-4 for 5–7 days, cells acquired the morphological features of iDC, including increased cell size, irregular shape, and the appearance of short cytoplasmic projections (Fig. 6A). Flow cytometric analysis confirmed that iDCs downregulated CD14 while acquiring DC phenotype, including increased expression of CD11c and HLA-DR, consistent with antigen-capturing capacity (Fig. 6C). At this stage, co-stimulatory molecules CD80, CD86, CD83 and CD40 remained at low to intermediate levels, confirming the immature state of the differentiated cells (Fig. 6C).

Following 24 hours of LPS stimulation, DCs underwent the characteristic morphological transition to mDC, displaying enlarged cell bodies with prominent dendritic processes extending from the cell surface (Fig. 6A). Flow cytometric analysis revealed the expected maturation-associated phenotypic changes characterized by marked upregulation of co-stimulatory molecules CD80, CD86, and CD40, the maturation marker CD83, the antigen presentation molecule HLA-DR, and the dendritic cell marker CD11c (Fig. 6C). Notably, the immune checkpoint molecule PD-L1 was substantially upregulated upon maturation, consistent with the known induction of counter-regulatory mechanisms during DC activation that serve to prevent excessive T cell stimulation (Brown et al., 2003; Selenko-Gebauer et al., 2003). Overall, these results demonstrated that our differentiation protocol reliably generated immunophenotypically validated immature and mature DCs from human peripheral blood

monocytes, establishing an experimental system for subsequent investigation of optineurin's role in human DC biology.

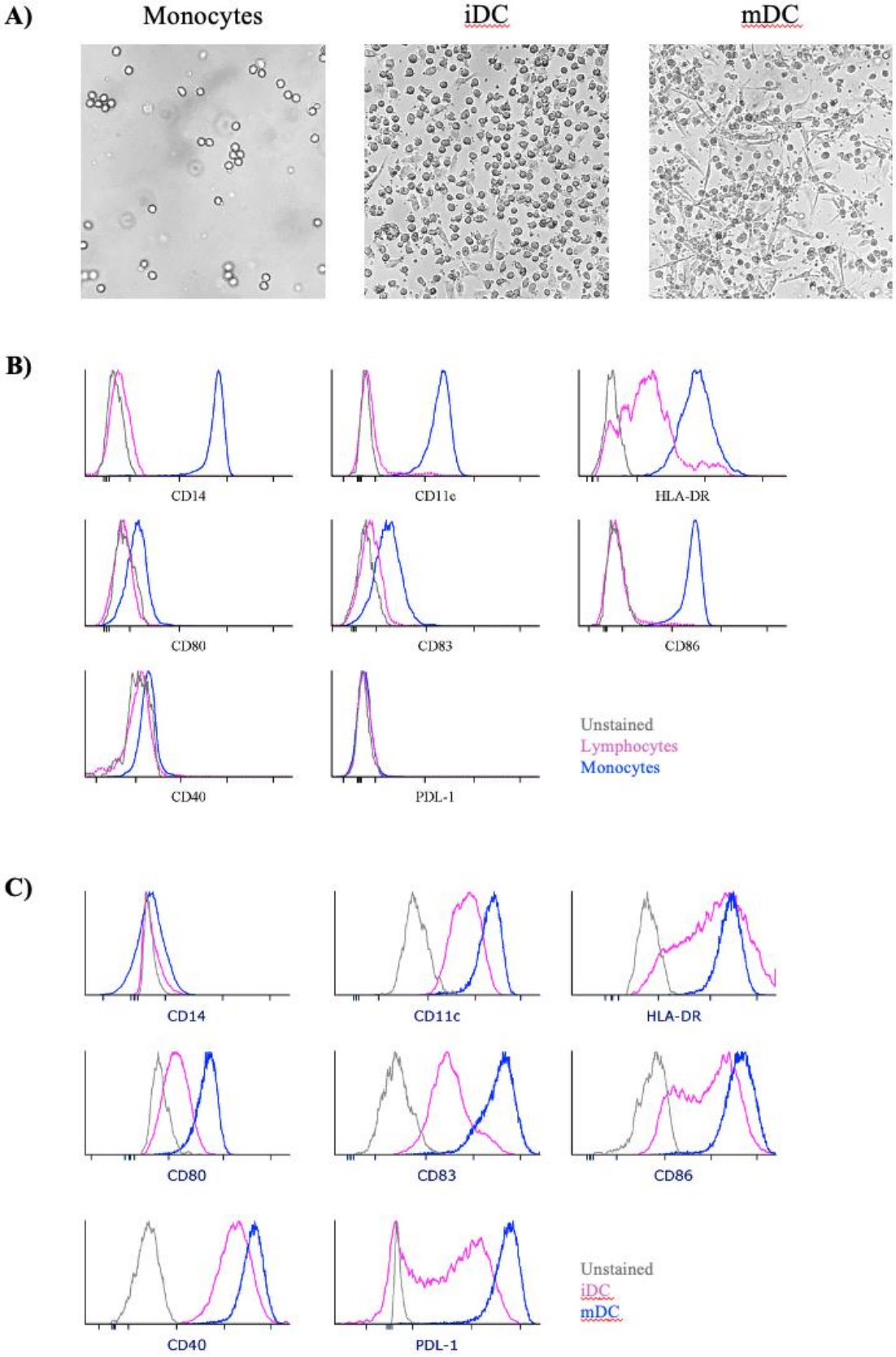

Figure 6. Validation of human monocyte-derived dendritic cell differentiation and maturation.

(A) Representative bright-field microscopy images showing morphological changes during differentiation: monocytes (left), iDCs (middle), and LPS-matured mDCs (right). (B) Representative flow cytometry histograms showing surface expression of CD14, CD11c, HLA-DR, CD80, CD83, CD86, CD40, and PD-L1 on monocytes (blue). Lymphocytes (gated by forward and side scatter) were used as biological internal control for the staining procedure (pink). (C) Representative flow cytometry of at least three independent experiments histograms showing surface expression of CD14, CD11c, HLA-DR, CD80, CD83, CD86, CD40, and PD-L1 on iDCs (pink) and mDCs (blue).

4.2. Optineurin expression is upregulated during dendritic cell differentiation and is preferentially induced by TLR4 stimulation

Given the established responsiveness of optineurin to inflammatory cues (Sudhakar et al., 2009; Sudhakar et al., 2013; Munitic et al., 2013), we next examined optineurin expression during DC differentiation and maturation in our experimental system. Freshly isolated CD14+ monocytes expressed negligible levels of optineurin protein, indicating that optineurin was not constitutively present at detectable levels in circulating human monocytes (Fig. 7 A). Upon differentiation into iDCs in the presence of GM-CSF and IL-4, optineurin expression became detectable but remained at low levels. However, by 24 hours of LPS stimulation, optineurin expression was markedly elevated, reaching approximately a 3-fold increase relative to iDCs (Fig. 7A; see Fig. 8A for quantification).

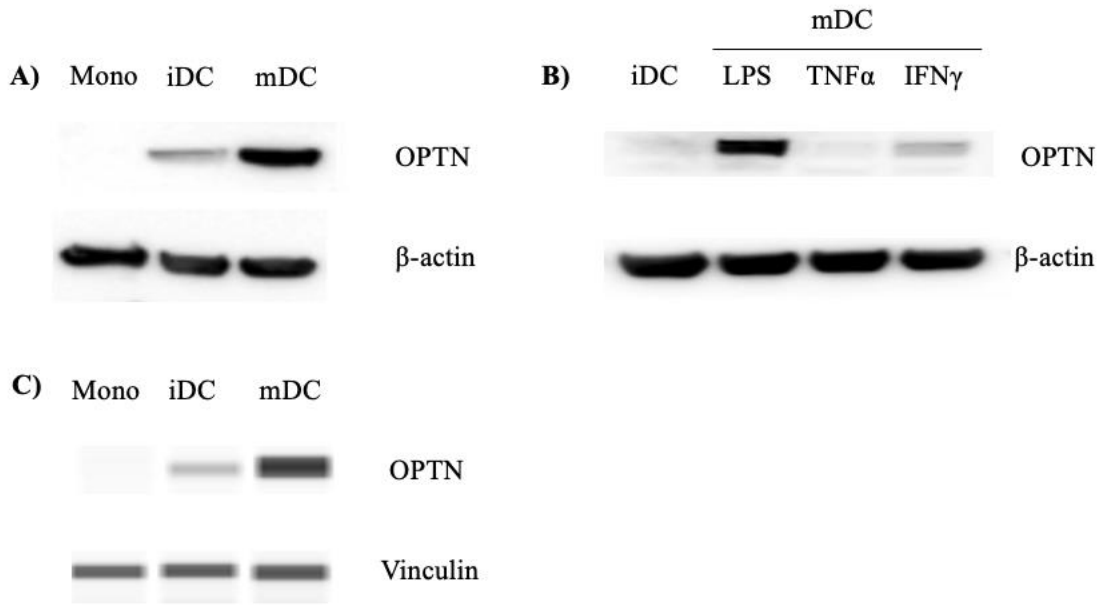

Figure 7. LPS induces optineurin expression during dendritic cell differentiation and maturation.

(A) Representative Western blot of OPTN in monocytes (Mono), immature dendritic cells (iDCs), and LPS-matured dendritic cells 24 upon stimulation (mDCs); β-actin was used as a loading control. (B) Representative Western blot of OPTN in iDCs and mDCs stimulated for 24 h with LPS, TNF-α, or IFN-γ. (C) Representative automated capillary Western immunoassay confirming OPTN upregulation from Mono to iDCs and mDCs, with vinculin as loading control.

Given that DC maturation can be triggered by diverse stimuli engaging distinct receptor systems and signaling cascades, we next sought to determine whether optineurin upregulation was specific to LPS-mediated TLR4 signaling or could be similarly induced by other physiologically relevant maturation stimuli. To address this question, iDCs were stimulated for 24 hours with LPS (100 ng/mL), TNF-α (10 ng/mL), or IFN-γ (50 ng/mL), and optineurin protein levels were measured by Western blot (Fig. 7 B). LPS was by far the strongest inducer of optineurin expression among the stimuli tested. In marked contrast, TNF-α stimulation did not upregulate optineurin above the baseline levels observed in iDCs, despite TNF-α being a potent activator of NF-κB signaling and a well-established DC maturation agent. IFN-γ produced only a modest increase of approximately 20% over iDC baseline, which was substantially lower than the robust LPS-driven induction (Fig. 7A and B). This stimulus-specific pattern of induction suggests that the full complement of signaling pathways activated downstream of TLR4, including both the NF-κB cascade and the TBK1/IRF3/IFN-β axis, may cooperate to maximally upregulate optineurin expression during DC maturation, whereas activation of NF-κB alone (as occurs with TNF-α) or IFN-γ receptor signaling in isolation is insufficient.

Finally, optineurin protein levels were assessed by automated capillary Western immunoassay (ProteinSimple Wes and Jess) and compared with standard Western blotting. Vinculin was used as the housekeeping protein for normalization and as a loading control in the Jess system. Capillary electrophoresis reduces the variability associated with gel-to-membrane transfer and the manual handling steps required in traditional Western blotting. In combination with chemiluminescent detection, it can provide a linear dynamic range of up to 6 logs, compared with approximately 3 logs for conventional Western blot. Both methods yielded comparable results for optineurin quantification, confirming that capillary electrophoresis provides sensitivity and accuracy equivalent to those of conventional Western blotting. It was therefore adopted for most downstream protein analyses in this thesis.

Overall, the progressive increase in optineurin expression from monocytes through iDCs to LPS-matured mDCs suggests that optineurin may play an increasingly important functional role as DCs acquire full immunostimulatory capacity. The strong and time-dependent induction of optineurin specifically upon TLR4 engagement positions it as a potential regulator of mature DC function in innate immune responses.

4.3. LPS-induced optineurin expression is delayed and remains sustained after transient stimulation

To define the kinetics of optineurin induction during dendritic cell maturation, iDCs were stimulated with LPS and protein expression was assessed at different time points. As shown in Fig. 8A, unstimulated iDCs (0 h) expressed low basal levels of optineurin and after 8 h of LPS stimulation, optineurin levels showed only a modest increase. In contrast, in mDC after 24 h of stimulation, optineurin expression was strongly elevated, reaching an approximately 3-fold induction relative to baseline iDC. These data indicated that LPS-induced optineurin upregulation was not an immediate early response to LPS stimulation but required more than 8 h to reach substantial levels, with strong induction observed by 24 h.

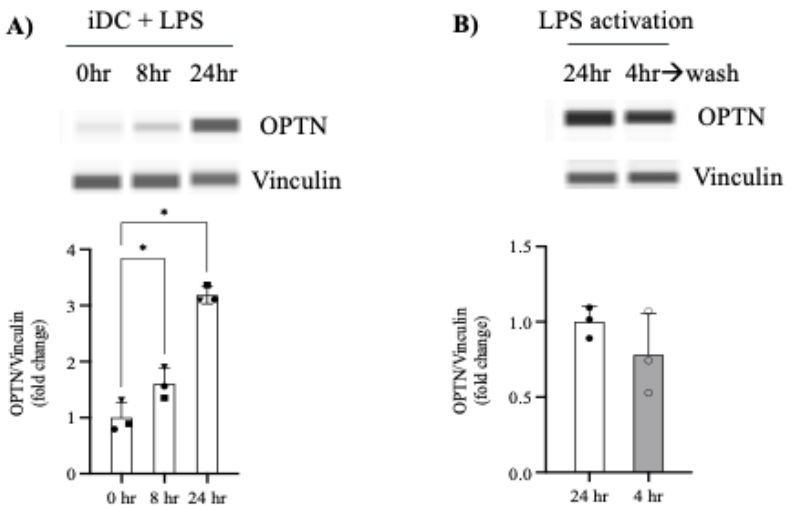

Figure 8. Optineurin induction by LPS was delayed and did not require continuous stimulation.

(A) Representative capillary Western immunoassay and quantification of OPTN expression after 0 h, 8 h, and 24 h of LPS stimulation. Basal OPTN expression was low in unstimulated iDCs, increased modestly at 8 h, and reached approximately 3-fold induction at 24 h. Vinculin was used as the loading control, and OPTN levels were normalized to vinculin. Statistical test: repeated measures one-way ANOVA. (B) Representative capillary

Western immunoassay and quantification of OPTN expression in cells stimulated either continuously with LPS for 24 h or with LPS for 4 h followed by washout and further incubation until 24 h. Data represent three independent donors. Statistical test: paired Student's t-test or multi comparison one-way ANOVA. * $p < 0.05$, ** $p < 0.01$, *** $p < 0.001$.

This delayed pattern suggested that optineurin accumulation during DC maturation was a progressive process that depended on continued signaling and/or transcriptional amplification over time. This is consistent with previous reports showing that the optineurin promoter contains NF-κB- and interferon-responsive elements, which can mediate inducible transcription in response to inflammatory stimuli (Schwamborn et al., 2000; Sudhakar et al., 2009; Sudhakar et al., 2009; Munitic et al., 2013). The requirement for prolonged stimulation further supports the idea that secondary mediators, such as autocrine IFN-β generated downstream of TLR4-TBK1 signaling, may contribute to the full magnitude of optineurin induction. To determine whether continuous LPS exposure was required throughout the entire stimulation period, iDCs were either stimulated with LPS for 24 h continuously or exposed to LPS for 4 h followed by washing and further incubation in LPS-free medium until the 24 h endpoint. Transient 4 h exposure to LPS resulted in a slight reduction in optineurin expression compared with continuous 24 h stimulation, but expression remained largely sustained (Fig. 8B). These findings demonstrate that optineurin induction is a delayed process requiring more than 8 hours for robust expression, but not persistent extracellular LPS presence, supporting a model in which early TLR4 engagement initiates a self-sustaining signaling program, potentially reinforced by secondary autocrine mediators such as IFN-β, that drives progressive optineurin accumulation even after stimulus removal.

4.4. siRNA-mediated reduction of optineurin in human monocyte-derived dendritic cells

Having established that optineurin is strongly upregulated upon LPS-induced DC maturation, we next aimed to silence optineurin expression to investigate its functional role in human DCs, given that several confirmed pathogenic ALS-linked OPTN variants are thought to act through loss-of-function mechanisms. Optineurin knockdown was achieved using ON-TARGETplus SMARTpool siRNA directed against human OPTN (OPTN siRNA), delivered to iDCs via HiPerFect transfection reagent, as described in the Methods section. Non-targeting scrambled siRNA (sc siRNA) served as control. Transfection was performed on

iDCs at days 5–7 of differentiation, and 24 hours post-transfection, cells were stimulated with LPS (100 ng/mL) to induce maturation. Knockdown efficiency was assessed by ProteinSimple Wes or Jess at multiple time points following LPS stimulation.

In scrambled siRNA-transfected cells, optineurin expression was low in unstimulated iDCs and increased slightly after 8 h of LPS stimulation (Fig. 9A), consistent with the delayed kinetics of optineurin induction described in section 4.3. By 24 h of LPS stimulation, optineurin protein levels increased markedly. In contrast, in OPTN siRNA-transfected cells, optineurin expression was modestly reduced at baseline, which corresponded to a total of 24 h of siRNA-mediated silencing, and remained substantially suppressed after both 8 h and 24 h of LPS stimulation, corresponding to a total of 32 h and 48 h of silencing, respectively. Densitometric analysis showed that OPTN knockdown efficiency was maintained throughout the time course, with an approximately 60-70% reduction in protein levels compared with scrambled control cells.

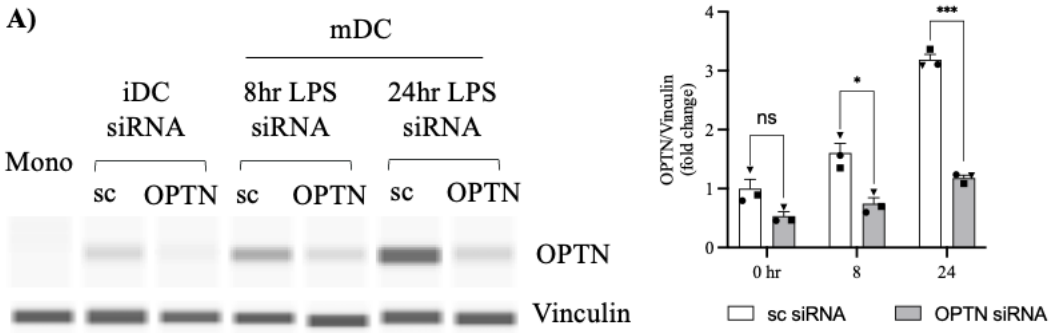

Figure 9. siRNA-mediated knockdown suppressed optineurin expression in dendritic cells.

(A) Representative automated capillary Western immunoassay and quantification of OPTN protein expression in monocytes (Mono) and in iDCs transfected with scrambled control siRNA (sc) or OPTN siRNA (OPTN), either left unstimulated or stimulated with LPS for 8 h or 24 h (mDC). Vinculin was used as a loading control, and OPTN levels were normalized to vinculin. Quantified data are shown as fold change relative to the indicated control; three independent donors. Statistics: multiple comparison two-way ANOVA; ns, not significant; * $p < 0.05$, ** $p < 0.01$, *** $p < 0.001$.

Overall, we established a reproducible model of markedly reduced optineurin expression in human monocyte-derived DCs. This system was used in subsequent experiments to examine

the effect of optineurin silencing on DC maturation, inflammatory signaling, and functional immune responses.

4.5. Optineurin silencing did not alter dendritic cell immunophenotype during differentiation or LPS-induced maturation

To determine whether optineurin contributes to DC differentiation and maturation, we performed comprehensive immunophenotyping by multicolor flow cytometry. iDCs transfected with either scrambled (scRNA) or OPTN-targeting siRNA were assessed for surface marker expression both in the immature state and following 24 hours of LPS stimulation. The panel included markers of monocyte lineage (CD14), DC identity (CD11c), co-stimulatory molecules (CD80, CD86, CD40), maturation markers (CD83), antigen presentation capacity (HLA-DR), and immune checkpoint molecules (PD-L1).

First, we compared the immunophenotype of iDCs transfected with scrambled siRNA versus OPTN siRNA in the absence of maturation stimuli. No differences were observed in the expression of CD14, CD11c, CD80, CD86, CD83, CD40, HLA-DR, and PD-L1 surface markers between scRNA and siOPTN iDCs (Fig. 10A), indicating that optineurin is dispensable for the basal surface marker profile of immature DCs. This result also suggested that the low levels of optineurin present in iDCs (see section 4.1) did not contribute to the maintenance of the immature DC phenotype.

Next, we assessed whether optineurin deficiency affected the phenotypic changes associated with LPS-induced DC maturation. Scrambled and OPTN siRNA-transfected iDCs were stimulated with LPS for 24 hours and their surface marker profiles were compared. The maturation-associated changes, including upregulation of CD80, CD83, CD86, CD40, HLA-DR, CD11c, and PD-L1, occurred to the same extent in both scRNA and siOPTN DCs (Fig. 10B). This demonstrated that optineurin silencing did not impair the capacity of human DCs to undergo full phenotypic maturation in response to TLR4 engagement.

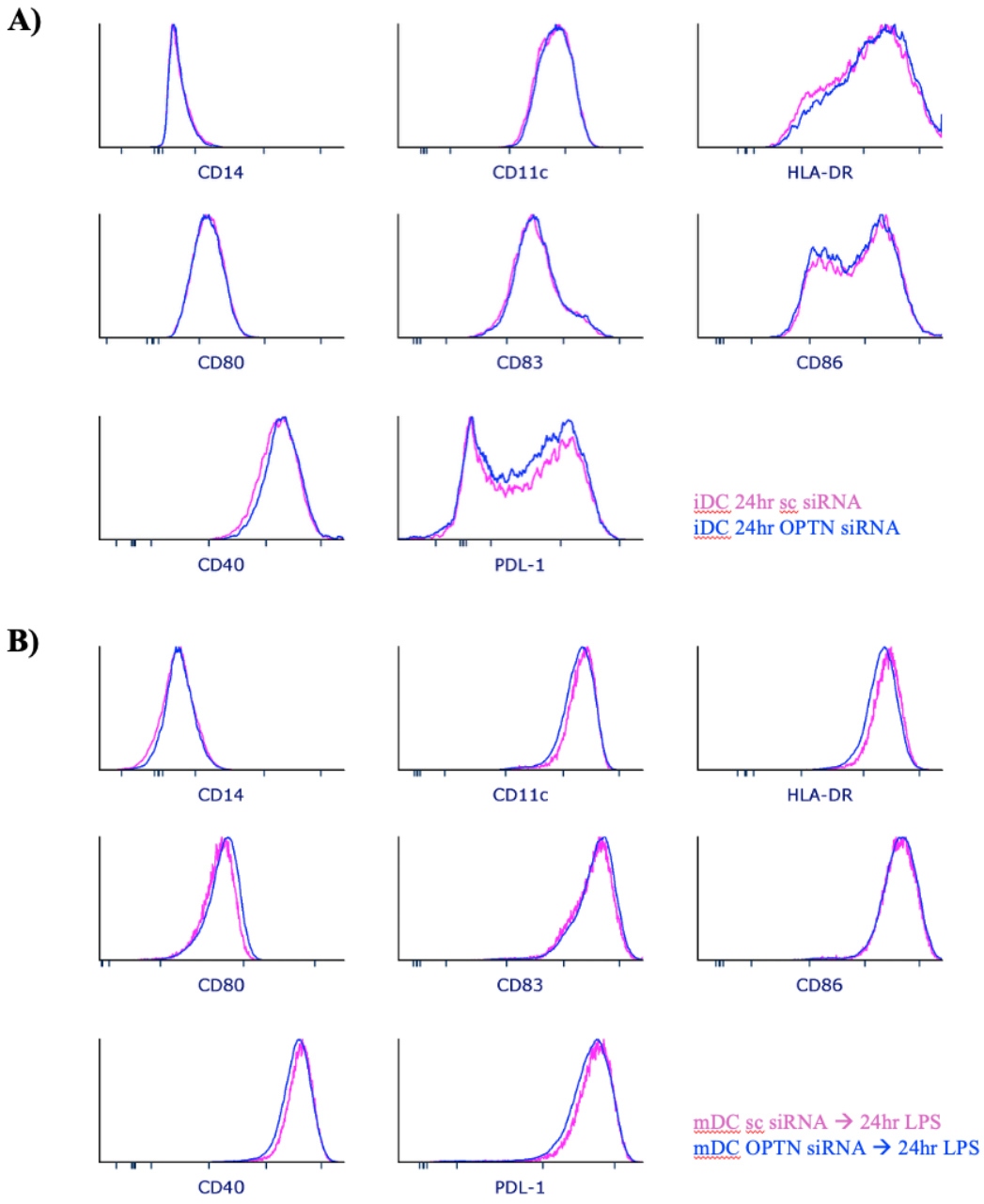

Figure 10. Optineurin silencing did not alter the iDC and mDC surface phenotype.

Immunophenotypic analysis of scrambled control siRNA (sc siRNA)- and OPTN siRNA-transfected human monocyte-derived dendritic cells by multicolor flow. Histograms show representative surface expression profiles of CD14, CD11c, HLA-DR, CD80, CD83, CD86, CD40, and PD-L1. (A) Comparison of unstimulated iDCs after 24 h from transfection with sc siRNA or OPTN siRNA. (B) Comparison of sc siRNA- and OPTN siRNA-transfected cells in mDC after 24 h of LPS stimulation. Representative overlays are shown from at least three independent PBMC donors, with sc siRNA in pink and OPTN siRNA in blue.

Taken together, these results indicated that optineurin was not required for the acquisition or maintenance of the DC immunophenotype in monocyte derived human cells, neither in the

immature resting state nor during LPS-driven maturation. Thus, despite the strong upregulation of optineurin itself during DC maturation (see section 4.1), its absence did not affect the surface expression of co-stimulatory molecules, antigen presentation machinery, or immune checkpoint receptors. This finding suggested that optineurin's functional role in mature DCs may lie downstream of surface marker acquisition, potentially in intracellular signaling, cytokine production, or antigen processing and presentation, rather than in the regulation of DC immunophenotype per se. This possibility was explored in the subsequent sections.

4.6. Optineurin silencing did not affect NF-κB activation but showed a trend toward reduced TBK1 phosphorylation in human dendritic cells

Having established that optineurin deficiency did not alter DC immunophenotype, we next investigated whether optineurin regulates the two major inflammatory signaling pathways downstream of TLR4 engagement: the NF-κB pathway and the TBK1/IFN-β pathway. Previous studies in murine primary cells demonstrated that optineurin is dispensable for acute NF-κB activation but is required for optimal TBK1 phosphorylation and IFN-β production (Gleason et al., 2011; Munitic et al., 2013; Pourcelot et al., 2016; Markovinovic et al., 2018). To determine whether these findings translate to human DCs, we stimulated scrambled and OPTN siRNA-transfected iDCs for 24 h with LPS (100 ng/mL) and assessed pathway activation by measuring phosphorylation of the NF-κB subunit p65 (Ser536) and TBK1 (Ser172) at multiple time points using the ProteinSimple Jess automated capillary Western system.

Phosphorylated p65 (P-p65) was present at low but detectable levels at baseline in unstimulated iDCs. Upon LPS stimulation, P-p65 levels increased rapidly, reaching a peak at 30 minutes post-stimulation. At 1 hour, P-p65 remained slightly elevated above baseline, and by 4 hours, levels had returned to basal values, indicating resolution of the acute NF-κB activation wave (Fig. 11 A and B). This kinetic profile is consistent with the well-characterized rapid and transient nature of canonical NF-κB signaling, in which IκBα degradation and p65 phosphorylation occur shortly upon TLR4 engagement, followed by negative feedback through IκBα resynthesis (Ghosh & Hayden, 2012).

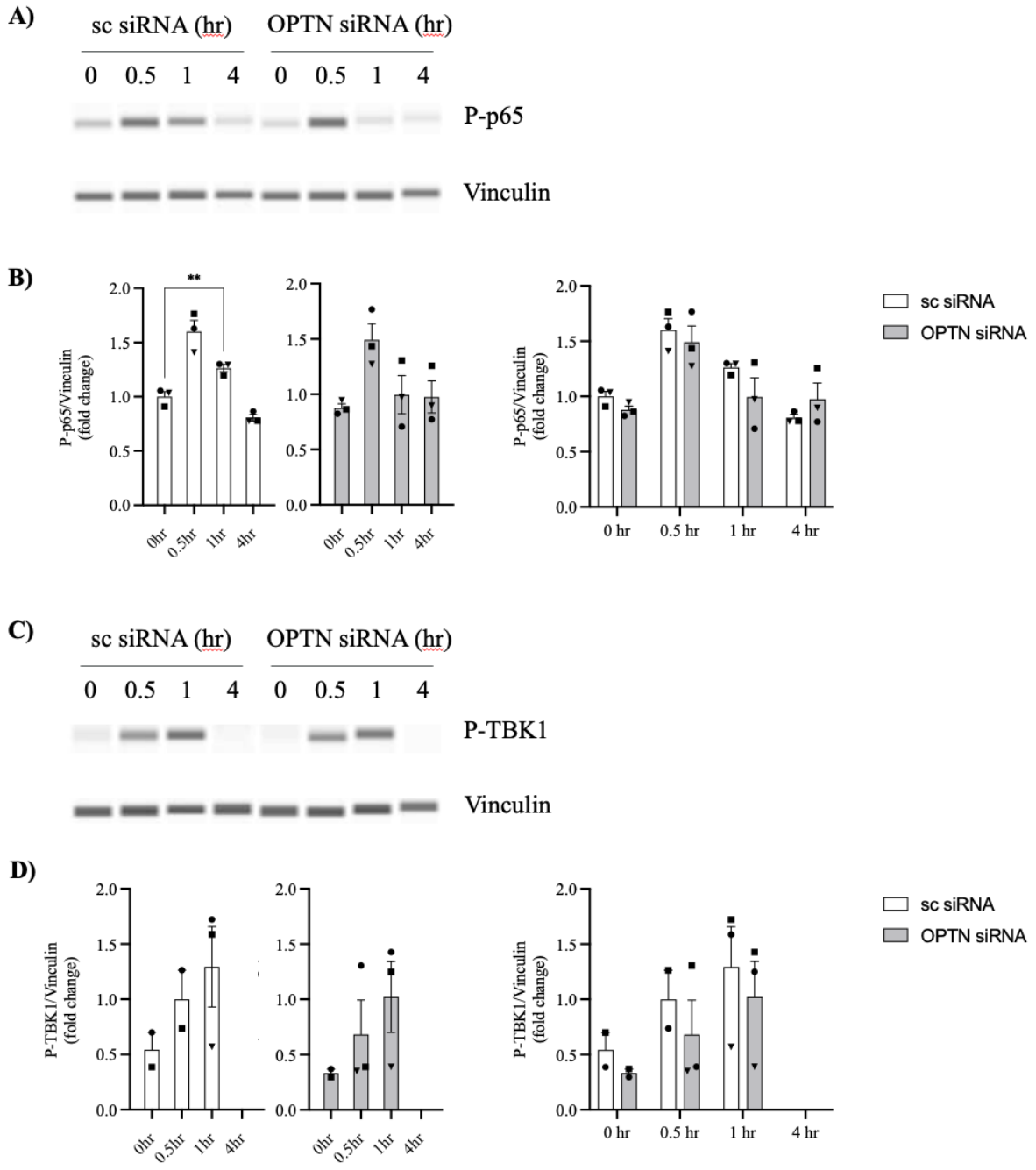

Figure 11. Optineurin silencing did not affect NF-κB activation but showed a trend toward reduced TBK1 phosphorylation

(A) Representative ProteinSimple Jess electropherograms showing phospho-p65 (Ser536) protein levels in scRNA and siOPTN DCs at baseline (unstimulated) and at 30 minutes, 1 hour, and 4 hours following LPS stimulation (100 ng/mL). Vinculin was used as loading control. (B) Quantification of P-p65 signal intensity normalized to total protein across the time course. Data represent mean ± SEM from 3 independent donors. (C) Representative ProteinSimple Jess electropherograms showing phospho-TBK1 (Ser172) protein levels in scRNA and siOPTN DCs at baseline and at 30 minutes, 1 hour, and 4 hours following LPS stimulation. (D) Quantification of P-TBK1 signal intensity normalized to total protein. Data represent mean ± SEM from three independent donors. Statistical comparisons between

scRNA and siOPTN conditions were performed using multi comparison two-way ANOVA. Statistical comparisons within scRNA alone or siOPTN alone conditions were performed using multi comparison one-way ANOVA. * $p < 0.05$, ** $p < 0.01$, *** $p < 0.001$.

Importantly, kinetics and magnitude of NF-κB activation measured by phosphorylation of p65 were similar between optineurin-sufficient and optineurin-deficient DCs at baseline, at the 30-minute peak, during the 1-hour decline phase, nor at the 4-hour resolution time point (Fig. 11 A and B). This finding is consistent with results from murine primary microglia, macrophages, and dendritic cells, where optineurin deficiency similarly did not affect acute NF-κB activation upon LPS stimulation (Gleason et al., 2011; Munitic et al., 2013; Slowicka et al., 2016; Markovinovic et al., 2018), confirming that this observation from mouse models extends to human monocyte-derived DCs. Together with our immunophenotyping data showing unaltered co-stimulatory molecule expression (section 4.3), these results demonstrate that optineurin is dispensable for canonical NF-κB signaling in human DCs upon acute TLR4 engagement.

In contrast to the robust and consistent P-p65 signal, phosphorylated TBK1 (P-TBK1 at Ser172) was more difficult to detect in human DCs and displayed greater inter-donor variability. At baseline, P-TBK1 was detectable as a faint band in only 2 out of 3 donors, indicating that constitutive TBK1 activity is minimal in unstimulated iDCs (Fig. 11 C and D). Upon LPS stimulation, P-TBK1 levels increased at 30 minutes and reached a peak at 1 hour post-stimulation, demonstrating slightly delayed kinetics compared to NF-κB activation, possibly driven by sequential engagement of the MyD88-dependent (NF-κB) and TRIF-dependent (TBK1) branches of TLR4 signaling (Kawai & Akira, 2010). By 4 hours post-stimulation, P-TBK1 was no longer detectable, indicating that TBK1 activation in human DCs is transient and confined to the early phase following TLR4 engagement (Fig. 11 C and D).

When comparing scrambled and OPTN siRNA-transfected DCs, P-TBK1 levels appeared lower in optineurin-silenced cells at the 30-minute and 1-hour time points (Fig. 11 D). This trend toward reduced TBK1 activation is directionally consistent with findings from murine $Optn^{470T}$ microglia, macrophages, and dendritic cells, where loss of optineurin's ubiquitin-binding region resulted in approximately 40–50% reduction in P-TBK1 levels upon LPS stimulation (Munitic et al., 2013; Pourcelot et al., 2016; Markovinovic et al., 2018).

However, in our human DC system, this reduction did not reach statistical significance (Fig. 11 C and D). Despite the lack of statistical significance, the consistent directional trend toward reduced TBK1 activation in optineurin-silenced DCs suggests that optineurin contributes to, but is not absolutely required for, TBK1 activation in human DCs. Of note, a similar trend was also present in macrophages (Figure 19 C and D). This partial effect may have downstream consequences for IFN-β production and interferon-stimulated gene expression, which were explored in the subsequent section on cytokine profiling.

4.7. **Optineurin silencing did not significantly alter STAT1 activation and TDP-43 expression in DC**

To extend our signaling analysis beyond the immediate TLR4-proximal events (NF-κB, TBK1), we examined STAT1 phosphorylation and TDP-43 protein levels in DCs. STAT1 phosphorylation (Tyr701) is a key downstream readout of the IFN-β/IFNAR/JAK signaling axis: upon LPS stimulation, TBK1-driven IFN-β production leads to autocrine/paracrine IFNAR engagement, JAK1/TYK2 activation, and STAT1/STAT2 phosphorylation, which drives ISG transcription (Lin et al., 1999; Sharma et al., 2003; Honda et al., 2005). Therefore, P-STAT1 serves as an indirect but functionally important indicator of this signaling cascade. TDP-43, the protein that aggregates in >95% of in ALS patients (Neumann et al., 2006), was assessed to determine whether optineurin deficiency or inflammatory activation alters its expression in human macrophages following OPTN silencing, a question of direct disease relevance given the reports that LPS-driven NF-κB activation can promote TDP-43 mislocalization and aggregation in glia (Correia et al., 2015).

P-STAT1 (Tyr701) was measured by ProteinSimple Jess/Wes at baseline (iDC), 4 hours, 8 hours, and 24 hours post-LPS stimulation (100 ng/mL) in scrambled and OPTN siRNA-transfected DCs (Fig. 12A and B). At baseline, P-STAT1 was detectable but at very low levels, consistent with minimal constitutive IFN-β/IFNAR signaling in immature DCs. Upon LPS stimulation, P-STAT1 increased substantially, reaching approximately 18-fold induction by 4 hours and continuing to rise to approximately 25-fold at 8 hours (Fig. 12A and B). By 24 hours, P-STAT1 had declined to approximately 5-fold above baseline, indicating resolution of the IFNAR-driven signaling wave while maintaining modestly elevated activity (Fig. 12A and B). When comparing scrambled and OPTN siRNA-transfected DCs, no differences in P-STAT1 levels were observed at any time point examined (Fig. 12B).

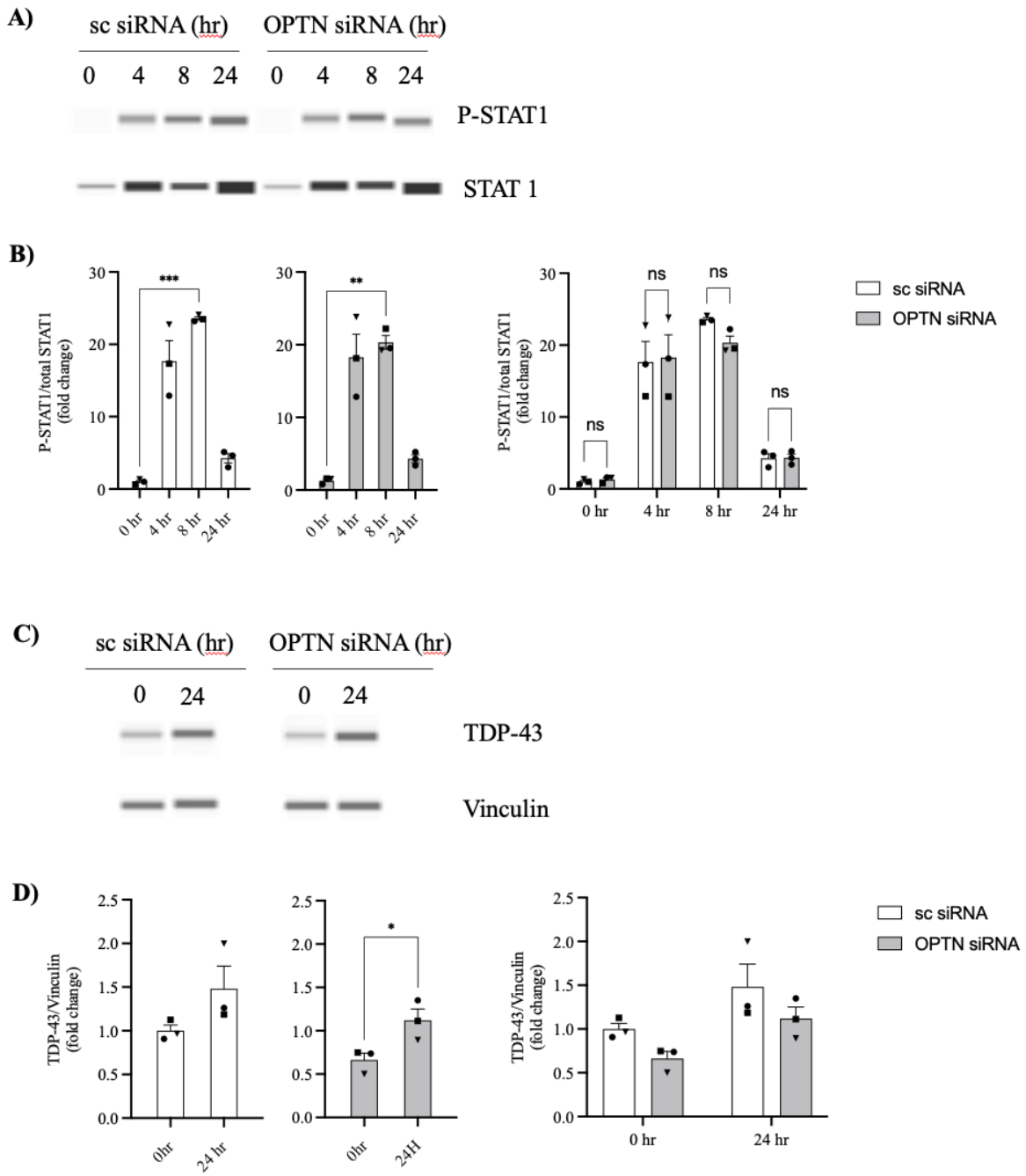

Figure 12. STAT1 activation and TDP-43 expression in optineurin-silenced dendritic cells.

(A) Representative ProteinSimple Jess electropherograms showing phospho-STAT1 (Tyr701) in scRNA and siOPTN DCs at baseline and post-LPS time points. (B) Quantification of P-STAT1 signal intensity normalized to STAT1. (C) Representative ProteinSimple Jess electropherograms showing total TDP-43 protein levels in scRNA and siOPTN DCs at baseline (iDC) and 24 hours post-LPS stimulation (100 ng/mL). (D) Quantification of TDP-43 signal intensity normalized to vinculin. Data represent mean ± SEM from 3 independent donors. Statistical comparisons between scRNA and siOPTN conditions were performed using multi comparison two-way ANOVA. Statistical comparisons within scRNA alone or

siOPTN alone conditions were performed using multi comparison one-way ANOVA. * $p < 0.05$, ** $p < 0.01$, *** $p < 0.001$.

Total TDP-43 protein was measured by ProteinSimple Jess/Wes at baseline (iDC) and 24 hours post-LPS stimulation in scrambled and OPTN siRNA-transfected DCs (Fig. 12C and D). TDP-43 was readily detectable in immature DCs, consistent with its ubiquitous expression. Following 24 hours of LPS stimulation, total TDP-43 levels showed a modest increase of approximately 50% relative to iDC baseline (Fig. 12C and D). While the mechanism underlying this increase was not investigated, it may reflect inflammatory regulation of TDP-43 expression during DC activation. No statistically significant differences in total TDP-43 levels were observed between scrambled and siOPTN DCs at either time point, although a trend toward lower TDP-43 expression was noted in siOPTN cells. Importantly, the modest increase in total TDP-43 following acute LPS stimulation does not exclude the possibility that inflammatory activation may additionally induce disease-relevant post-translational modifications, cytoplasmic redistribution, or aggregation of TDP-43 without major changes in total protein abundance (Swarup et al., 2011; Correia et al., 2015). In conclusion, optineurin reduction alone was insufficient to substantially alter total TDP-43 levels under these experimental conditions.

4.8. Optineurin silencing did not significantly alter cytokine production by LPS-stimulated dendritic cells

To determine whether optineurin deficiency affects the cytokine secretory profile of human DCs, we measured a comprehensive panel of pro-inflammatory and anti-inflammatory cytokines in cell culture supernatants from scrambled and OPTN siRNA-transfected DCs at baseline (iDC), 8 hours, and 24 hours following LPS stimulation (100 ng/mL). Cytokine quantification was performed using the MSD V-PLEX Proinflammatory Panel 1 (measuring IFN-γ, IL-1β, IL-2, IL-4, IL-6, IL-8, IL-10, IL-12p70, IL-13, and TNF-α) and a standard ELISA platform for IFN-β, as described in the Methods section.

IL-1β, a key inflammasome-dependent pro-inflammatory cytokine, was present at levels below 1 pg/mL in unstimulated iDCs. Upon LPS stimulation, IL-1β increased to approximately 10 pg/mL by 8 hours and remained at comparable levels at 24 hours (Fig. 13 A), indicating sustained but modest IL-1β secretion consistent with the requirement for secondary inflammasome activation signals for maximal IL-1β release.

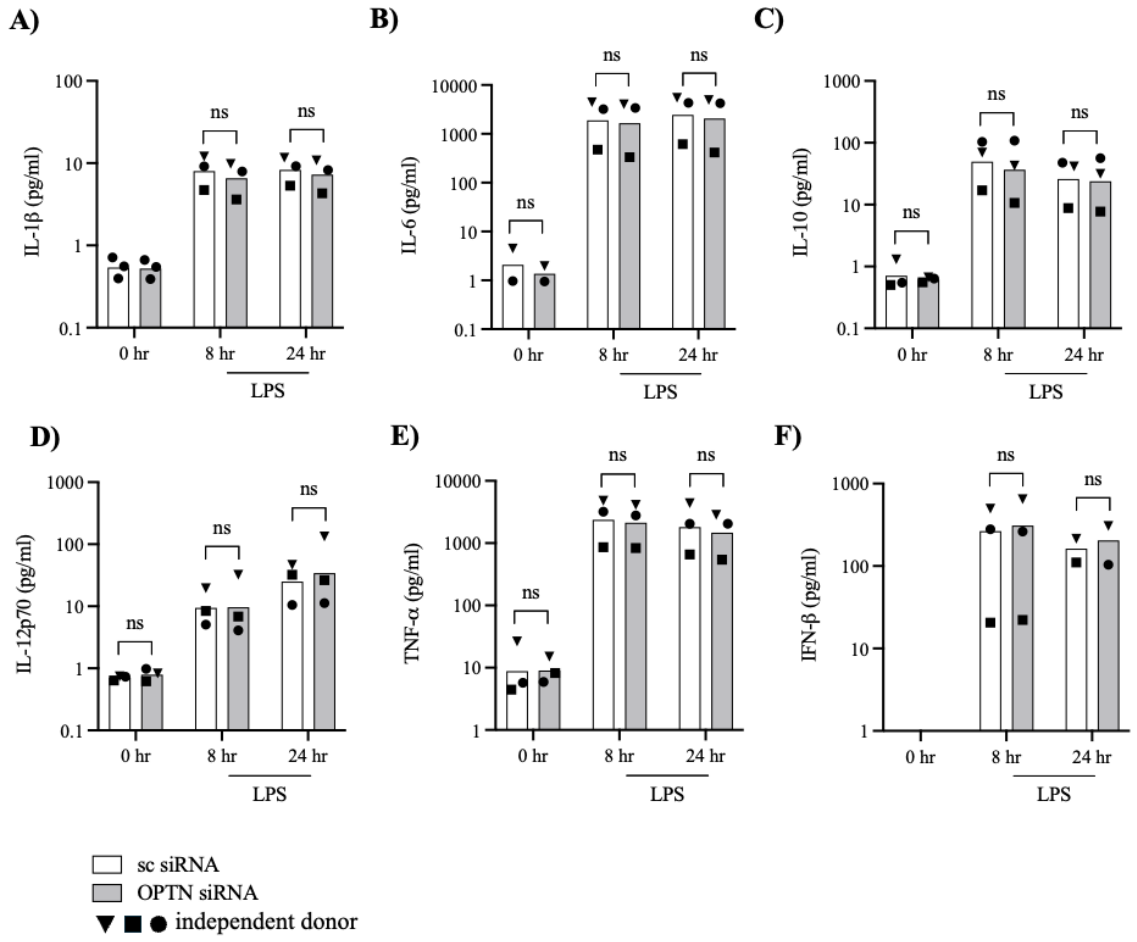

Figure 13. Cytokine production by optineurin-silenced dendritic cells upon LPS stimulation.

(A–F) Cytokine levels measured in culture supernatants from scRNA and siOPTN DCs at baseline (iDC, unstimulated), 8 hours, and 24 hours following LPS stimulation (100 ng/mL). (A) IL-1β, (B) IL-6, (C) IL-10, (D) IL-12p70, (E) TNF-α, and (F) IFN-β. Cytokines were quantified using MSD V-PLEX Proinflammatory Panel 1 (A–E) and Abcam Simplestep ELISA (F). Each symbol represents an individual donor. The donor with low IFN-β production and reduced P-TBK1 activation is indicated a square symbol. Statistical comparisons between scRNA and siOPTN conditions were performed using multi comparison two-way ANOVA; ns= not significant, * $p < 0.05$, **$p < 0.01$, *** $p < 0.001$.

IL-6, a pleiotropic cytokine with both pro-inflammatory and immunoregulatory functions, was present at approximately 1 pg/mL in iDCs and showed a dramatic increase to over 1,000 pg/mL by 8 hours post-LPS stimulation, remaining stable at 24 hours (Fig. 13 B). This rapid and robust IL-6 induction reflected the strong NF-κB-driven transcriptional response to TLR4 engagement.

IL-10, an anti-inflammatory cytokine that counterbalances pro-inflammatory responses, followed a time-dependent induction pattern upon LPS stimulation (Fig. 13 C). IL-10 production is known to be regulated by both NF-κB and IFN-β/STAT1 signaling, and its induction in our system is consistent with the engagement of both pathways downstream of TLR4.

IL-12p70, the bioactive heterodimer critical for Th1 polarization, was present at approximately 1 pg/mL in iDCs and increased to around 10 pg/mL at 8 hours, with further accumulation around 30 pg/mL by 24 hours (Fig. 13 D). This progressive increase in IL-12p70 is consistent with its known delayed kinetics relative to other NF-κB-driven cytokines, reflecting the requirement for both p35 and p40 subunit transcription and heterodimer assembly.

TNF-α, a prototypical early-response pro-inflammatory cytokine, was already detectable at approximately 10 pg/mL in iDC supernatants, likely reflecting low-level constitutive secretion or residual activation from the differentiation process. Upon LPS stimulation, TNF-α levels increased sharply to approximately 1,000 pg/mL by 8 hours, with a slight decrease yet insignificant decrease by 24 hours (Fig. 13 E), consistent with the known early kinetics of TNF-α transcription and secretion following NF-κB activation.

IFN-β, the principal type I interferon produced downstream of TBK1/IRF3 activation, was not detectable in unstimulated iDCs. Upon LPS stimulation, IFN-β levels increased to over 100 pg/mL by 8 hours, followed by two-fold reduction by 24 hours (Fig. 13 F), consistent with the known transient kinetics of IFN-β transcription driven by IRF3 activation within the first hours of TLR4 engagement. Notably, one donor exhibited substantially lower IFN-β production at 8 hours (approximately 22 pg/mL) with undetectable levels by 24 hours. This same donor was the individual in whom P-TBK1 was not detectable at baseline and showed the lowest P-TBK1 levels at 1-hour post-LPS stimulation (see section 4.6), suggesting a correlation between TBK1 activation capacity and IFN-β output at the individual donor level. This observation, while based on a single donor, is mechanistically coherent with the established role of TBK1 as the upstream kinase driving IRF3-dependent IFN-β transcription and suggests that inter-individual variation in TBK1 pathway activity may contribute to heterogeneity in type I interferon responses among healthy donors.

Despite the robust cytokine responses observed upon LPS stimulation, no statistically significant differences were detected between scrambled and OPTN siRNA-transfected DCs

for any of the measured cytokines at any time point (Fig. 13 A–F). IL-1β, IL-6, IL-12p70, TNF-α, IL-10, and IFN-β levels were comparable between optineurin-sufficient and optineurin-deficient DCs at baseline, 8 hours, and 24 hours post-LPS stimulation. The preservation of NF-κB-driven cytokines (TNF-α, IL-6, IL-1β, IL-12p70) aligns with the unaltered p65 phosphorylation, confirming that NF-κB-dependent cytokine output is independent of optineurin in human DCs and macrophages. The lack of significant IFN-β reduction is consistent with the modest, non-significant P-TBK1 decrease, potentially insufficient to affect IFN-β secretion given the IRF7-mediated amplification loop and redundant TBK1 adaptors. Nevertheless, the single-donor correlation between low P-TBK1 and reduced IFN-β supports the optineurin–TBK1–IFN-β functional axis, suggesting that more complete ablation or increased statistical power might reveal significant differences, as demonstrated in murine models (Munitic et al., 2013; Pourcelot et al., 2016; Markovinovic et al., 2018).

IFN-γ, IL-2, and IL-13 (not shown) were barely detectable across all conditions and time points, which is expected given that these cytokines are primarily produced by T cells and not by DCs upon TLR4 stimulation. IL-4 was excluded because the DC differentiation medium contains exogenous IL-4, rendering the measured levels uninterpretable as endogenous DC production.

4.9. Optineurin silencing did not impair phagocytosis by immature or LPS-matured dendritic cells

Having established that optineurin deficiency does not alter DC immunophenotype or signaling pathway activation, we next investigated whether it affects phagocytosis, a core functional property of dendritic cells. As the principal professional antigen-presenting cells of the immune system, DCs rely on phagocytosis as the critical first step in their immunological function: the capture and internalization of pathogens, apoptotic cells, and particulate antigens from the extracellular environment, which are subsequently processed and loaded onto MHC molecules for presentation to T cells. Immature DCs are highly phagocytic, actively sampling their surroundings for foreign material, while upon maturation they downregulate phagocytic capacity and shift toward antigen presentation and T cell activation (Banchereau & Steinman, 1998). Given optineurin's known interactions with vesicular trafficking machinery (myosin VI, Rab8) and its involvement in autophagosome–lysosome

fusion, we hypothesized that optineurin deficiency might impair the phagocytic uptake or phagosomal processing of particulate antigens.

To address this, we assessed phagocytosis using pHrodo™ *E. coli* BioParticles in both immature and LPS-matured DCs transfected with either scRNA or OPTN-targeting siRNA. These particles are conjugated with the pH-sensitive pHrodo dye, which is non-fluorescent at neutral extracellular pH but fluoresces brightly upon acidification within phagolysosomes (Fig. 14A). This property ensures that only particles successfully internalized and delivered to acidic phagolysosomal compartments generate a fluorescent signal, providing a specific readout of completed phagocytosis, including both engulfment and phagosome–lysosome fusion, rather than mere surface binding. Phagocytosis was quantified by flow cytometry measuring the percentage of fluorescence-positive cells and median fluorescence intensity (MFI).

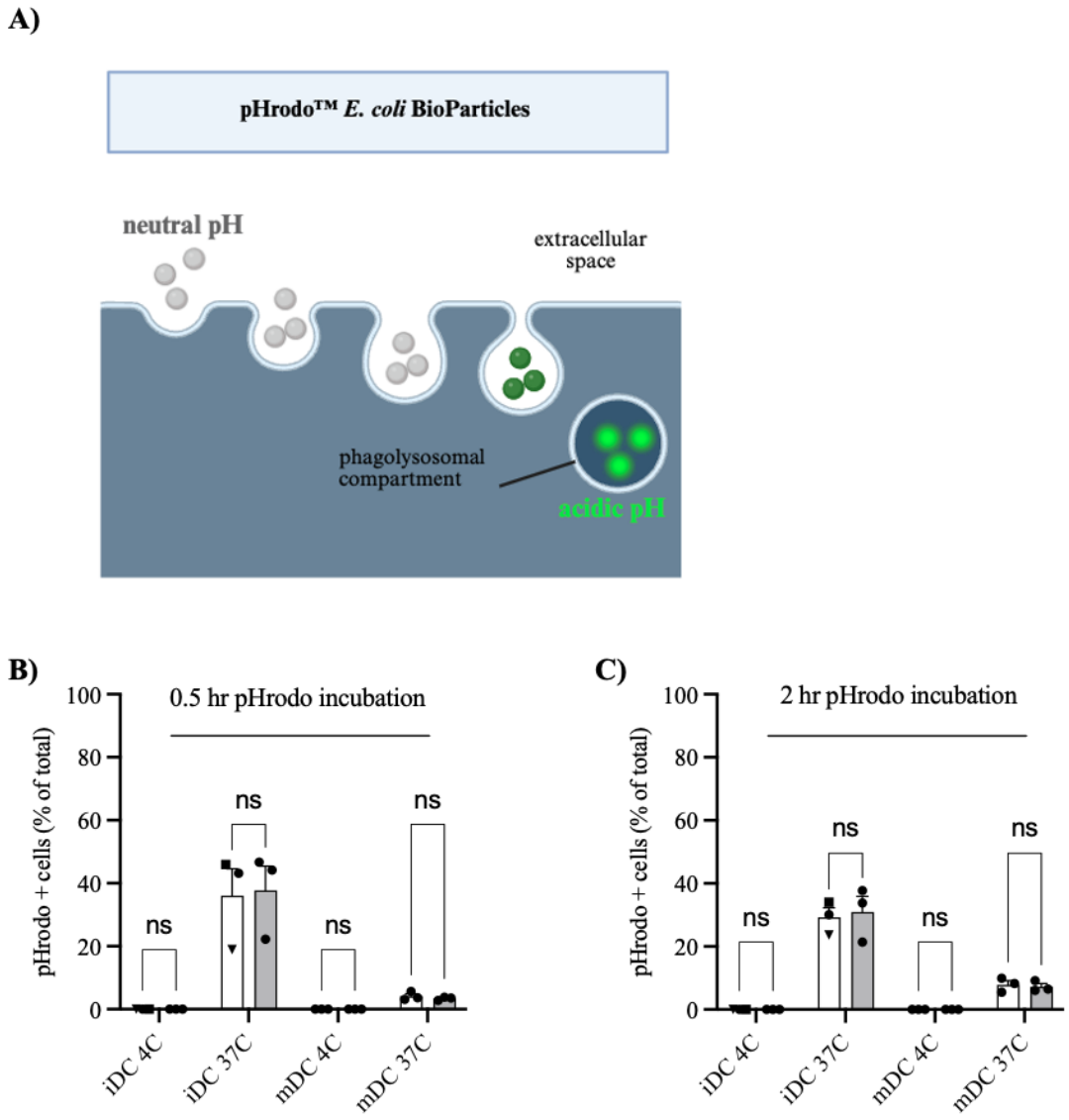

Figure 14. Optineurin silencing did not impair phagocytosis by dendritic cells.

(A) Schematic of the pHrodo phagocytosis assay. pHrodo™ *E. coli* BioParticles are non-fluorescent at neutral extracellular pH; upon internalization and delivery to acidic phagolysosomes, the pH-sensitive dye fluoresces, providing a specific readout of completed phagocytosis including phagosome–lysosome fusion. (B) Quantification of phagocytosis (percentage of pHrodo-positive cells) in scRNA and siOPTN iDCs (left) and LPS-matured mDCs (right) after 0.5 hr of incubation with pHrodo. (C) Quantification of phagocytosis (percentage of pHrodo-positive cells) in scRNA and siOPTN iDCs (left) and LPS-matured mDCs (right) after 3 hr of incubation with pHrodo. Data represent mean ± SEM from 3 independent donors. Statistics: multi comparison 2-way ANOVA; ns = not significant.

As expected, immature DCs displayed robust phagocytic activity, while LPS-matured DCs showed a marked reduction (80%), confirming the well-established maturation-associated downregulation of phagocytic capacity. Importantly, no differences in phagocytosis were observed between scRNA and siOPTN DCs in either the immature or LPS-matured state (Fig. 14B). The percentage of phagocytic cells were comparable between conditions, demonstrating that optineurin is dispensable for phagocytosis in human DCs regardless of maturation state. This indicates that despite optineurin's roles in vesicular trafficking and autophagy, its deficiency did not measurably affect the capacity of DCs to engulf bacterial particles or deliver them to acidic phagolysosomal compartments, suggesting that redundant trafficking mechanisms compensate or that optineurin's functional contributions in DCs lie in other aspects of immune function.

4.10. Optineurin silencing did not impair antigen processing and presentation by dendritic cells

A critical function of DCs is their capacity to capture, process, and present protein antigens to CD4+ T cells via MHC class II molecules, thereby initiating adaptive immune responses. Given that our phagocytosis assay (section 4.8) showed no difference in particle uptake between optineurin-sufficient and optineurin-deficient DCs, we sought to determine whether optineurin might instead affect downstream steps — specifically antigen processing, MHC II loading, and T cell activation. To address this, we employed a CD154 (CD40L) upregulation assay, which detects antigen-specific CD4+ T cell activation by measuring transient CD154 surface expression upon cognate TCR engagement with peptide–MHC II complexes (Frentsch et al., 2005; Chattopadhyay et al., 2005). The experimental design is schematically represented in Figure 15 A: anti-CD40 blocking antibody was first added to prevent CD154 internalization by DCs, followed by antigen pulsing to allow DC uptake and processing, and

subsequent co-culture with autologous CD4+ T cells. Successful antigen processing and presentation results in antigen-specific T cell activation detected as CD154 upregulation by flow cytometry.

Before performing the assay, we optimized the LPS concentration for DC maturation in this context (Fig. 15 B). Saturating LPS concentrations (100 ng/mL) can drive excessive co-stimulatory molecule expression and cytokine release, leading to non-specific bystander T cell activation that obscures antigen-specific responses. We determined that 3 ng/mL LPS was sufficient to induce optineurin expression at 24 hours while avoiding system saturation, and this sub-saturating dose was used for the antigen presentation experiment.

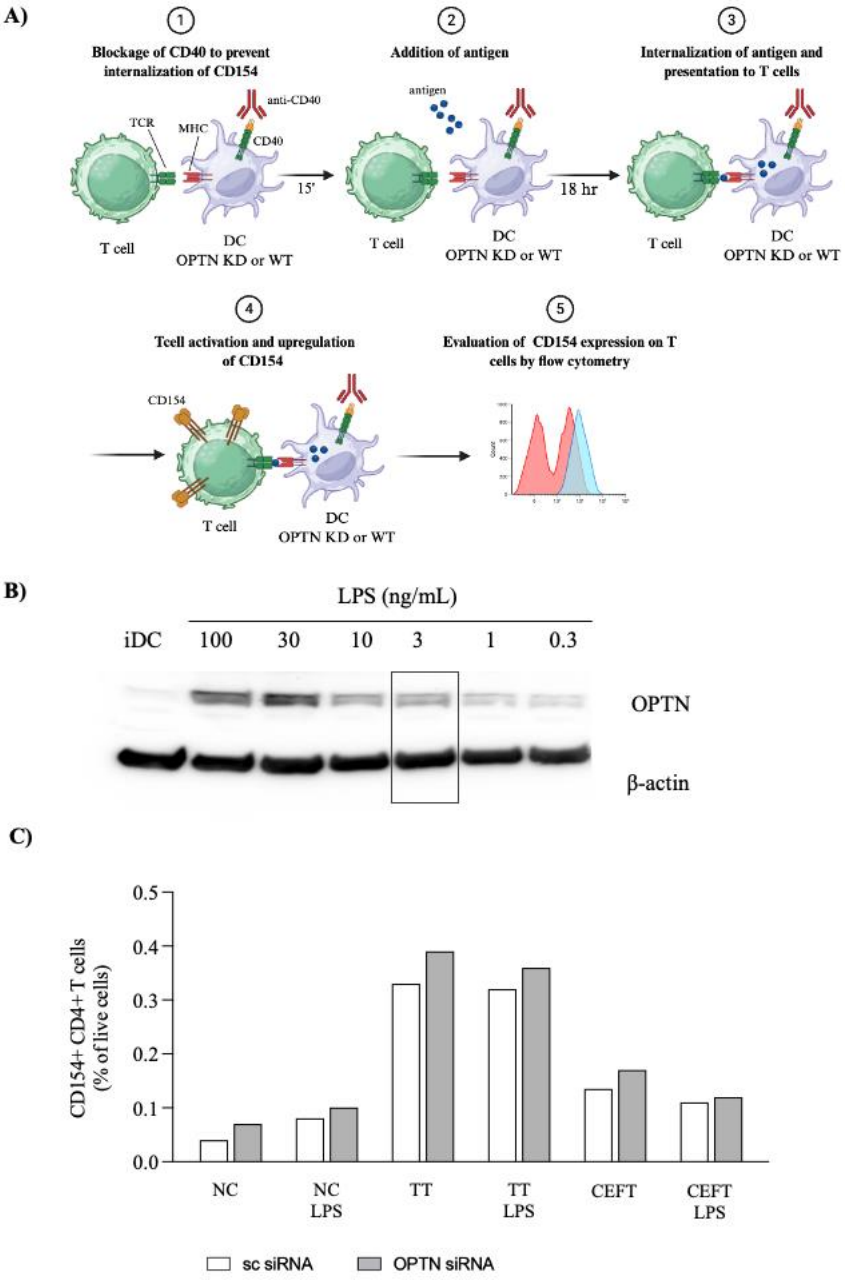

Figure 15. Optineurin silencing did not impair antigen-specific T cell activation by dendritic cells.

(A) Schematic of the CD154 antigen-specific T cell activation assay. Anti-CD40 blocking antibody prevents CD154 internalization by DCs; antigen is added and internalized; processed peptides are presented on MHC II; antigen-specific CD4+ T cells upregulate CD154, detected by flow cytometry. (B) LPS titration showing optineurin expression at 2 ng/mL LPS (24 hours), confirming induction at a sub-saturating dose. (C) Percentage of CD154+ CD4+ T cells across conditions: DC+T (negative control), LPS only, TT, TT+LPS, CEFT, CEFT+LPS, in scRNA and siOPTN DCs. Data from a single donor; no differences observed between conditions.

We tested multiple conditions: unstimulated DCs co-cultured with T cells (negative control; DC+T), LPS-only treated DCs, tetanus toxoid (TT) alone, TT plus LPS, CEFT peptide pool alone, and CEFT plus LPS, all in both sc and OPTN siRNA-transfected DCs (Fig. 14 C). TT is a recall protein antigen requiring full endosomal processing and MHC II loading, providing a readout of the entire antigen presentation pathway. CEFT is a pre-processed peptide pool (CMV, EBV, influenza, tetanus) that bypasses endosomal processing and reports primarily on MHC II surface expression and co-stimulatory capacity.

As expected, unstimulated DC+T co-cultures showed minimal background CD154 expression, while antigen-pulsed DCs induced detectable CD154 upregulation that was further enhanced by LPS co-treatment. No differences were observed between scRNA and siOPTN DCs in any condition tested (Fig. 15 C). It should be noted that this experiment was performed as a preliminary trial with a single donor; while the results were consistent across all conditions tested and aligned with our immunophenotyping data showing unaltered HLA-DR, CD80, CD86, and CD40 expression (section 4.3), confirmation with additional donors would be required to draw definitive conclusions. Nevertheless, the absence of any trend toward impaired antigen presentation in optineurin-silenced DCs, across both whole protein (TT) and pre-processed peptide (CEFT) antigens, with and without LPS, suggests that optineurin is dispensable for the antigen processing and presentation machinery in human DCs.

4.11. Establishment and validation of the human monocyte-derived macrophage model

4.11.1. Experimental strategy for investigating optineurin function in human macrophages

To investigate the role of optineurin in human macrophages, we designed an experimental workflow encompassing monocyte isolation, macrophage differentiation, optineurin silencing, and functional characterization (Fig. 16).

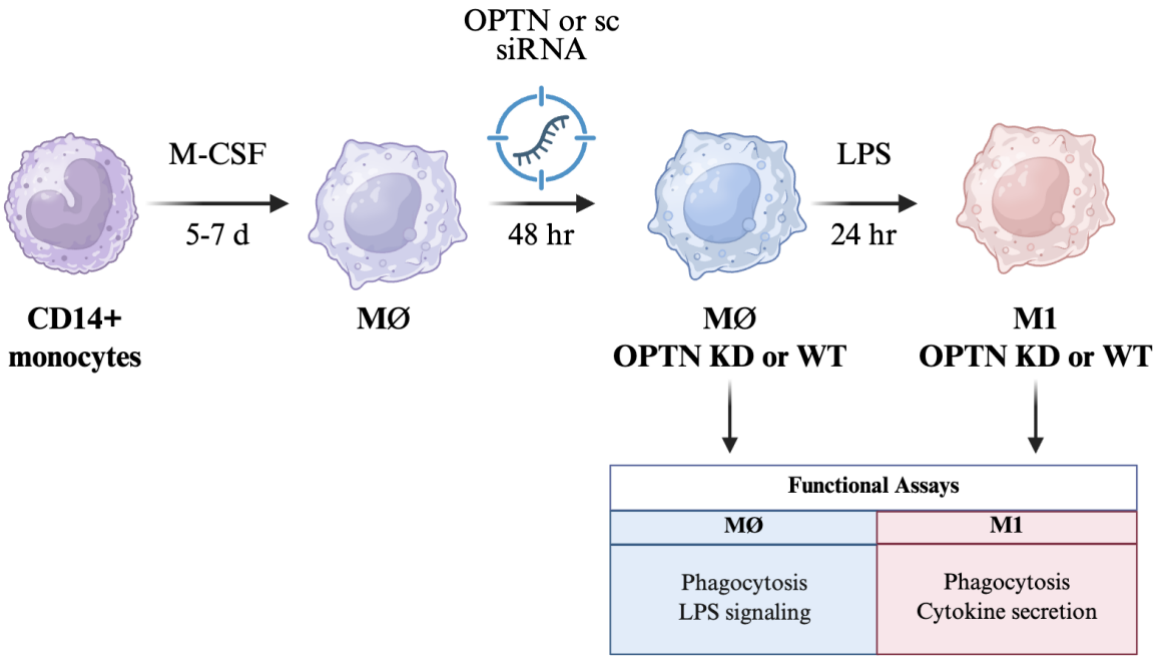

Figure 16. Workflow for optineurin silencing in human monocyte-derived macrophages

Schematic overview of the experimental workflow used to assess the effects of optineurin silencing during human monocyte-derived macrophage differentiation, activation, and functional assays. CD14+ human monocytes were positively selected from PBMCs, differentiated in macrophages (MØ) using M-CSF, and analyzed either under unstimulated conditions (M0 or resting macrophages) or following stimulation with LPS, which induced generation of M1-like macrophages (M1). Remark: M2 polarization experiments for a limited set of experiments (see chapter 4.13.) and are not depicted. Image was generated with Biorender.

CD14+ monocytes were isolated from healthy donor peripheral blood mononuclear cells (PBMCs) by magnetic bead positive selection, routinely achieving purity >95% as confirmed by flow cytometry (Fig. 6). Isolated monocytes were subsequently cultured in the presence of M-CSF for 5–7 days to generate resting macrophages (M0). Optineurin silencing was then performed using OPTN or scrambled control siRNA for 48 hours. This differentiation

protocol, described in detail in the Methods section, recapitulates the physiological transition from circulating monocytes to tissue-resident-like monocyte-derived macrophages.

4.11.2 Validation of macrophage differentiation and activation by light microscopy and flow cytometry

To confirm successful differentiation and activation at each stage of monocyte differentiation, we performed morphological assessment by light microscopy and immunophenotyping by multicolor flow cytometry.

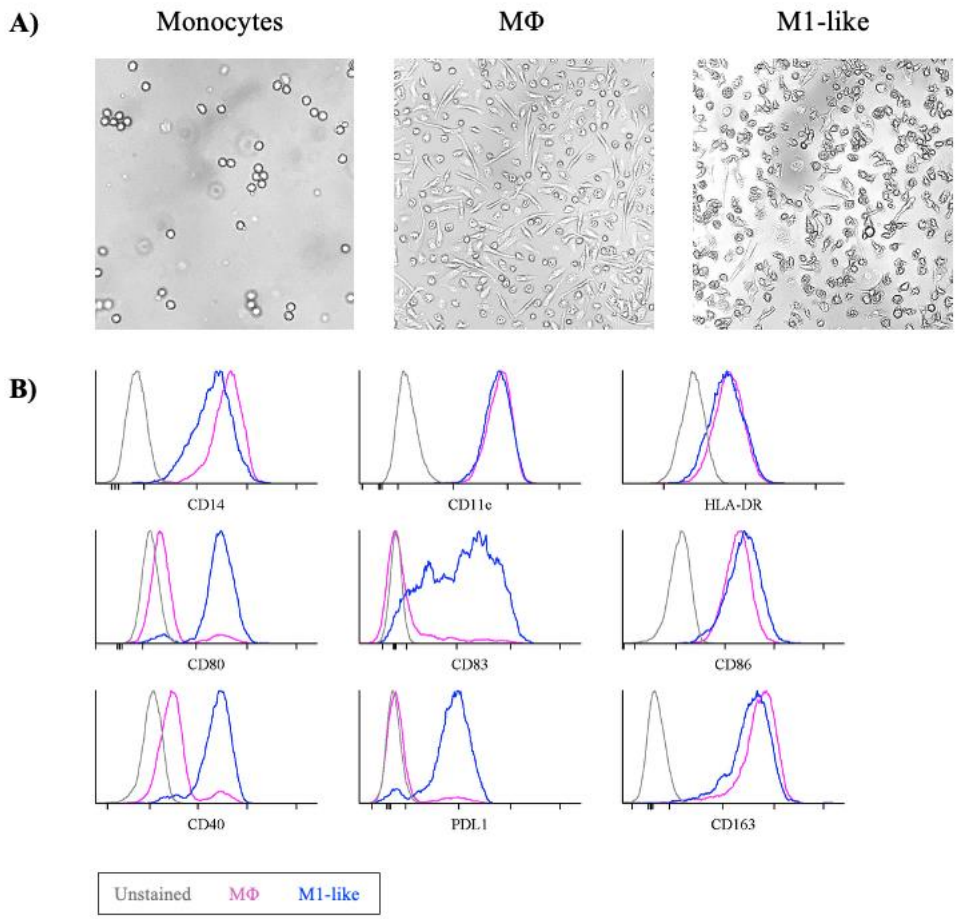

Figure 17. Validation of macrophage differentiation and activation by morphology and flow cytometry

(A) Representative light microscopy images showing the morphological transition from freshly isolated CD14+ monocytes to resting macrophages (M0) after culture with M-CSF for 5–7 days, and to LPS-activated M1-like macrophages (M1) following 24 hours of stimulation. (B) Representative multicolor flow cytometry histograms from three individual donors showing expression of CD14, CD11c, HLA-DR, CD80, CD83, CD86, CD40, and PD-L1 across differentiation stages (unstained, grey; M0, blue; M1-like, pink).

Freshly isolated CD14+ monocytes culture with M-CSF for 5–7 days acquired the morphological features of resting macrophages (M0), including increased cell size, an adherent and spread appearance, abundant cytoplasm, and a more irregular cellular outline (Fig. 17 A). Flow cytometric analysis confirmed the transition from monocytes to macrophages: differentiated M0 macrophages expressed CD14, HLA-DR, CD86 and CD163. Co-stimulatory molecules CD80, and CD40 remained at low to intermediate levels, while the maturation markers CD83 and PDL-1 were largely absent (Fig. 17 B). This surface phenotype is consistent with the generation of resting, non-activated macrophages poised to respond to inflammatory stimuli (Moschetti et al., 2026).

Following 24 hours of LPS stimulation, macrophages underwent further phenotypic and morphological changes consistent with inflammatory activation toward an M1-like state. By light microscopy, activated cells displayed a more spread and flattened morphology with increased cellular complexity compared with resting M0 macrophages (Fig. 17 A). Flow cytometric analysis revealed the expected activation-associated upregulation of co-stimulatory molecules CD80, CD86, and CD40, the maturation marker CD83, and induction of the immune checkpoint molecule PD-L1. CD163, a scavenger receptor specific for the identification of macrophages, was included to exclude differentiation of monocyte in DC (Fig. 17 B). These changes are characteristic of classically activated M1-like macrophages with enhanced antigen-presenting capacity and pro-inflammatory function. Together, these observations validated the generation of both resting M0 macrophages and LPS-activated M1-like macrophages in our experimental system.

Overall, these results demonstrated that our differentiation and activation protocol reliably produces immunophenotypically validated human monocyte-derived macrophages in both the resting and inflammatory states, establishing a robust experimental platform for subsequent investigation of optineurin function in macrophage biology.

4.12. Optineurin is constitutively expressed in resting macrophages and further upregulated upon M1-like but not M2 differentiation

Having established the macrophage differentiation system, we next characterized optineurin protein expression across the stages of macrophage differentiation and polarization. In contrast to the DC lineage, where optineurin was virtually undetectable in monocytes and

only modestly expressed in iDCs (see section 4.1), M-CSF-differentiated resting macrophages (M0) already expressed optineurin at substantial and readily detectable levels (Fig. 18 A). This constitutive expression in M0 macrophages represents a notable difference from the DC differentiation pathway, where optineurin accumulation required inflammatory stimulation, and suggests that M-CSF-driven differentiation programs are sufficient to induce and maintain optineurin expression in the macrophage lineage.

Upon stimulation with LPS for 24 hours to generate M1-like macrophages, optineurin expression was further increased above M0 levels (Fig. 18 A), consistent with the pattern observed in DCs where TLR4 engagement drove robust optineurin upregulation. This finding confirms that inflammatory activation amplifies optineurin expression in both DC and macrophage lineages, likely through the combined action of NF-κB and interferon-responsive elements in the optineurin promoter (Sudhakar et al., 2009; Sudhakar et al., 2013).

To determine whether optineurin upregulation is specific to pro-inflammatory polarization, we also differentiated M0 macrophages toward an M2-like anti-inflammatory phenotype using IL-4. Strikingly, M2-polarized macrophages did not show an increase in optineurin expression (Fig. 18 A). This polarization-dependent expression pattern, elevated in M1-like but not in M2-like macrophages, has not been previously reported. It suggests that optineurin expression is selectively associated with pro-inflammatory macrophage programs driven by TLR signaling and NF-κB/IFN-β pathways, rather than being a general feature of macrophage activation. The absence of optineurin upregulation in M2-polarized cells is consistent with the fact that IL-4 signals primarily through STAT6 rather than NF-κB or interferon-responsive elements, the pathways known to regulate optineurin transcription (Sudhakar et al., 2009; Sudhakar et al., 2013, Munitic et al., 2013).

4.13. Efficient siRNA-mediated silencing of optineurin in human macrophages

To study the consequences of optineurin loss-of-function associated with several confirmed pathogenic ALS-linked *OPTN* variants, we performed optineurin silencing in human monocyte-derived macrophages. Given the high basal expression of optineurin in resting M0 macrophages, and its further upregulation in M1-like macrophages, cells were transfected for 48 hours before functional assessment. After 48 hours of transfection with OPTN siRNA, optineurin protein levels in M0 macrophages were reduced by approximately 50% compared to sc siRNA controls (Fig. 18 B). While this knockdown efficiency is somewhat lower than

the 60–70% achieved in DCs (section 4.2), it is consistent with the higher baseline optineurin levels in M0 macrophages requiring greater protein turnover for depletion, and with the known challenges of transfecting fully differentiated macrophages.

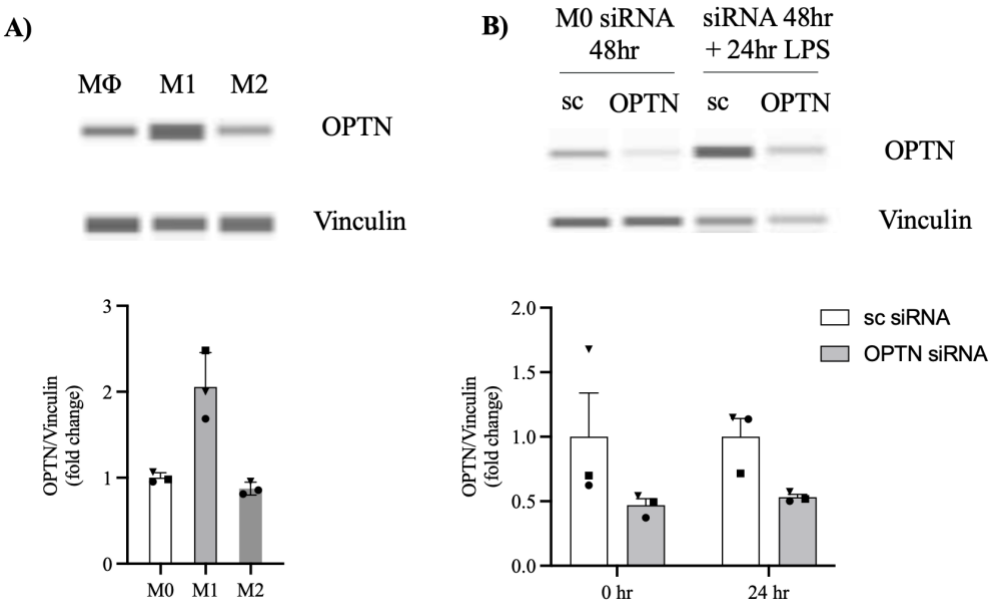

Figure 18. Optineurin expression during macrophage differentiation and polarization, and validation of siRNA-mediated silencing

(A) Optineurin protein expression measured by ProteinSimple Jess in freshly isolated monocytes, M-CSF-differentiated resting macrophages (M0), LPS-activated M1-like macrophages (M1; 24 hours, 100 ng/mL LPS), and IL-4-polarized M2-like macrophages (M2). Total protein normalization was used as loading control. Data represent mean ± SEM from three independent donors. (B) Optineurin protein levels scRNA and OPTN siRNA-transfected macrophages at 48 hours post-transfection (M0 state) and following subsequent LPS stimulation for 24 hours (M1-like state). Data represent mean ± SEM from 3 independent donors. Statistical comparisons were performed using paired t-test; *$p < 0.05$, **$p < 0.01$.

Following 24 hours of LPS stimulation, scrambled siRNA-transfected macrophages showed the expected increase in optineurin expression characteristic of M1-like polarization, confirming that the transfection procedure itself did not impair the capacity of macrophages to upregulate optineurin upon inflammatory activation or induce nonspecific optineurin upregulation through cellular stress or innate immune activation (Fig. 18 B). In OPTN siRNA-transfected macrophages stimulated with LPS, optineurin levels remained approximately 50% lower than in scrambled controls at the M1-like stage (Fig. 18 B). This

demonstrated that the knockdown was maintained through the LPS stimulation period and that the siRNA continued to suppress new optineurin synthesis driven by TLR4 engagement.

In summary, we established siRNA-mediated optineurin silencing in human monocyte-derived macrophages, achieving approximately 50% reduction in both resting M0 and LPS-activated M1-like states. This system was subsequently used to investigate the consequences of optineurin deficiency on macrophage signaling and functional capacity.

4.14. Optineurin silencing did not alter macrophage immunophenotype in resting or LPS-activated states

Having established a substantial reduction of optineurin via silencing in human monocyte-derived macrophages (section 4.12), we next assessed whether optineurin deficiency affected the surface marker profile of macrophages in either the resting (M0) or LPS-activated (M1-like) state. Scrambled and OPTN siRNA-transfected macrophages were analyzed by multicolor flow cytometry for expression of lineage markers (CD14, CD11c), co-stimulatory molecules (CD80, CD86, CD40), the maturation marker CD83, the antigen presentation molecule HLA-DR, and the immune checkpoint molecule PD-L1 and the scavenger receptor CD163.

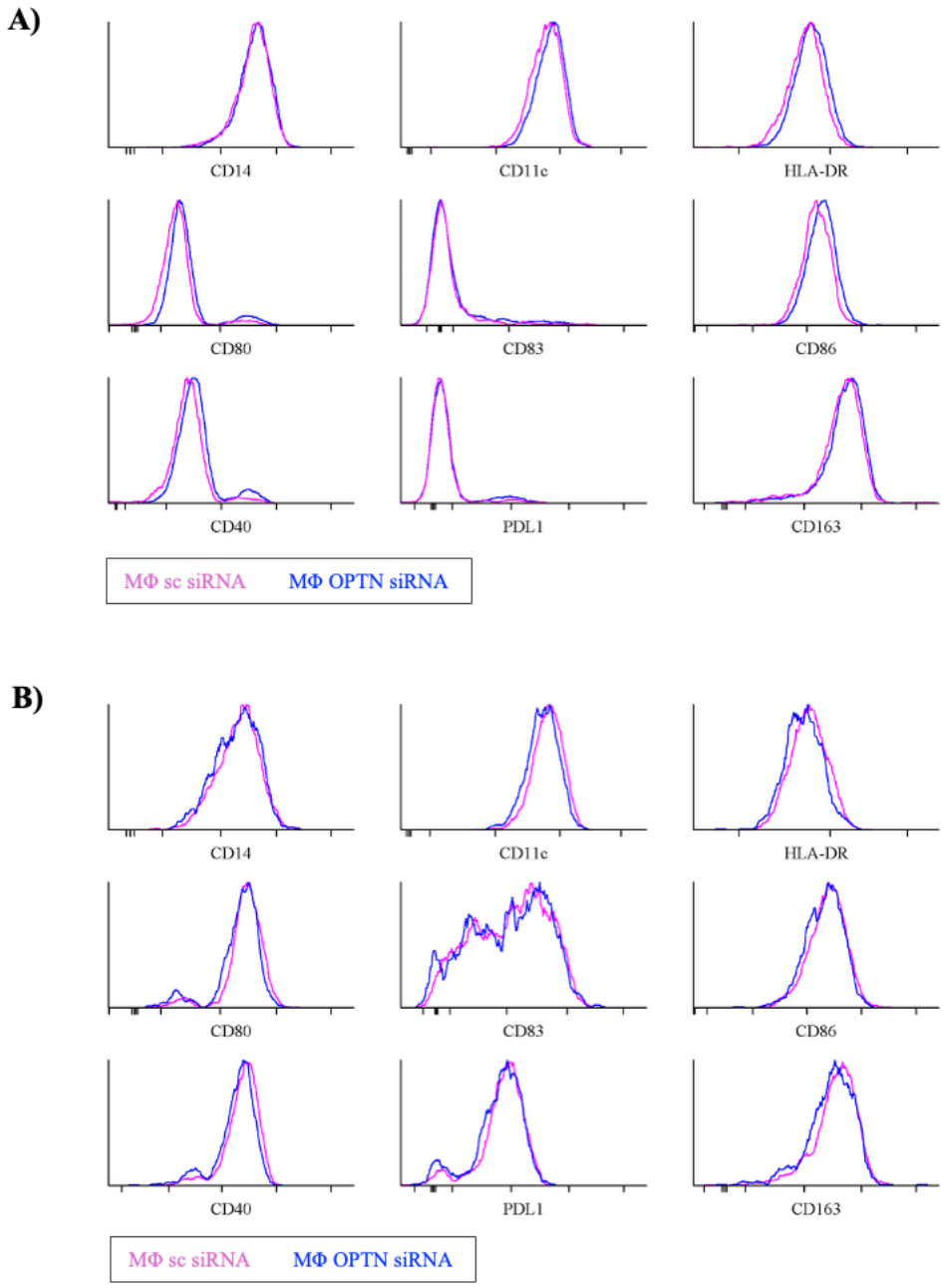

Figure 19. Optineurin silencing does not alter macrophage surface marker expression in resting or LPS-activated states

(A) Quantification of surface marker expression (MFI or percentage positive) in M0 macrophages transfected with scRNA or OPTN siRNA for 48 hours. Markers assessed: CD14, CD11c, HLA-DR, CD80, CD83, CD86, CD40, and PD-L1. (B) Quantification of the same surface markers in macrophages stimulated with LPS (100 ng/mL) for 24 hours following siRNA transfection.

In the resting M0 state, 48 hours post-transfection, no differences were observed in the expression of CD14, CD11c, HLA-DR, CD80, CD86, CD40, CD83, or PD-L1 surface

markers between scrambled and OPTN siRNA-transfected macrophages (Fig. 19 A), indicating that the approximately 50% reduction in optineurin protein achieved by siRNA did not affect the basal surface phenotype or differentiation state of M-CSF-derived macrophages.

Following 24 hours of LPS stimulation, both scrambled and OPTN siRNA-transfected macrophages underwent the expected activation-associated phenotypic changes, including upregulation of CD80, CD86, CD40, CD83, HLA-DR, and PD-L1 characteristic of M1-like polarization (Fig. 19 B). However, the magnitude of these changes was indistinguishable between scRNA and siOPTN macrophages, demonstrating that optineurin was dispensable for the acquisition of the M1-like surface phenotype in human macrophages. Together, these results indicate that partial optineurin silencing does not substantially affect the basal or LPS-induced surface phenotype of human monocyte-derived macrophages under the conditions tested.

Of note, these findings mirror our observations in dendritic cells (section 4.3), where optineurin silencing similarly failed to alter the immunophenotype of either immature or LPS-matured cells. The consistency of this result across both myeloid lineages, DCs and macrophages, reinforces the conclusion that optineurin does not regulate the surface expression of co-stimulatory molecules, antigen presentation machinery, or immune checkpoint receptors in human myeloid cells, despite its strong upregulation during inflammatory activation. This suggests that optineurin's functional contributions in activated macrophages, as in DCs, likely reside in intracellular signaling outputs or other functional domains rather than in the regulation of surface immunophenotype.

4.15. Optineurin silencing did not affect NF-κB activation but showed a trend toward reduced TBK1 phosphorylation in human macrophages

To determine whether optineurin regulates inflammatory signaling pathways in human macrophages, we assessed the activation of the NF-κB and TBK1 pathways in sc siRNA and OPTN siRNA-transfected macrophages following LPS stimulation (100 ng/mL). Pathway activation was measured by phosphorylation of the NF-κB subunit p65 (Ser536) and TBK1 (Ser172) at multiple time points (baseline, 30 minutes, 1 hour, and 4 hours) using the ProteinSimple Jess automated capillary Western system.

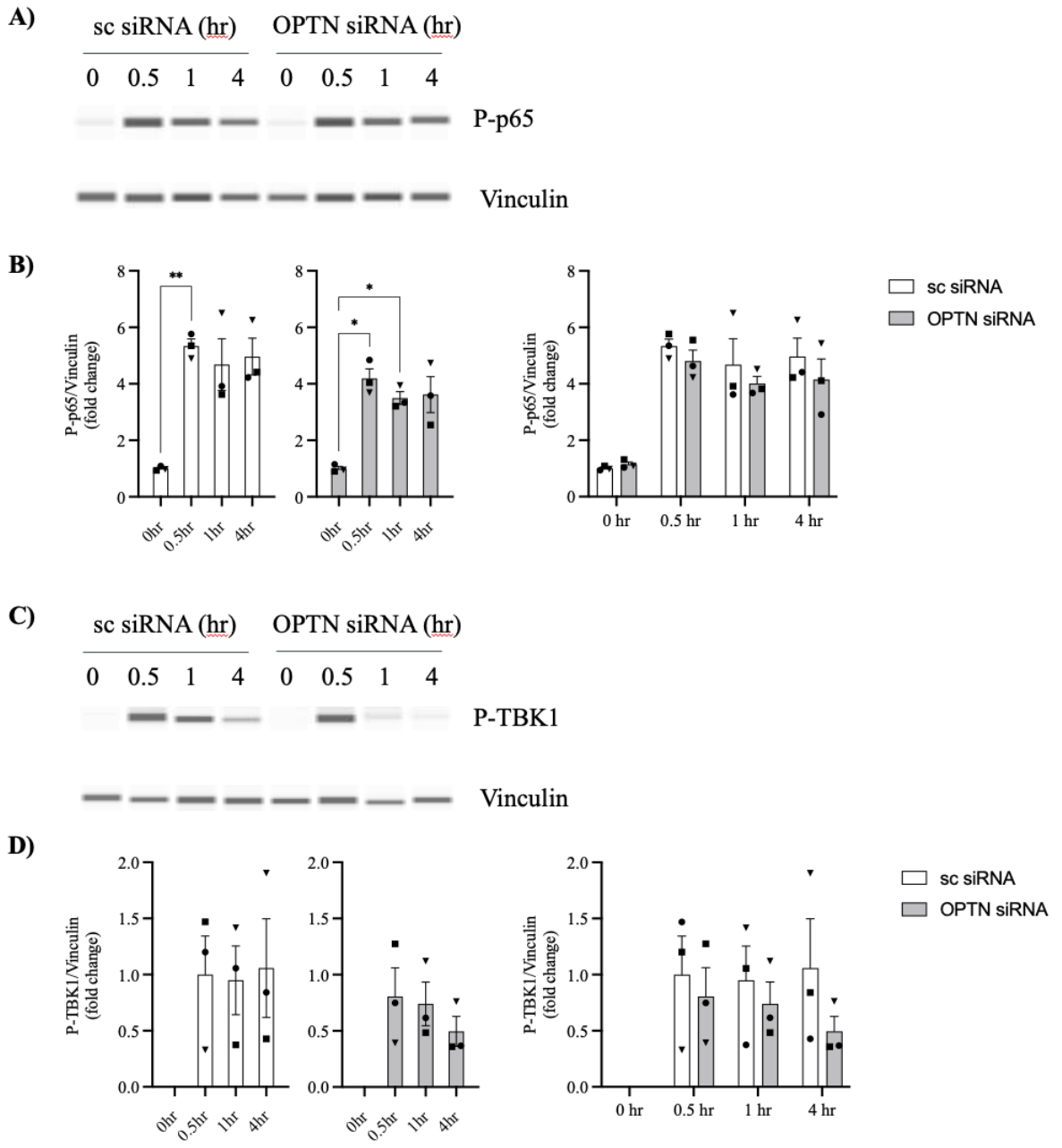

Figure 20. Analysis of NF-κB and TBK1 signaling pathway activation in optineurin-silenced macrophages.

(A) Representative ProteinSimple Jess electropherograms showing phospho-p65 (Ser536) protein levels in scRNA and siOPTN macrophages at baseline (M0, unstimulated) and at 30 minutes, 1 hour, and 4 hours following LPS stimulation (100 ng/mL). Vinculin normalization was used as loading control. (B) Quantification of P-p65 signal intensity normalized to total protein across the time course. Data represent mean ± SEM from 3 independent donors. (C) Representative ProteinSimple Jess electropherograms showing phospho-TBK1 (Ser172) protein levels in scRNA and siOPTN macrophages at baseline and at 30 minutes, 1 hour, and 4 hours following LPS stimulation. (D) Quantification of P-TBK1 signal intensity normalized to total protein. Data represent mean ± SEM from 3 independent donors. Statistical comparisons between scRNA and siOPTN conditions were performed using multi

comparison two-way ANOVA. Statistical comparisons within scRNA alone or siOPTN alone conditions were performed using multi comparison one-way ANOVA. * $p < 0.05$, ** $p < 0.01$, *** $p < 0.001$.

Phosphorylated p65 (P-p65) was present at low levels in resting M0 macrophages at baseline (Fig. 20 A and B). Upon LPS stimulation, P-p65 levels increased rapidly, reaching approximately a 4-fold increase by 30 minutes post-stimulation. At 1 hour, P-p65 showed a slight reduction to approximately 3-fold above baseline and remained at comparable levels through 4 hours (Fig. 20 A and B). This kinetic profile differs somewhat from that observed in DCs (section 4.7), where P-p65 returned to baseline by 4 hours. The sustained p65 phosphorylation in macrophages is consistent with reports of prolonged NF-κB activity in macrophages compared to DCs, potentially reflecting differences in IκBα resynthesis kinetics or the contribution of autocrine TNF-α signaling that sustains NF-κB activation in macrophages (Covert et al., 2005; Werner et al., 2005).

Importantly, no difference in P-p65 levels was observed between sc siRNA and OPTN siRNA-transfected macrophages at any time point examined (Fig. 20 A and B). The kinetics and magnitude of NF-κB activation were indistinguishable between optineurin-sufficient and optineurin-deficient macrophages at baseline, at the 30-minute peak, and throughout the sustained activation phase at 1 and 4 hours. This finding is consistent with our results in human DCs (section 4.7) and with previous reports from murine macrophages and dendritic cells demonstrating that optineurin is dispensable for acute NF-κB activation upon TLR4 engagement (Gleason et al., 2011; Munitic et al., 2013; Slowicka et al., 2016). Together, these data confirm that optineurin does not regulate canonical NF-κB signaling in human myeloid cells, regardless of whether the cells are DCs or macrophages.

Phosphorylated TBK1 (P-TBK1 at Ser172) was not detectable in resting M0 macrophages at baseline, indicating minimal constitutive TBK1 activity in the absence of inflammatory stimulation (Fig. 19 C and D). Upon LPS stimulation, P-TBK1 became detectable at 30 minutes and remained stable through 1 hour and 4 hours post-stimulation (Fig. 20 C and D). This sustained TBK1 activation in macrophages contrasts with the transient P-TBK1 signal observed in DCs (section 4.7), where phosphorylation peaked at 1 hour and was undetectable by 4 hours. The prolonged TBK1 activation in macrophages may reflect sustained TRIF-dependent signaling or autocrine IFN-β-driven positive feedback through

IFNAR/JAK/STAT/IRF7 that maintains TBK1 activity over a longer time course in this cell type.

In sc siRNA-transfected macrophages, P-TBK1 levels increased at 30 minutes and remained relatively stable through 4 hours. In OPTN siRNA-transfected macrophages, P-TBK1 was also induced at 30 minutes, reaching levels that were initially comparable to scrambled controls at this early time point (Fig. 20 C and D). However, over the subsequent time course, P-TBK1 levels in siOPTN macrophages showed a progressive decline relative to scrambled controls. At 1 hour, a modest reduction was apparent, and by 4 hours, the difference between scRNA and siOPTN macrophages was most pronounced, with a trend toward lower P-TBK1 in optineurin-silenced cells (Fig. 20 C and D). The pattern, most pronounced at later time points in macrophages, is directionally consistent with 40–50% P-TBK1 reductions reported in murine Optn470T cells (Munitic et al., 2013; Pourcelot et al., 2016; Markovinovic et al., 2018), and could potentially corroborate the concept that across both human DCs and macrophages optineurin contributes to TBK1 activation in human myeloid cells.

4.16. Optineurin silencing did not significantly alter STAT1 activation and TDP-43 expression in macrophages

To further assess downstream IFN-β signaling and TDP-43 regulation, STAT1 phosphorylation and TDP-43 protein levels were analyzed in scrambled and OPTN siRNA-transfected macrophages. P-STAT1 was measured by ProteinSimple Jess/Wes at baseline (M0), 4 hours, and 24 hours post-LPS stimulation (100 ng/mL) in scrambled and OPTN siRNA-transfected macrophages (Fig. 21A). At baseline, P-STAT1 was detectable but at very low levels, consistent with minimal constitutive IFN-β signaling in resting macrophages. Upon LPS stimulation, P-STAT1 increased dramatically, reaching approximately a 30-fold induction by 4 hours (Fig. 21A and B). By 24 hours, P-STAT1 levels had declined to approximately 7–8-fold above baseline, indicating partial resolution of IFNAR-driven signaling while maintaining elevated activity above resting levels (Fig. 21A and B).

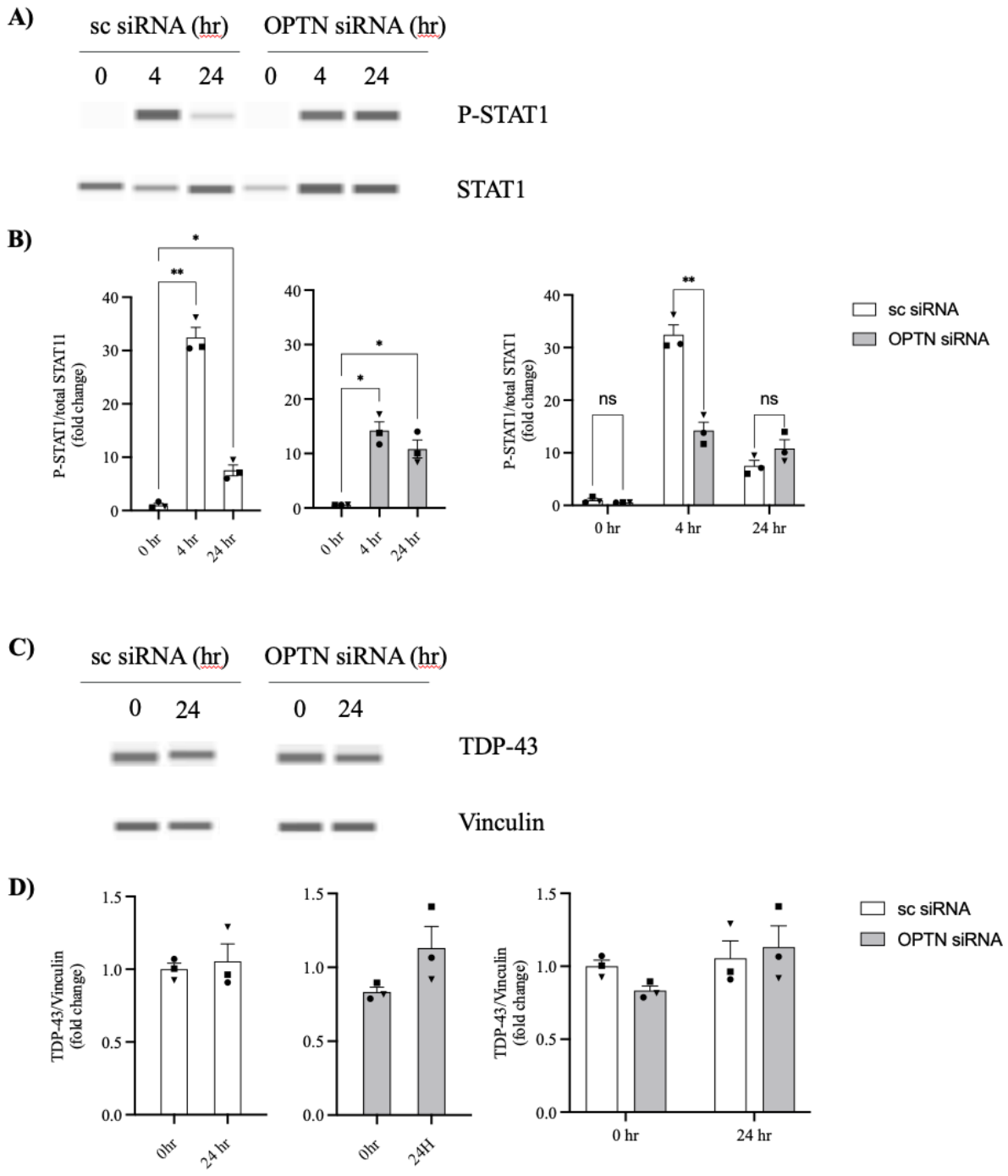

Figure 21. STAT1 phosphorylation and TDP-43 expression in optineuirn-silenced macrophages.

(A) Representative ProteinSimple Jess electropherograms showing phospho-STAT1 (Tyr701) in scRNA and siOPTN macrophages at baseline (M0), 4 hours, and 24 hours post-LPS stimulation (100 ng/mL). (B) Quantification of P-STAT1 signal intensity normalized to STAT-1. Representative blots (C) and total TDP-43 protein levels (D) at baseline and 24 hours post-LPS in scRNA and siOPTN macrophages normalized to vinculin. Data represent mean ± SEM from 3 independent donors. Statistical comparisons between scRNA and siOPTN conditions were performed using multi comparison two-way ANOVA. Statistical

comparisons within scRNA alone or siOPTN alone conditions were performed using multi comparison one-way ANOVA. * $p < 0.05$, ** $p < 0.01$, *** $p < 0.001$.

When comparing scrambled and OPTN siRNA-transfected macrophages, P-STAT1 levels, normalized to total STAT1, were comparable at baseline and at 24 hours. However, at the 4-hour peak, siOPTN macrophages showed a statistically significant reduction in P-STAT1 induction, reaching only approximately 15-fold above baseline compared to the 30-fold induction observed in scrambled controls (Fig. 21B). This finding is mechanistically coherent with the trend toward reduced TBK1 phosphorylation in siOPTN macrophages (section 4.15): diminished TBK1 activation would result in reduced IRF3 phosphorylation and consequently attenuated IFNAR/JAK-mediated STAT1 activation. The comparable P-STAT1 levels at 24 hours suggest that compensatory mechanisms, potentially including the IRF7-mediated positive feedback loop, eventually restore STAT1 signaling in both conditions. This finding provides evidence in our human primary cell system that optineurin silencing functionally impacts the TBK1–IFN-β–STAT1 signaling axis, potentially supporting the conservation of this pathway from murine to human myeloid cells.

Total TDP-43 protein was measured at baseline (M0) and 24 hours post-LPS stimulation in scrambled and OPTN siRNA-transfected macrophages (Fig. 21C). TDP-43 was readily detectable in resting macrophages. Importantly, LPS stimulation for 24 hours did not increase total TDP-43 protein levels above baseline in either condition (Fig. 21C). Furthermore, no differences in TDP-43 expression were observed between scRNA and siOPTN macrophages at either time point.

4.17. Optineurin silencing did not significantly alter cytokine production by LPS-activated macrophages

To determine whether optineurin deficiency affects the cytokine secretory profile of human macrophages, we measured pro-inflammatory and anti-inflammatory cytokines in cell culture supernatants from scrambled and OPTN siRNA-transfected macrophages at baseline (M0) and 24 hours following LPS stimulation (100 ng/mL). As with the DC experiments, IFN-γ, IL-2, and IL-13 were not further analysed as they were barely detectable, which is expected for myeloid cells.

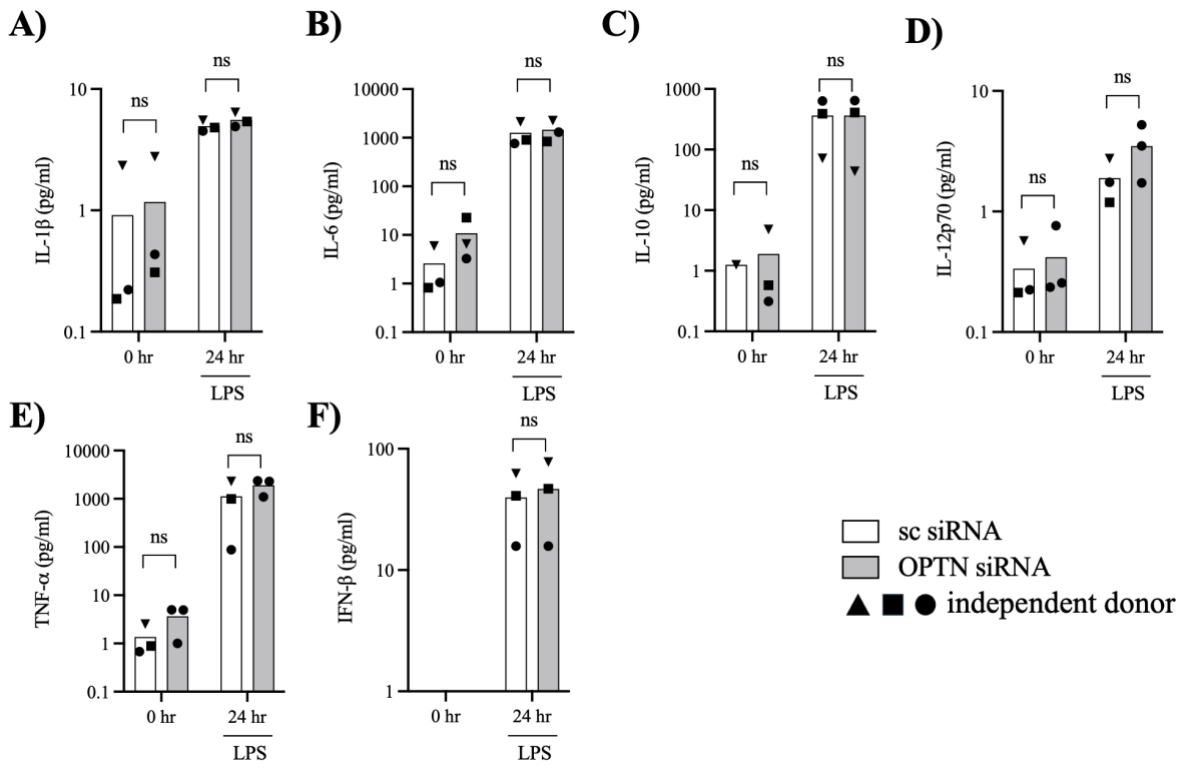

Figure 22. Cytokine production by optineurin-silenced macrophages upon LPS stimulation

(A–F) Cytokine levels measured in culture supernatants from scRNA and siOPTN macrophages at baseline (M0, unstimulated) and 24 hours following LPS stimulation (100 ng/mL). (A) IL-1β, (B) IL-10, (C) IL-6, (D) IL-12p70, (E) TNF-α, and (F) IFN-β. Cytokines were quantified using MSD V-PLEX Proinflammatory Panel 1 (A–E) and MSD U-PLEX (F). Each symbol represents an individual donor; bars represent mean ± SEM from three independent donors. Statistical comparisons between scRNA and siOPTN conditions were performed using multiple comparison 2-Way ANOVA; ns = not significant.

IL-1β was present at approximately 1 pg/mL in resting M0 macrophages and increased to around 8 pg/mL following 24 hours of LPS stimulation (Fig. 22 A). This modest but consistent induction is comparable to the levels observed in DCs (section 4.8) and reflects the requirement for secondary inflammasome activation signals for maximal IL-1β processing and release; LPS alone provides the priming signal that induces pro-IL-1β transcription via NF-κB without fully engaging caspase-1-mediated cleavage and secretion.

IL-10 increased from approximately 1 pg/mL in M0 macrophages to low hundreds of pg/mL upon LPS activation (Fig. 22 B), consistent with the induction of this anti-inflammatory cytokine as part of the negative feedback program that limits excessive pro-inflammatory

responses. The magnitude of IL-10 induction was comparable to that observed in LPS-stimulated DCs (section 4.8).

IL-6, a pleiotropic cytokine with both pro-inflammatory and immunoregulatory functions, was present at low pg/mL levels in resting M0 macrophages and showed a dramatic increase to approximately 1,000 pg/mL following 24 hours of LPS stimulation (Fig. 22 C). This robust IL-6 induction mirrors the response observed in DCs (section 4.8) and reflects the strong NF-κB-driven transcriptional program activated downstream of TLR4 engagement. The comparable magnitude of IL-6 production between macrophages and DCs is consistent with IL-6 being a major NF-κB target gene in both myeloid lineages.

IL-12p70 was present at less than 1 pg/mL in resting macrophages and increased only modestly to approximately 3–4 pg/mL following LPS stimulation (Fig. 22 D). This low level of IL-12p70 production is notably lower than that observed in LPS-matured DCs, where IL-12p70 reached between 10 and 100 pg/mL by 24 hours (section 4.8). This difference is consistent with the well-established role of DCs as the primary producers of IL-12p70 for Th1 polarization, while macrophages typically produce lower amounts unless additionally stimulated with IFN-γ (Trinchieri, 2003; Mosser & Edwards, 2008).

TNF-α showed the most dramatic induction, increasing from approximately 1 pg/mL in M0 macrophages to over 1,000 pg/mL upon LPS stimulation (Fig. 22 E). This robust TNF-α production is characteristic of classically activated macrophages and confirms strong NF-κB-driven transcriptional activity, consistent with the sustained p65 phosphorylation observed in our signaling experiments (section 4.15).

IFN-β was not detectable in resting M0 macrophages and increased to approximately 50 pg/mL following 24 hours of LPS stimulation (Fig. 22 F). These levels were in the range of those observed in LPS-stimulated DC cultures (section 4.8), although the multiplex cytokine assay performed on bulk culture supernatants precludes precise direct quantitative comparison between cell types.

Despite the robust cytokine responses observed upon LPS stimulation, no statistically significant differences were detected between scrambled and OPTN siRNA-transfected macrophages for any of the measured cytokines (Fig. 22 A–F). IL-1β, IL-10, IL-6, IL-12p70, TNF-α, and IFN-β levels were comparable between optineurin-sufficient and optineurin-deficient macrophages at both baseline and 24 hours post-LPS stimulation. The preservation of TNF-α, IL-6, IL-1β, and IL-12p70 production aligns with the intact NF-κB activation

observed in siOPTN macrophages (section 4.8), confirming that NF-κB-driven cytokine output is independent of optineurin in human macrophages. The maintenance of IL-10 secretion is also consistent with intact upstream signaling, as IL-10 transcription in myeloid cells is driven by both NF-κB and STAT3 pathways (Saraiva & O'Garra, 2010). The preservation of IFN-β secretion, despite the trend toward reduced P-TBK1 at later time points in siOPTN macrophages, suggests that the approximately 50% reduction in optineurin achieved by siRNA is insufficient to produce a measurable deficit in IFN-β protein output. The consistency of these findings across both DCs and macrophages strengthens the conclusion that partial optineurin reduction by siRNA is insufficient to produce significant functional deficits in cytokine production in human primary myeloid cells under acute LPS stimulation conditions.

4.18. Optineurin silencing did not impair phagocytosis by resting or LPS-activated macrophages

To extend our functional analysis to the macrophage lineage, we assessed phagocytosis in resting M0 and LPS-activated M1-like macrophages transfected with either scrambled (scRNA) or OPTN-targeting siRNA. Macrophages are professional phagocytes that serve as the primary effector cells for clearance of pathogens, apoptotic cells, and cellular debris in both peripheral tissues and the CNS. In the context of ALS, macrophage phagocytic function is particularly relevant, as peripheral monocyte-derived macrophages infiltrate the CNS and neuromuscular junctions during disease progression, where efficient clearance of damaged neurons, myelin debris, and protein aggregates (e.g., TDP-43, SOD1) is critical for limiting chronic inflammation and DAMP-driven feedforward loops (Ajami et al., 2011; Nógrádi et al., 2025). Unlike DCs, which downregulate phagocytosis upon maturation, macrophages retain substantial phagocytic capacity even after inflammatory activation, although the efficiency and specificity of uptake may be modulated by polarization state.

Phagocytosis was assessed using pHrodo™ *E. coli* BioParticles as described for DCs (see section 4.8). For macrophages, we expected robust phagocytic activity in both M0 and M1-like states, given that macrophages are constitutive phagocytes that maintain this function throughout their activation spectrum, in contrast to DCs where maturation suppresses phagocytosis.

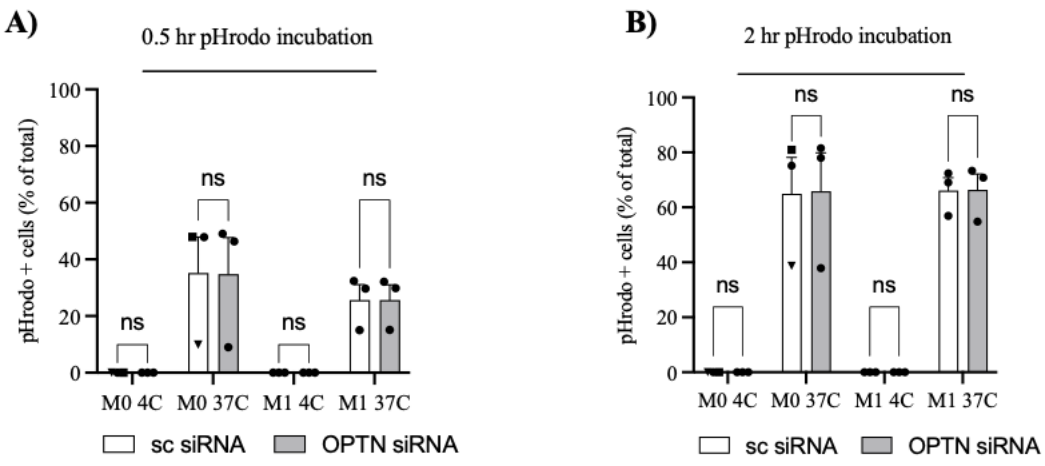

Figure 23. Optineurin silencing did not impair phagocytosis by macrophages.

(A) Quantification of phagocytosis (percentage of pHrodo-positive cells) in scRNA and siOPTN M0 (left) and LPS-matured M1 (right) after 0.5 hr of incubation with pHrodo. (C) Quantification of phagocytosis (percentage of pHrodo-positive cells) in scRNA and siOPTN M0 (left) and LPS-matured M1 (right) after 2 hr of incubation with pHrodo. Phagocytosis was assessed using pHrodo™ *E. coli* BioParticles as described in section 4.8. Data represent mean ± SEM from 3 independent donors. Statistics: multiple comparison 2-way ANOVA; ns = not significant.

As anticipated, resting **M0 macrophages** exhibited high phagocytic activity, with approximately **40%** of cells internalizing **pHrodo *E. coli*** particles at **0.5 h**, increasing to **more than 60%** by **3 h**, with the particles subsequently trafficked to acidic phagolysosomal compartments. (Fig. 23 A). LPS-activated M1-like macrophages retained substantial phagocytic capacity, consistent with the functional requirement for activated macrophages to continue clearing pathogens and debris at sites of inflammation. Importantly, no differences in phagocytosis were observed between scRNA and siOPTN macrophages in either the M0 or M1-like state (Fig. 23 B). Both the percentage of phagocytic cells were comparable between optineurin-sufficient and optineurin-deficient macrophages across both conditions.

These results demonstrated that optineurin was dispensable for macrophage phagocytosis, mirroring our findings in DCs (section 4.8) and indicating that this observation extends across human myeloid lineages. Despite optineurin's interactions with vesicular trafficking components (myosin VI, Rab8) and its role in autophagosome–lysosome fusion, its partial

reduction does not compromise the phagocytic machinery in human macrophages. This suggests that the initial steps of particle recognition, engulfment, and phagosomal acidification operate independently of optineurin, and that redundant trafficking adaptors maintain phagocytic function in its absence.

5. DISCUSSION

In this study, we investigated the functional consequences of optineurin reduction in human monocyte-derived dendritic cells and macrophages, aiming to bridge the gap between findings from model models and human disease mechanisms in the context of ALS-associated neuroinflammation.

Previous studies from our group demonstrated that optineurin insufficiency ($Optn^{470T}$) in murine myeloid cells impaired TBK1/IFN-β signaling and altered inflammatory responses (Munitic et al., 2013; Markovinovic et al., 2018), yet produced relatively subtle downstream functional phenotypes, including limited effects on phagocytosis, age-associated neuroinflammation and neurodegeneration in vivo (Peradinovic et al., 2022; Mohovic et al., 2023). Similar lack of overt neurological phenotype was reported for Optn-/- models generated by different groups (Ito et al., 2016; Slowicka et al., 2016). These observations raised the possibility that murine systems may incompletely capture optineurin-dependent immune mechanisms relevant to human ALS pathogenesis, particularly given known species-specific differences in innate immune signaling between mice and humans.

The choice of human monocyte-derived macrophages and dendritic cells as experimental models in this study was guided by both biological and practical considerations. Peripheral innate immune dysfunction is increasingly recognized as an important contributor to ALS pathogenesis, with alterations in monocytes, macrophages, dendritic cells, and other myeloid populations reported in both ALS patients and experimental models (Beers and Appel, 2019; Béland et al., 2020). Moreover, we recently reported broadly comparable inflammatory and phagocytic phenotypes between optineurin-insufficient murine macrophages and microglia, supporting peripheral myeloid cells as a translationally relevant surrogate system for studying innate immune regulation (Prtenjaca et al., 2022; Peradinovic et al., 2022). While human monocyte-derived microglia-like models have emerged as valuable tools for studying neuroimmune interactions in ALS (Quek et al., 2022), monocyte-derived macrophages and DCs can be generated more reproducibly from peripheral blood and allow controlled investigation of inflammatory signaling, phagocytosis, and antigen-presenting-cell function in primary human cells.

Overall, our results demonstrated that partial siRNA-mediated optineurin reduction did not produce significant functional deficits in human myeloid cells under acute inflammatory conditions, while revealing novel aspects of optineurin biology including its polarization-selective expression in macrophages.

Optineurin expression was dynamically regulated and lineage-specific in human myeloid cells

An important finding of this study is the distinct optineurin expression pattern between DCs and macrophages. Optineurin was virtually absent in monocytes and iDCs and required sustained LPS stimulation (24 hours) for robust upregulation, while in macrophages, M-CSF-driven differentiation alone was sufficient to induce substantial optineurin expression. We also showed that optineurin is upregulated only upon M1 but not M2 polarization, which is a novel finding that positions optineurin as a marker selectively associated with pro-inflammatory programs. This is consistent with the known regulation of the optineurin promoter by NF-κB and interferon-responsive elements (Sudhakar et al., 2009; Sudhakar et al., 2013). The interferon-responsive regulation described by Sudhakar et al. involved IFN-γ/IRF1 signaling and was characterized in immortalized cell lines rather than primary myeloid cells. In contrast, previous work from our group demonstrated that type I IFN-inducing stimuli can also upregulate optineurin expression in primary murine myeloid cells, although the underlying promoter mechanisms were not examined (Munitic et al., 2013). The findings of this study extend these observations to primary human dendritic cells and macrophages, providing a more physiologically relevant context for optineurin regulation. Given that M1 polarization engages both NF-κB and TBK1/IFN-β pathways, whereas IL-4-driven M2 polarization signals primarily through STAT6, which promotes anti-inflammatory transcriptional programs, our findings further support the association of optineurin expression with pro-inflammatory programs. The finding that TNF-α alone fails to upregulate optineurin in DCs, despite being a potent NF-κB activator, suggests that the full complement of TLR4-driven signals, including the TRIF-dependent TBK1/IFN-β axis, is required for maximal optineurin induction. The delayed IFN-β-dependent induction pattern raises the possibility that optineurin functions primarily in the resolution or sustained phases of inflammation rather than in the initial acute response. At the same time, the substantial induction of optineurin during M-CSF-driven macrophage differentiation suggests that its regulation is not exclusively linked to classical inflammatory activation but may also involve pathways engaged during macrophage maturation.

Optineurin was dispensable for NF-κB activation in human DCs and macrophages

Our finding that optineurin silencing did not affect p65 phosphorylation in either DCs or macrophages upon LPS stimulation is consistent with the body of evidence from murine primary cells. Studies in BMDMs, BMDCs, and MEFs from $Optn^{470T}$, $Optn^{-/-}$, and $Optn^{D477N}$ mice consistently demonstrated that optineurin is dispensable for acute NF-κB activation (Gleason et al., 2011; Munitic et al., 2013; Slowicka et al., 2016). The discrepancy with earlier cell line studies reporting NF-κB hyperactivation upon optineurin silencing could reflect overexpression artifacts, or cell-line-specific contexts where the relative abundance of optineurin, NEMO, and ABIN family members differs from primary cells (Zhu et al., 2007; Sudhakar et al., 2009). Notably, our results extend the findings from primary murine systems to primary human myeloid cells and confirm that, regardless of species or myeloid cell subtype, optineurin does not regulate canonical NF-κB signaling under acute stimulation conditions. This was corroborated by the unchanged production of TNF-α, IL-6, IL-1β, and IL-12p70, indicating preserved NF-κB-dependent cytokine responses in human DCs and macrophages. However, we cannot exclude the possibility that optineurin may restrain NF-κB during chronic or repeated stimulation, as demonstrated in RANKL-driven osteoclastogenesis (Obaid et al., 2015), or under necroptotic conditions where RIPK1-dependent signaling amplifies NF-κB through DAMP release (Ito et al., 2016; Nakazawa et al., 2016). Additionally, disease-relevant chronic stimuli, such as exposure to aggregated TDP-43, which has been shown to enhance NF-κB activation and pro-inflammatory factor production when overexpressed in microglia (Swarup et al., 2011) may be required to reveal optineurin's regulatory function. Such chronic paradigms were not tested in our system and represent an important avenue for future investigation.

Notably, our findings contrast with earlier reports proposing optineurin as a negative regulator of NF-κB signaling through competition with NEMO and CYLD recruitment, much of which relied on transformed cell lines and overexpression systems (Zhu et al., 2007; Nagabhushana et al., 2011, PLoS One, 6, e17477). However, not all transformed cell line studies supported a model of NF-κB hyperactivation upon optineurin loss. A study using the THP-1 monocytic cell line instead proposed that optineurin deficiency impaired cytokine trafficking and secretion without major defects in cytokine transcription; in that system, approximately 60% optineurin silencing reduced TNF-α and IL-6 secretion following bacterial stimulation without evidence of NF-κB hyperactivation upon optineurin loss {Smith et al., 2015, Immunology, 144, 45-55}. Notably, the degree of optineurin reduction achieved

in this monocytic line was comparable to that obtained in our primary human DCs and macrophages, yet no effect on NF-κB-dependent cytokine output was observed in our system. Taken together, the available literature now suggests that the originally proposed role of optineurin as a universal negative regulator of canonical NF-κB signaling may have been overstated, at least in the context of acute TLR-driven responses in monocyte-derived human myeloid cells. Under these conditions, optineurin appears dispensable for early NF-κB activation, highlighting the importance of validating signaling models directly in primary human immune cells.

Partial optineurin reduction showed a trend toward diminished TBK1 activation and, in macrophages, reduction in STAT1 phosphorylation

The consistent trend toward reduced TBK1 phosphorylation observed in DCs and macrophages following optineurin silencing, although not statistically significant, is in line with murine studies in which complete loss of optineurin ubiquitin-binding function produced partial (~40–50%) reductions in TBK1 activation (Munitic et al., 2013; Pourcelot et al., 2016; Markovinovic et al., 2018). Similarly, the lack of significant IFN-β reduction is consistent with the modest and statistically non-significant decrease in P-TBK1 observed in siOPTN cells, suggesting that residual TBK1 activity may have remained above the threshold required to sustain downstream IFN-β production. Importantly, however, phosphorylated STAT1, a distal readout of the TBK1–IFN-β–IFNAR signaling cascade, was significantly reduced by approximately 50% in optineurin-silenced macrophages at the 4-hour peak, providing the first statistically significant evidence in our system that optineurin silencing functionally impacts this signaling axis. The fact that significance was achieved at the STAT1 level but not at TBK1 could potentially reflects signal amplification inherent in cytokine-mediated signaling: even a modest reduction in IFN-β secretion is amplified through IFNAR/JAK engagement to produce a more measurable downstream effect. This reduction was not observed in DCs, where higher absolute IFN-β production may saturate STAT1 activation regardless of upstream optineurin status.

The temporal pattern of TBK1 reduction differed between cell types. In DCs, where TBK1 activation was transient (peaking at 1 hour and undetectable by 4 hours), the trend toward reduction was evident at the peak. In macrophages, where TBK1 activation was sustained over 4 hours, the reduction became progressively more pronounced at later time points. This

temporal pattern suggests that while the initial triggering of TBK1 phosphorylation does not require optineurin, the sustained maintenance of TBK1 activation over time may depend on optineurin's scaffolding function. This is mechanistically plausible: optineurin's bivalent interaction with TBK1, constitutive binding via CC1 and inducible recognition of K63-ubiquitinated TBK1 via UBAN/ZF, is thought to promote TBK1 dimerization and trans-autophosphorylation (Li et al., 2016; Pourcelot et al., 2016). In line with this, the E3 ligase ANKIB1 was recently reported to drive type I and type III IFN induction downstream of TLR3, TLR4, and cGAS–STING, but not RIG-I, signaling pathways (Betrancourt et al., 2026). Mechanistically, ANKIB1 deposits K11-linked ubiquitin chains on TRIF, STING, NEMO, and optineurin itself, which are required for signalosome assembly, where optineurin serves as an adaptor for TBK1 recruitment and activation. Notably, Ankib1$^{-/-}$ mice displayed markedly increased mortality following intranasal herpex simplex virus 1 (HSV-1) infection (Betrancourt et al., 2026), while independent studies similarly showed impaired survival and enhanced neuroinvasive disease in Optn$^{-/-}$ mice following ocular HSV-1 infection (Ames et al., 2021). Consistent with a broader role of optineurin in innate immune regulation, transcriptome-wide profiling of CRISPR–Cas9 optineurin knockout BV2 microglia demonstrated broad attenuation of LPS-induced interferon, antiviral, and inflammatory programs (Cappelli et al., 2025).Thus, although the TBK1 and IFN-β trends observed in our system did not reach statistical significance, they remain consistent with the emerging view that optineurin is an important regulator of the type I IFN-inducing arm of innate immune signalling. The significant 50% reduction in P-STAT1 in macrophages further strengthens this conclusion, demonstrating that even partial optineurin reduction can produce measurable downstream consequences.

The subtle phenotype observed in our system likely reflects, at least in part, the considerable inter-donor variability inherent to primary human myeloid cell models, together with the technical challenges of achieving efficient siRNA-mediated silencing in primary cells. Consistent with this, while initial conventional Western blot analyses suggested stronger optineurin suppression (~80–90%), subsequent quantitative Jess/Wes-based measurements demonstrated more modest silencing efficiencies of approximately 60–70% in DCs and ~50% in macrophages. Given the role of optineurin as a scaffold, the residual protein levels may have been sufficient to support downstream signaling and functional responses.

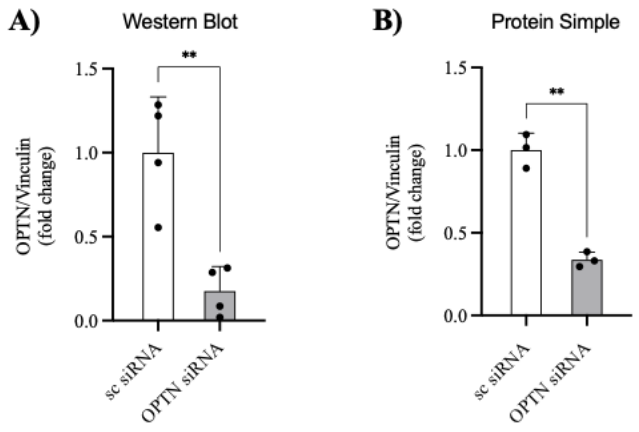

Figure 24. Comparison of optineurin knockdown quantification by conventional Western blot versus ProteinSimple Jess/Wes.

(A) Conventional Western blot analysis of optineurin protein levels in scrambled (scRNA) and OPTN siRNA-transfected DC with densitometric quantification normalized to housekeeping protein. (B) ProteinSimple Jess/Wes automated capillary Western analysis of the same samples with total protein normalization. Statistical comparison: Paired Student's t-test (*$p < 0.05$; **$p < 0.01$; ***$p < 0.001$; ****$p < 0.0001$).

This difference may be attributed to the higher quantitative accuracy of the automated capillary-based format, in which digital electropherogram output across a broad linear range enables more reliable quantification of proteins across different expression levels while reducing analytical bias (Fig. 24).

Taken together, our findings indicate that the strong inflammatory phenotypes reported in murine complete-knockout systems are not readily reproduced in human primary myeloid cells under partial, acute optineurin reduction. The degree and duration of optineurin loss, together with the nature of the inflammatory stimulus and cellular background, likely critically determine whether functional consequences become measurable. More broadly, these findings raise the possibility that partial optineurin deficiency or insufficiency in humans may be functionally tolerated under basal or acute inflammatory conditions, whereas more profound or chronic loss may be required to unmask disease-relevant phenotypes. The correlation observed at the single-donor level between low P-TBK1 activation and reduced IFN-β production provides indirect support for the functional link between TBK1 signaling and IFN-β output in human DCs, and suggests that in a system with greater statistical power,

either through increased donor numbers or more complete optineurin ablation (e.g., CRISPR-mediated knockout), a significant reduction in IFN-β might become apparent, as has been consistently demonstrated in murine primary cells with complete loss of optineurin's ubiquitin-binding function (Munitic et al., 2013; Pourcelot et al., 2016; Markovinovic et al., 2018). The fact that this trend is observed in both human DCs and macrophages, and is concordant with murine data, strengthens the interpretation that optineurin contributes to TBK1 activation in human myeloid cells, even though the effect did not achieve significance in our siRNA-based system.

Implications for ALS pathogenesis and the multihit hypothesis

The absence of overt functional deficits upon partial optineurin reduction in human myeloid cells under acute conditions aligns with the clinical evidence that ALS, including *OPTN*-linked ALS, is a late-onset disease requiring decades to manifest (Feldman et al., 2022; Maruyama et al., 2010). This supports a multifactorial, threshold-dependent model in which optineurin insufficiency alone is insufficient to cause immune dysfunction, but may become pathologically relevant when combined with additional hits: aging-related immune decline (inflammaging, reduced autophagy capacity, macrophage/microglial priming), chronic or repeated inflammatory challenges that exhaust compensatory mechanisms, accumulation of protein aggregates (TDP-43, SOD1) that overwhelm residual clearance capacity, or co-occurring mutations in other ALS-associated genes (oligogenic model) (Al-Chalabi et al., 2014; van Blitterswijk et al., 2012; Chio et al., 2018). Indeed, neither $Optn^{470T}$ nor $Optn^{-/-}$ mice develop spontaneous motor neuron loss (Gleason et al., 2011; Munitic et al., 2013; Ito et al., 2016; Mohovic et al., 2023), reinforcing the concept that optineurin deficiency creates vulnerability rather than directly causing neurodegeneration. Our TDP-43 data support this interpretation: while acute LPS stimulation modestly increased TDP-43 protein levels in DCs (~50%) and did not alter them in macrophages, optineurin silencing alone was insufficient to perturb TDP-43 homeostasis in either cell type. However, the trend toward lower TDP-43 in siOPTN DCs raises the possibility that chronic inflammatory stimulation, driving repeated cycles of TDP-43 upregulation in the context of impaired optineurin-dependent autophagy, could progressively overwhelm the cellular capacity for TDP-43 clearance, ultimately contributing to the cytoplasmic mislocalization and aggregation that characterizes ALS pathology.

Increasing evidence suggests that impaired phagocytosis is an important component of ALS-associated myeloid dysfunction. Monocyte-derived microglia-like cells from ALS patients exhibit defective phagocytosis associated with disease progression (Quek et al., 2022), while recent iPSC-derived C9ORF72 microglia models similarly demonstrated altered uptake of pHrodo-labelled bioparticles and dysregulated inflammatory responses following LPS stimulation (Gao et al., 2026). In this context, our finding that optineurin silencing did not impair phagocytosis, antigen processing, or antigen presentation suggests that partial optineurin reduction alone is insufficient to disrupt these core myeloid immune functions under acute conditions. The intact phagocytosis through both TLR/scavenger receptor pathways assessed using pHrodo E. coli particles further suggested that optineurin's known interactions with vesicular trafficking machinery (myosin VI, Rab8) were either not rate-limiting for particle uptake, or that redundant mechanisms involving other trafficking adaptors compensated for optineurin loss. Similarly, the preservation of antigen processing (tetanus toxoid) and direct peptide presentation (CEFT) demonstrated that the entire MHC class II pathway, from endosomal proteolysis through peptide loading to surface presentation and co-stimulation, remains functionally intact.

The novel finding that optineurin expression is selectively associated with M1 but not M2 macrophage polarization adds a new dimension to understanding optineurin's role in ALS. If optineurin is preferentially expressed in pro-inflammatory macrophages, its loss may specifically impair the TBK1/IFN-β-mediated resolution programs that facilitate the M1-to-M2 transition potentially trapping cells in a dysregulated inflammatory state. This is consistent with the immunodeficiency hypothesis in ALS, which proposes that defects in immune-regulating genes may produce inefficient or maladaptive immune responses rather than overt hyperinflammation (Béland et al., 2020). This model may extend beyond *OPTN* to other immune-regulating ALS genes such as *TBK1* and *C9ORF72*, in which defective innate immune homeostasis, impaired debris clearance, or dysfunctional inflammatory resolution are increasingly recognized as contributors to disease progression. Given the growing recognition that peripheral innate immune cells actively contribute to ALS pathogenesis and disease progression (Nógrádi et al., 2025), our findings open a possibility that optineurin-deficient monocytes and macrophages may participate in shaping the chronic inflammatory milieu of ALS not through overt hyperactivation, but through subtle defects in TBK1/IFN-β-dependent immune regulation and inflammatory resolution.

Limitations and future directions

This study has several limitations. The siRNA approach achieves only partial and transient knockdown, which may be insufficient to reveal optineurin's full functional contributions, a fundamental limitation when studying a scaffolding protein where residual levels may maintain partial complex assembly above the functional threshold. CRISPR/Cas9-mediated knockout in human iPSC-derived myeloid cells would provide complete and stable ablation, enabling more accurate assessment of optineurin's functions. Additionally, our experiments assessed only acute LPS stimulation; chronic or repeated stimulation paradigms, exposure to disease-relevant DAMPs (aggregated TDP-43, oxidized SOD1), or co-culture systems incorporating neuronal stress signals may be required to unmask optineurin-dependent phenotypes. The use of monocyte-derived cells, while experimentally accessible, may not fully recapitulate the biology of tissue-resident macrophages or microglia, which have distinct transcriptional programs and functional properties. Finally, testing optineurin deficiency in the context of aging-related immune changes, where autophagy capacity is diminished, mitochondrial damage accumulates, and innate immune pathways are chronically activated, would provide the most disease-relevant context for understanding how optineurin insufficiency contributes to ALS pathogenesis.

In conclusion, this study establishes that optineurin is dynamically regulated during human myeloid cell differentiation, with a novel M1-selective expression pattern in macrophages, and demonstrates that partial optineurin reduction is insufficient to impair acute immune function in human DCs and macrophages. The consistent trend toward reduced TBK1 activation, together with reduced STAT1 phosphorylation in macrophages, suggests that optineurin contributes to TBK1/IFN-β signaling in human myeloid cells, although partial reduction alone was insufficient to produce major downstream functional consequences.

6. CONCLUSIONS

(1) Optineurin expression was dynamically regulated during human myeloid cell differentiation: negligible in monocytes, low in iDCs, and strongly upregulated (~3-fold) upon LPS-induced DC maturation. In macrophages, optineurin was already expressed in resting M0 cells, due to M-CSF, and further increased upon M1 polarization, but not upon M2 polarization with IL-4.

(2) LPS was the strongest inducer of optineurin in human DCs, whereas TNF-α had no effect and IFN-γ produced only a modest (~20%) increase. Optineurin upregulation was delayed, requiring more than 8 h for robust induction (~3-fold at 24 h), but once initiated, remained largely sustained even after transient LPS exposure and washout.

(3) Optineurin silencing did not alter the immunophenotype (CD80, CD86, CD40, CD83, HLA-DR, PD-L1, CD163) of DCs or macrophages in either resting or LPS-activated states.

(4) Optineurin was dispensable for acute NF-κB activation (p65 phosphorylation) in both human DCs and macrophages upon LPS stimulation, confirming murine findings in human primary cells.

(5) A consistent trend toward reduced TBK1 phosphorylation was observed in optineurin-silenced DCs and macrophages, most pronounced at later time points in macrophages, but did not reach statistical significance.

(6) Cytokine production (IL-1β, IL-6, IL-10, IL-12p70, TNF-α, IFN-β) was not significantly altered by optineurin silencing in either DCs or macrophages. A single-donor correlation between low P-TBK1 and reduced IFN-β supports the optineurin–TBK1–IFN-β axis.

(7) Phagocytic capacity (pHrodo *E. coli* uptake) was unaffected by optineurin silencing in both DCs and macrophages, indicating that optineurin was dispensable for particle internalization through TLR/scavenger pathways.

(8) Antigen processing and presentation, assessed by CD154 upregulation using tetanus toxoid and CEFT peptide pool, were not impaired by optineurin silencing in human DCs.

(9) Partial optineurin reduction by siRNA (~50–70%) in human myeloid cells was insufficient to produce significant functional deficits under acute stimulation. Complete ablation, chronic stimulation, or the context of aging may be required to unmask optineurin's contributions, consistent with the multifactorial nature of ALS pathogenesis.

7. LITERATURE

Abe K, Aoki M, et al. Safety and efficacy of edaravone in well-defined patients with amyotrophic lateral sclerosis: a randomized, double-blind, placebo-controlled trial. Lancet Neurol. 2017;16(7):505–512. https://doi.org/10.1016/S1474-4422(17)30115-1

Agrawal A, Gupta S. Impact of aging on human dendritic cell functions. Ageing Res Rev. 2011;10(3):336–345. https://doi.org/10.1016/j.arr.2010.10.005

Ahmad S, et al. TBK1 in IFN-β production and innate signaling. FEBS Lett. 2016;590(6):726–738.

Ajami B, Bennett JL, Krieger C, Tetzlaff W, Rossi FMV. Local self-renewal of microglia. Nat Neurosci. 2011;14(12):1538–1543. https://doi.org/10.1038/nn.2967

Akçimen F, Lopez ER, Landers JE, Nath A, Chiò A. Amyotrophic lateral sclerosis: translating genetic discoveries into therapies. Nat Rev Genet. 2023;24(6):360–378. https://doi.org/10.1038/s41576-023-00592-y

Akizuki M, Yamashita H, Uemura K, Kawamoto Y, Takahashi R. Optineurin suppresses TNFα-induced NF-κB activation. J Neurochem. 2013;127(5):685–689. https://doi.org/10.1111/jnc.12406

Akutsu M, Dikic I, Bremm A. Ubiquitin chain diversity at a glance. J Cell Sci. 2016;129(5):875–880. https://doi.org/10.1242/jcs.183954

Al-Chalabi A, et al. Multifactorial risk in ALS: genetics and environment. Lancet Neurol. 2014;13(12):1256–1258. https://doi.org/10.1016/S1474-4422(14)70222-6

Al Chalabi A, et al. Edaravone commentary in ALS. Neurotherapeutics. 2017;14(1):4–5. https://doi.org/10.1007/s13311-016-0499-2

Albagha OME, et al. Genome-wide association identifies OPTN variants in Paget's disease. Nat Genet. 2011;43(8):585–589. https://doi.org/10.1038/ng.840

Andersen PM, Al-Chalabi A. Clinical genetics of amyotrophic lateral sclerosis. Nat Rev Neurol. 2011;7(11):603–615. https://doi.org/10.1038/nrneurol.2011.130

Anborgh PH, Godin C, Pampillo M, Dhami GK, Dale LB, Cregan SP, et al. Inhibition of metabotropic glutamate receptor signaling by the huntingtin-binding protein optineurin. J Biol Chem. 2005;280(34):30212–30220. https://doi.org/10.1074/jbc.M501100200

Arai T, Hasegawa M, Akiyama H, Ikeda K, Nonaka T, Mori H, et al. TDP-43 is a component of ubiquitin-positive inclusions in ALS. Biochem Biophys Res Commun. 2006;351(3):602–611. https://doi.org/10.1016/j.bbrc.2006.10.093

Arenzana-Seisdedos F, Thompson J, Rodriguez MS, Bachelerie F, Thomas D, Hay RT. Inducible nuclear expression of newly synthesized IκBα negatively regulates NF-κB. J Cell Sci. 1997;110(Pt 3):369–378. https://doi.org/10.1242/jcs.110.3.369

Beers DR, Henkel JS, Zhao W, Wang J, Huang A, Wen S, et al. Endogenous regulatory T

lymphocytes ameliorate ALS in mice. Brain. 2011;134(Pt 5):1293–1314. https://doi.org/10.1093/brain/awr074

Beers DR, Appel SH. Immune dysregulation in amyotrophic lateral sclerosis: mechanisms and emerging therapies. Lancet Neurol. 2019;18(2):211–220. https://doi.org/10.1016/S1474-4422(18)30394-6

Beers DR, et al. Wild-type microglia extend survival of mutant SOD1 motor neurons. Proc Natl Acad Sci U S A. 2006;103(5):16021–16026. https://doi.org/10.1073/pnas.0607423103

Béland LC, Markovinovic A, Jakovac H, De Marchi F, Bilic E, Mazzini L, et al. Immunity in amyotrophic lateral sclerosis: blurred lines between excessive inflammation and inefficient immune responses. Brain Commun. 2020;2(2):fcaa124. https://doi.org/10.1093/braincomms/fcaa124

Betrancourt A, Cinko MT, Varanda AB, Arias M, Uranga-Murillo I, Peña N, et al. Lysine-11 ubiquitination drives type-I/III interferon induction by cGAS-STING and Toll-like receptors 3 and 4. Nat Cell Biol. 2026;28(3):608–621. https://doi.org/10.1038/s41556-026-01886-z

Bhakar AL, Tannis LL, Zeindler C, Russo MP, Jobin C, Park DS, et al. Constitutive nuclear NF-κB activity is required for CNS neuron survival. J Neurosci. 2002;22(19):8466–8475. https://doi.org/10.1523/JNEUROSCI.22-19-08466.2002

Bjørkøy G, Lamark T, Brech A, Outzen H, Perander M, Øvervatn A, et al. p62/SQSTM1 aggregates are degraded by autophagy and protect against huntingtin toxicity. J Cell Biol. 2005;171(4):603–614. https://doi.org/10.1083/jcb.200507002

Boillée S, Yamanaka K, Lobsiger CS, Copeland NG, Jenkins NA, Kassiotis G, et al. Onset and progression in inherited ALS determined by motor neurons and non-neuronal cells. Science. 2006;311(5768):636–639. https://doi.org/10.1126/science.1123511

Braak H, Brettschneider J, et al. Amyotrophic lateral sclerosis: staging. Acta Neuropathol. 2010;119(6):739–752. https://doi.org/10.1007/s00401-010-0664-0

Brenner D, et al. TBK1 variant that does not bind optineurin in ALS/FTD. J Exp Med. 2024;221:e20221190. https://doi.org/10.1084/jem.20221190

Brown RH, Al-Chalabi A. Amyotrophic lateral sclerosis. N Engl J Med. 2017;377(2):162–172. https://doi.org/10.1056/NEJMra1603471

Bsibsi M, et al. Toll-like receptors on human glial cells: TLR2/3/4 expression and function. J Immunol. 2002;168(2):792–799. https://doi.org/10.4049/jimmunol.168.2.792

Butovsky O, et al. Monocyte polarization in SOD1 mice. Proc Natl Acad Sci U S A. 2012;109(41):16129–16134. https://doi.org/10.1073/pnas.1209307109

Butovsky O, Siddiqui S, Gabriely G, Lanser AJ, Dake B, Murugaiyan G, et al. Modulating inflammatory monocytes with a unique microRNA gene signature ameliorates murine ALS. J Clin Invest. 2012;122(9):3063–3087. https://doi.org/10.1172/JCI62636

Cappelli S, Peradinovic J, Mohovic N, Mandal P, Stuani C, Longo A, et al. Optineurin shapes basal and LPS-induced transcriptomes in BV2 microglia. Int J Mol Sci. 2025;26(21):10453. https://doi.org/10.3390/ijms262110453

Carletta O, et al. Genotype-specific interferon signatures in amyotrophic lateral sclerosis relate to disease severity. Brain. 2026. https://doi.org/10.1093/brain/awaf324

Cherry JD, Olschowka JA, O'Banion MK. Neuroinflammation and M1/M2 microglia. J Neuroinflammation. 2014;11:98. https://doi.org/10.1186/1742-2094-11-98

Chi C, Trinkle-Mulcahy L, Chalmers A, Lamond AI. Visualization of Rab8-GTPase trafficking using BiFC. Biochem Soc Trans. 2010;38(5):1283–1288. https://doi.org/10.1042/BST0381283

Chiu IM, et al. A neurodegeneration-specific role of T cells at neuromuscular junctions in ALS mice. Science. 2009;326(5951):1549–1554. https://doi.org/10.1126/science.1180204

Clement AM, Nguyen MD, Roberts EA, Garcia ML, Boillée S, Rule M, et al. Nonneuronal cells extend survival of SOD1 mutant motor neurons in chimeric mice. Science. 2003;302(5642):113–117. https://doi.org/10.1126/science.1086071

Coan G, Mitchell C. TDP-43: mechanisms of pathogenesis. Neurodegener Dis Manag. 2015;5(6):421–440. https://doi.org/10.2217/nmt.15.40

Cohen M, et al. IFN-β restrains microglial activation and promotes resolution. EMBO J. 2014;33(9):1105–1121. https://doi.org/10.1002/embj.201387937

Conn PJ, Pin JP. Pharmacology and functions of metabotropic glutamate receptors. Annu Rev Pharmacol Toxicol. 1997;37:205–237. https://doi.org/10.1146/annurev.pharmtox.37.1.205

Correia AS, Patel P, Dutta K, Julien JP. Inflammation induces TDP-43 mislocalization in microglia and neurons. J Neuroinflammation. 2015;12:144. https://doi.org/10.1186/s12974-015-0366-1

Daugaard M, Nitsch R, Razaghi B, McDonald L, Jarrar A, Torrino S, et al. HACE1 controls ROS generation of vertebrate Rac1-dependent NADPH oxidase complexes. Nat Commun. 2013;4:2180. https://doi.org/10.1038/ncomms3180

de Majo M, Topp SD, Smith BN, Nishimura AL, Chen HJ, Gkazi AS, et al. ALS-associated TBK1 mutations disrupt optineurin binding and IFN signalling. Neurobiol Aging. 2018;64:39–50. https://doi.org/10.1016/j.neurobiolaging.2017.12.025

DeJesus-Hernandez M, Mackenzie IR, Boeve BF, Boxer AL, Baker M, Rutherford NJ, et al. Expanded GGGGCC repeat in C9ORF72 causes ALS and FTD. Neuron. 2011;72(2):245–256. https://doi.org/10.1016/j.neuron.2011.09.011

Del Bo R, Tiloca C, Pensato V, Corrado L, Redaelli T, Carelli V, et al. Novel OPTN mutations in familial ALS. J Neurol Neurosurg Psychiatry. 2011;82(11):1239–1242. https://doi.org/10.1136/jnnp.2010.232470

del Toro D, Alberch J, Lázaro-Diéguez F, Martín-Ibáñez R, Xifró X, Egea G, et al. Mutant huntingtin impairs post-Golgi trafficking to lysosomes by delocalizing the optineurin/Rab8 complex. Mol Biol Cell. 2009;20(5):1478–1492. https://doi.org/10.1091/mbc.E08-06-0607

di Penta A, Moreno B, Reix S, Fernandez-Diez B, Villanueva M, Errea O, et al. IFN-β protects neurons and astrocytes from oxidative stress. PLoS One. 2013;8(6):e66114. https://doi.org/10.1371/journal.pone.0066114

Dobson-Stone C, et al. CYLD is a causative gene for frontotemporal dementia-amyotrophic lateral sclerosis. Brain. 2020;143(3):783–799. https://doi.org/10.1093/brain/awaa039

Dong XX, Wang Y, Qin ZH. Molecular mechanisms of excitotoxicity and neurodegeneration. Acta Pharmacol Sin. 2009;30(4):379–387. https://doi.org/10.1038/aps.2009.24

Ejlerskov P, et al. Lack of neuronal IFN-β signalling causes Parkinson-like neurodegeneration. Cell. 2015;163(6):1974–1987. https://doi.org/10.1016/j.cell.2015.11.018

Engelke DR, Ng SY, Shastry BS, Roeder RG. Specific interaction of a purified transcription factor with an internal control region of 5S RNA genes. Cell. 1980;19(3):717–728. https://doi.org/10.1016/S0092-8674(80)80047-4

Es MA van, Hardiman O, Chio A, Al-Chalabi A, Pasterkamp RJ, Veldink JH, et al. Amyotrophic lateral sclerosis. Lancet. 2017;390(10107):2084–2098. https://doi.org/10.1016/S0140-6736(17)31287-4

Fecto F, Yan J, Vemula SP, Liu E, Yang Y, Chen W, et al. SQSTM1 mutations in familial and sporadic ALS. Arch Neurol. 2011;68(11):1440–1446. https://doi.org/10.1001/archneurol.2011.250

Ferraiuolo L, Kirby J, Grierson AJ, Sendtner M, Shaw PJ. Molecular pathways in ALS. Nat Rev Neurol. 2011;7(11):616–630. https://doi.org/10.1038/nrneurol.2011.153

Fitzgerald KA, McWhirter SM, Faia KL, Rowe DC, Latz E, Golenbock DT, et al. IKKε and TBK1 are essential components of the IRF3 signalling pathway. Nat Immunol. 2003;4(5):491–496. https://doi.org/10.1038/ni921

Frakes AE, Ferraiuolo L, Haidet-Phillips AM, Schmelzer L, Braun L, Miranda CJ, et al. Microglial activation by NF-κB drives neurodegeneration in ALS models. Neuron. 2014;81(6):1249–1262. https://doi.org/10.1016/j.neuron.2014.01.010

Franceschi C, Garagnani P, Parini P, Giuliani C, Santoro A. Inflammaging: a new immune-metabolic viewpoint for age-related diseases. Nat Rev Endocrinol. 2018;14(10):576–590. https://doi.org/10.1038/s41574-018-0059-4

Freischmidt A, Wieland T, Richter B, Ruf W, Schaefer J, et al. Haploinsufficiency of TBK1 causes familial ALS and FTD. Nat Neurosci. 2015;18(3):364–371. https://doi.org/10.1038/nn.4000

Gao JJ, Filla MB, Fultz MJ, Vogel SN, Russell SW, Murphy WJ. Autocrine/paracrine IFN-β mediates chemokine induction. J Immunol. 1998;160(7):3503–3509.

Gao J, Ohtsubo M, et al. Oligomerization and structural organization of optineurin. PLoS One. 2014;9(6):e101206. https://doi.org/10.1371/journal.pone.0101206

Gate D, Saligrama N, et al. Clonally expanded CD8 T cells patrol CSF in Alzheimer's disease. Nature. 2020;577(7790):399–404. https://doi.org/10.1038/s41586-019-1895-7

Gerbino V, Kaunga E, Ye J, Canzio D, O'Keeffe S, Rudnick ND, et al. The loss of TBK1 kinase activity in motor neurons or in all cell types differentially impacts ALS disease progression in SOD1 mice. Neuron. 2020;106(5):789–805.e5. https://doi.org/10.1016/j.neuron.2020.05.003

Ghosh S, Hayden MS. Celebrating 25 years of NF-κB. Immunol Rev. 2012;246(1):5–13. https://doi.org/10.1111/j.1600-065X.2012.01111.x

Gleason CE, Ordureau A, Gourlay R, Arthur JSC, Cohen P. Recruitment of optineurin to TBK1-dependent signalling complexes is required for IFN-β production. J Biol Chem. 2011;286(39):35663–35674. https://doi.org/10.1074/jbc.M111.246074

Gong YH, Parsadanian AS, Isacson O, Arenas E. Non-cell-autonomous mechanisms in ALS revealed by chimeric mice. J Neurosci. 2000;20(19):724–732. https://doi.org/10.1523/JNEUROSCI.20-19-07224.2000

Graber DJ, Hickey WF, Harris BT. Progressive changes in macrophages at the neuromuscular junction in SOD1 mice. Muscle Nerve. 2010;41(5):679–688. https://doi.org/10.1002/mus.21542

Green DR, Oguin TH, Martinez J. The clearance of dying cells: efferocytosis. Nat Rev Immunol. 2016;16(4):229–244. https://doi.org/10.1038/nri.2016.26

Gudkov AV, et al. Aging of glial cells in context of neuroinflammation. Cell. 2022;185(24):4573–4588.e20.

Gurney ME, Pu H, Chiu AY, Dal Canto MC, Polchow CY, Alexander DD, et al. Motor neuron degeneration in mice expressing human mutant SOD1. Science. 1994;264(5166):1772–1775. https://doi.org/10.1126/science.8209258

Hardiman O, Al-Chalabi A, Chio A, Corr EM, Logroscino G, Robberecht W, et al. Amyotrophic lateral sclerosis. Nat Rev Dis Primers. 2017;3:17085. https://doi.org/10.1038/nrdp.2017.71

Hattula K, Peränen J. FIP-2 links huntingtin to Rab8 and modulates morphogenesis. Curr Biol. 2000;10(24):1603–1606. https://doi.org/10.1016/S0960-9822(00)00860-9

Hattula K, Furuhjelm J, Tikkanen J, Tanhuanpää K, Laakkonen P, Peränen J. Characterization of the Rab8-specific membrane traffic route linked to protrusion formation. J Cell Sci. 2006;119(23):4866–4877. https://doi.org/10.1242/jcs.03275

Helgason E, Phung QT, Dueber EC. Recent insights into the regulation of TBK1 and IKKε. FEBS Lett. 2013;587(8):1274–1279. https://doi.org/10.1016/j.febslet.2013.03.040

Heneka MT, et al. NLRP3 is activated in neurodegeneration. Nature. 2013;493(7434):674–678. https://doi.org/10.1038/nature11729

Henkel JS, et al. Immune alterations in ALS: T cells and cytokines. Brain Behav Immun. 2013;32:1–11. https://doi.org/10.1016/j.bbi.2013.01.004

Hernandez A, Burger M, Blomberg BB, Ross WA, Gaynor JJ, Lindner I, Cirocco R, Mathew JM, Carreno M, Jin Y, Lee KP, Esquenazi V, Miller J. Inhibition of NF-κB during human dendritic cell differentiation generates anergy and regulatory T cell activity for one-but not two-HLA-DR mismatches. Hum Immunol. 2007;68(9):715–729. https://doi.org/10.1016/j.humimm.2007.06.008

Heo JM, Ordureau A, Paulo JA, Rinehart J, Harper JW. The PINK1-PARKIN mitochondrial ubiquitylation pathway drives a program of OPTN/NDP52 recruitment and TBK1 activation to promote mitophagy. Mol Cell. 2015;60(1):7–20.

Huber LA, Pimplikar S, Parton RG, Virta H, Zerial M, Simons K. Rab8 in vesicular traffic. J Cell Biol. 1993;123(1):35–45. https://doi.org/10.1083/jcb.123.1.35

Hu H, Sun SC. Ubiquitin signaling in immune responses. Cell Res. 2016;26(4):457–483. https://doi.org/10.1038/cr.2016.39

Ising C, et al. NLRP3 drives tau pathology. Nat Med. 2019;25(11):1761–1772. https://doi.org/10.1038/s41591-019-0503-z

Ito Y, Ofengeim D, Najafov A, Das S, Saberi S, Li Y, et al. RIPK1 mediates axonal degeneration in ALS. Science. 2016;353(6299):603–608. https://doi.org/10.1126/science.aaf6803

Ivashkiv LB, Donlin LT. Regulation of type I interferon responses. Nat Rev Immunol. 2014;14(1):36–49. https://doi.org/10.1038/nri3581

Jin S, Kawakami Y. Interferon β is neuroprotective in glia. Brain Res. 2007;1165:62–70. https://doi.org/10.1016/j.brainres.2007.06.043

Jin X, Yamashita T. Microglia in cell death. J Biochem. 2016;159(4):305–315. https://doi.org/10.1093/jb/mvv128

Jo M, et al. TDP 43 C terminal fragments. Acta Neuropathol. 2020;140(1):91–111. https://doi.org/10.1007/s00401-020-02135-3

Kachaner D, Pinson X, Labbe JC, et al. Plk1 dependent phosphorylation of MYPT1 in mitosis. Mol Cell. 2012;45(4):533–546. https://doi.org/10.1016/j.molcel.2011.12.028

Kaltschmidt B, Kaltschmidt C, Baeuerle PA. NF κB in the nervous system. Biochim Biophys Acta. 2005;1745(3):287–299. https://doi.org/10.1016/j.bbamcr.2005.05.009

Kaveti S, Jain N. Optineurin calibrates STING-mediated type I interferon response. FEBS J. 2025.

Kawamata T, Akiyama H, Yamada T, McGeer PL. Immunologic reactions in ALS brain and spinal cord. J Neurol Sci. 1992;107(2):107–114. https://doi.org/10.1016/0022-510X(92)90210-6

Kawai T, Akira S. Signaling to NF κB by Toll like receptors. Trends Mol Med. 2010;16(4):153–164. https://doi.org/10.1016/j.molmed.2010.02.002

Keren-Shaul H, et al. A unique microglial type associated with restricting development of Aβ plaques. Cell. 2017;169(7):1276–1290.e17. https://doi.org/10.1016/j.cell.2017.05.018

Komander D, Rape M. The ubiquitin code. Annu Rev Biochem. 2012;81:203–229. https://doi.org/10.1146/annurev-biochem-060310-170328

Komatsu M, Kurokawa H, Waguri S, Taguchi K, Kobayashi A, Ichimura Y, et al. The selective autophagy substrate p62 activates Nrf2 by inactivating Keap1. Nat Cell Biol. 2010;12(3):213–223. https://doi.org/10.1038/ncb2021

Korac J, Schaeffer V, Kovacevic I, Clement AM, Jungblut B, Behl C, et al. Ubiquitin independent function of optineurin in autophagic clearance of protein aggregates. J Cell Sci. 2013;126(Pt 2):580–592. https://doi.org/10.1242/jcs.114926

Kovalenko A, Chable Bessia C, Cantarella G, Israel A, Wallach D, Courtois G. The tumour suppressor CYLD negatively regulates NF κB signalling. Nature. 2003;424(6950):801–805. https://doi.org/10.1038/nature01802

Krach F, Batra R, Wheeler EC, Vu AQ, Wang R, Hutt K, et al. Transcriptome-pathology correlation identifies interplay between TDP 43 and CK1ε in sporadic ALS. Acta Neuropathol. 2022;143(6):639–656. https://doi.org/10.1007/s00401-022-02479-6

Knödler A, Feng S, Zhang J, Zhang X, Das A, Peränen J, et al. Coordination of Rab8 and Rab11 in primary ciliogenesis. Proc Natl Acad Sci U S A. 2010;107(14):6346–6351. https://doi.org/10.1073/pnas.1002401107

Kwiatkowski TJ Jr, Bosco DA, Leclerc AL, Tamrazian E, Vanderburg CR, Russ C, et al. Mutations in FUS/TLS in familial ALS. Science. 2009;323(5918):1205–1208. https://doi.org/10.1126/science.1166066

Laplantine E, Fontan E, Chiaravalli J, Lopez T, Lakisic G, Véron M, et al. NEMO specifically recognizes K63 linked polyubiquitin through its UBAN domain. EMBO J. 2009;28(21):3094–3104. https://doi.org/10.1038/emboj.2009.257

Lazarou M, Sliter DA, Kane LA, Sarraf SA, Wang C, Burman JL, et al. The ubiquitin kinase PINK1 recruits autophagy receptors to induce mitophagy. Nature. 2015;524(7565):309–314. https://doi.org/10.1038/nature14895

Li F, Xie X, Wang Y, Liu J, Zhao N, Yan Z, et al. Structural insights into TBK1-optineurin interaction. Nat Commun. 2016;7:12646. https://doi.org/10.1038/ncomms12646

Li Y, Tarassishin L, Ye J, et al. Identification of a 14.7K interacting protein (FIP 2) that activates NF κB. Mol Cell Biol. 1998;18(11):6759–6768. https://doi.org/10.1128/MCB.18.11.6759

Li Y, Barres BA. Microglia and neurodevelopment. Annu Rev Neurosci. 2018;41:211–229. https://doi.org/10.1146/annurev-neuro-080317-061940

Liu T, Zhang L, Joo D, Sun SC. NF κB signaling in inflammation. Signal Transduct Target Ther. 2017;2:17023. https://doi.org/10.1038/sigtrans.2017.23

Liu Z, Chen P, Gao H, Gu Y, Yang J, Peng H, et al. Ubiquitylation of optineurin by HACE1 activates selective autophagy. Cancer Cell. 2014;26(1):106–120. https://doi.org/10.1016/j.ccr.2014.05.015

Lobo Silva D, Carriche GM, Castro AG, Roque S, Saraiva M. IFN β in neuroinflammation. Glia. 2017;65(8):1296–1310. https://doi.org/10.1002/glia.23157

Lomen-Hoerth C, Anderson T, Miller B. The overlap of ALS and FTD. Neurology. 2002;59(7):1077–1079. https://doi.org/10.1212/WNL.59.7.1077

López-Otín C, Blasco MA, Partridge L, Serrano M, Kroemer G. The hallmarks of aging. Cell. 2013;153(6):1194–1217. https://doi.org/10.1016/j.cell.2013.05.039

Louveau A, Smirnov I, et al. Meningeal lymphatic vessels link CSF and deep cervical lymph nodes. Nature. 2015;523(7560):337–341. https://doi.org/10.1038/nature14432

Mahmoudi S, et al. Ageing human macrophages impair efferocytosis. Nat Commun. 2019;10:264. https://doi.org/10.1038/s41467-018-08097-1

Manna S, et al. IFN α suppresses TNF induced NF κB activation. J Immunol. 2000;165(2):103–112. https://doi.org/10.4049/jimmunol.165.2.103

Markovinović A, Ljutic T, Belina S, Kriz J, Rogelj B, Munitic I. Optineurin in amyotrophic lateral sclerosis. Prog Neurobiol. 2017;154:1–21. https://doi.org/10.1016/j.pneurobio.2017.07.003

Maruyama H, Morino H, Ito H, Izumi Y, Kato H, Watanabe Y, et al. Mutations of optineurin in amyotrophic lateral sclerosis. Nature. 2010;465(7295):223–226. https://doi.org/10.1038/nature08971

Masrori P, Van Damme P. Amyotrophic lateral sclerosis: a clinical review. J Neurol. 2020;267(4):1024–1059. https://doi.org/10.1007/s00415-019-09663-0

Mattson MP, Arumugam TV. Hallmarks of brain aging: from synaptic plasticity to neuroinflammation. Nat Rev Neurosci. 2018;19(12):747–765. https://doi.org/10.1038/s41583-018-0068-6

McCauley ME, Baloh RH. Inflammation in ALS/FTD pathogenesis. Nat Neurosci. 2019;22(5):711–713. https://doi.org/10.1038/s41593-019-0396-0

McCauley ME, O'Rourke JG, Yáñez A, Markman JL, Ho R, Wang X, et al. C9orf72 in myeloid cells suppresses STING-induced inflammation. Nature. 2020;585(7823):96–101. https://doi.org/10.1038/s41586-020-2625-x

McGeer PL, McGeer EG. Inflammatory processes in ALS. Ann Neurol. 1991;29(5):505–513. https://doi.org/10.1002/ana.410290502

Mead RJ, et al. Emerging therapies for ALS. Lancet Neurol. 2022;21(5):455–469. https://doi.org/10.1016/S1474-4422(21)00454-9

Mead RJ, Shan N, Reiser HJ, Marshall F, Shaw PJ. Amyotrophic lateral sclerosis: a neurodegenerative disorder poised for successful therapeutic translation. Nat Rev Drug Discov. 2023;22(3):185–212. https://doi.org/10.1038/s41573-022-00612-2

Meena NP, Kandasamy RK, Sugumar A, et al. The TBK1 binding region of optineurin positively regulates antiviral signalling. FEBS Lett. 2016;590(8):1141–1151. https://doi.org/10.1016/j.febslet.2015.12.036

Mildner A, Schmidt H, Nitsche M, et al. CCR2+ Ly 6C(hi) monocytes are crucial for the effector phase of EAE. J Neurosci. 2007;27(41):11103–11111. https://doi.org/10.1523/JNEUROSCI.4607-06.2007

Minegishi Y, Iemura S, Ishitani R, Mizushima N. Significance of optineurin in retinal disease and oligomerization. Prog Retin Eye Res. 2016;55:120–138. https://doi.org/10.1016/j.preteyeres.2016.04.002

Mohovic N, Peradinovic J, Markovinovic A, Cimbro R, Minic Z, Dominovic M, et al. Neuroimmune characterization of optineurin insufficiency mouse model during ageing. Sci Rep. 2023;13(1):11840. https://doi.org/10.1038/s41598-023-38875-3

Moschetti G, Oliveri D, De Matteis V, Zaccaria M, Rondelli D, Griego A, Scarpa E, Rizzello L. A critical guideline for controlling monocyte-derived macrophages phenotypes. Front Immunol. 2026. https://doi.org/10.3389/fimmu.2025.1694625

Munitic I, Giardino Torchia ML, Meena NP, Zhu G, Ashwell JD. Optineurin insufficiency impairs IRF3 but not NF κB activation in myeloid cells. J Immunol. 2013;190(6):2620–2630. https://doi.org/10.4049/jimmunol.1202325

Nagabhushana A, Chalasani ML, Jain N, Radha V, Rangaraj N, Balasubramanian D, et al. Optineurin is required for CYLD dependent inhibition of TNFα induced NF κB activation. PLoS One. 2011;6(3):e17477. https://doi.org/10.1371/journal.pone.0017477

Nakazawa S, Oikawa D, Ishii R, Ayaki T, Takahashi H, Takeda H, et al. Linear ubiquitination is involved in the pathogenesis of optineurin associated ALS. Nat Commun. 2016;7:12547. https://doi.org/10.1038/ncomms12547

Neumann M, Sampathu DM, Kwong LK, Truax AC, Micsenyi MC, Chou TT, et al. Ubiquitinated TDP 43 in FTLD and ALS. Science. 2006;314(5796):130–133. https://doi.org/10.1126/science.1134108

Newton K, Manning G. Necroptosis and inflammation. Annu Rev Biochem. 2016;85:743–770. https://doi.org/10.1146/annurev-biochem-060815-014830

Nimmerjahn A, Kirchhoff F, Helmchen F. Resting microglia surveil the brain. Science. 2005;308(5726):1314–1318. https://doi.org/10.1126/science.1110647

Ning S, Pagano JS, Barber GN. IRF7: activation, regulation, function. Genes Immun. 2011;12(3):198–206. https://doi.org/10.1038/gene.2010.64

Obaid R, Wani A, Azfer A, Hadi SM, et al. Optineurin recruits CYLD to restrain RANKL induced NF κB signalling. Cell Rep. 2015;13(4):716–728. https://doi.org/10.1016/j.celrep.2015.09.034

Olmos G, Lladó J. TNF α: a link between neuroinflammation and excitotoxicity. Mediators Inflamm. 2014;2014:861231. https://doi.org/10.1155/2014/861231

Osawa T, et al. Optineurin in neuropathology. Neuropathology. 2011;31(6):546–557. https://doi.org/10.1111/j.1440-1789.2011.01299.x

Özoğuz A, Uyan Ö, Birdal G, Iskender C, Kartal E, Lahut S, et al. Genetic architecture of ALS in Turkey with OPTN variants. Neurobiol Aging. 2015;36(4):1764.e9–1764.e18. https://doi.org/10.1016/j.neurobiolaging.2015.01.012

Paolicelli RC, et al. Microglia in neurodegeneration. Nat Rev Neurosci. 2022;23(7):447–458. https://doi.org/10.1038/s41583-022-00595-2

Pankiv S, Clausen TH, Lamark T, Brech A, Bruun JA, Outzen H, et al. p62 binds LC3 to facilitate degradation of ubiquitinated aggregates. J Biol Chem. 2007;282(33):24131–24145. https://doi.org/10.1074/jbc.M702824200

Paul S, Biswas SR, Milner JP, Tomsick PL, Pickrell AM. Adaptor-mediated trafficking of tank binding kinase 1 during diverse cellular processes. Traffic. 2025;26(1–3):e70000. https://doi.org/10.1111/tra.70000

Peradinovic J, Mohovic N, Bulic K, Markovinovic A, Cimbro R, Munitic I, et al. Ageing-induced decline in primary myeloid cell phagocytosis is unaffected by optineurin insufficiency. Biology (Basel). 2023;12(2):240. https://doi.org/10.3390/biology12020240

Platanias LC. Mechanisms of type I and II interferon mediated signalling. Nat Rev Immunol. 2005;5(5):375–386. https://doi.org/10.1038/nri1604

Pohl C, Dikic I. Cellular quality control by the ubiquitin proteasome system and autophagy. Science. 2019;366(6467):818–822. https://doi.org/10.1126/science.aax3769

Polymenidou M, Cleveland DW. Misregulated RNA processing in ALS. Brain Res. 2012;1462:3–20. https://doi.org/10.1016/j.brainres.2012.02.059

Pottier C, et al. Whole genome approaches in ALS/FTD. Acta Neuropathol. 2015;129(4):553–564. https://doi.org/10.1007/s00401-015-1390-9

Pourcelot M, Zemirli N, Silva Da Costa L, Loyant R, Garcin D, Vitour D, et al. The Golgi apparatus acts as a platform for TBK1 activation after viral RNA sensing. BMC Biol. 2016;14:69. https://doi.org/10.1186/s12915-016-0299-6

Prasad A, et al. TDP 43 proteolysis and aggregation. Mol Neurobiol. 2019;56(6):3886–3905. https://doi.org/10.1007/s12035-018-1331-5

Prinz M, Priller J. Microglia and brain macrophages in the CNS. Nat Rev Neurosci. 2014;15(5):300–312. https://doi.org/10.1038/nrn3727

Prtenjaca N, Rob M, Alam MS, Markovinovic A, Stuani C, Buratti E, et al. Optineurin deficiency and insufficiency lead to higher microglial TDP-43 protein levels. Int J Mol Sci. 2022;23(12):6829. https://doi.org/10.3390/ijms23126829

Pulko V, et al. Human memory T cells with aging. Proc Natl Acad Sci U S A. 2016;113(16):4093–4098. https://doi.org/10.1073/pnas.1525607113

Ransohoff RM, Brown MA. Innate immunity in the CNS: cross talk with periphery. Trends Immunol. 2012;33(6):311–317. https://doi.org/10.1016/j.it.2012.03.002

Rauch I, Müller M, Decker T. Regulation of interferon stimulated gene expression. JAK STAT. 2013;2(1):e23820. https://doi.org/10.4161/jkst.23820

Rezaie T, Child A, Hitchings R, Brice G, Miller L, Coca Prados M, et al. Adult onset primary open angle glaucoma caused by OPTN mutations. Science. 2002;295(5557):1077–1079. https://doi.org/10.1126/science.1066901

Richter B, Sliter DA, Herhaus L, Stolz A, Wang C, Beli P, et al. Phosphorylation of OPTN by TBK1 enhances binding to ubiquitin chains and promotes mitophagy. Proc Natl Acad Sci U S A. 2016;113(15):4039–4044. https://doi.org/10.1073/pnas.1523810113

Ringholz GM, Appel SH, Bradshaw M, Cooke NA, Mosnik DM, Schulz PE. Prevalence and patterns of cognitive impairment in ALS. Neurology. 2005;65(4):586–590. https://doi.org/10.1212/01.wnl.0000172911.39167.b6

Rogov VV, Suzuki H, Marinković M, Lang V, Kato R, Kawasaki M, et al. Phosphorylation of Nix enhances its interaction with LC3. EMBO Rep. 2013;14(3):317–324. https://doi.org/10.1038/embor.2013.7

Rosen DR, Siddique T, Patterson D, Figlewicz DA, Sapp P, Hentati A, et al. Mutations in Cu/Zn superoxide dismutase gene in familial amyotrophic lateral sclerosis. Nature. 1993;362(6415):59–62. https://doi.org/10.1038/362059a0

Rusconi M, Gerardi F, Santus W, Lizio A, Sansone VA, Lunetta C, et al. Inflammatory role of dendritic cells in amyotrophic lateral sclerosis revealed by an analysis of patients' peripheral blood. Front Immunol. 2017;8:565. https://doi.org/10.3389/fimmu.2017.00565

Ryan TA, Tumbarello DA. Optineurin: a coordinator of membrane-associated cargo trafficking and autophagy. Front Immunol. 2018;9:1024. https://doi.org/10.3389/fimmu.2018.01024

Sahlender DA, Roberts RC, Arden SD, Spudich G, Taylor MJ, Luzio JP, et al. Optineurin links myosin VI to the Golgi complex and is involved in Golgi organization and exocytosis. J Cell Biol. 2005;169(2):285–295. https://doi.org/10.1083/jcb.200501162

Saresella M, Piancone F, Tortorella P, Marventano I, Gatti A, Caputo D, et al. T helper-17 activation dominates the immunologic milieu of both amyotrophic lateral sclerosis and progressive multiple sclerosis. J Neuroimmunol. 2013;261(1–2):57–63. https://doi.org/10.1016/j.jneuroim.2013.04.010

Schwamborn K, Weil R, Courtois G, Whiteside ST, Israël A. Phorbol esters and cytokines induce NEMO-related protein, a possible inhibitor of NF-κB activation. J Biol Chem. 2000;275(30):22780–22789. https://doi.org/10.1074/jbc.M000672200

Segal BM. Dendritic cells and CNS autoimmunity. J Exp Med. 2019;216(8):1723–1725. https://doi.org/10.1084/jem.20190730

Sen R, Smale ST. Selectivity of the NF-κB response. Cold Spring Harb Perspect Biol. 2010;2(4):a000257. https://doi.org/10.1101/cshperspect.a000257

Sharma S, tenOever BR, Grandvaux N, Zhou GP, Lin R, Hiscott J. Triggering the interferon antiviral response through an IKK-related pathway. Science. 2003;300(5622):1148–1151. https://doi.org/10.1126/science.1081315

Shih RH, Wang CY, Yang CM. NF-κB signaling pathways in neurological inflammation: a mini review. Front Mol Neurosci. 2015;8:77. https://doi.org/10.3389/fnmol.2015.00077

Slowicka K, Vereecke L, van Loo G. Cellular functions of optineurin in health and disease. Trends Immunol. 2016;37(9):621–633. https://doi.org/10.1016/j.it.2016.07.002

Smith AM, Rahman FZ, Hayee B, Graham SJ, Marks DJB, Sewell GW, et al. Disordered macrophage cytokine secretion underlies impaired acute inflammation and bacterial clearance in Crohn's disease. J Exp Med. 2009;206(9):1883–1897. https://doi.org/10.1084/jem.20091233

Smith AM, Sewell GW, Levine AP, Chew TS, Dunne J, O'Shea NR, et al. Disruption of macrophage pro-inflammatory cytokine release in Crohn's disease is associated with reduced optineurin expression in a subset of patients. Immunology. 2015;144(1):45–55. https://doi.org/10.1111/imm.12338

Sudhakar C, Nagabhushana A, Jain N, Swarup G. NF-κB mediates constitutive expression of

optineurin and its therapeutic inactivation by small interfering RNA induces cancer cell death. FEBS J. 2009;276(22):6338–6351. https://doi.org/10.1111/j.1742-4658.2009.07319.x

Sudhakar C, Vaibhava V, Swarup G. IRF-1-binding site in the first intron mediates interferon-γ-induced optineurin promoter activation. Biochem Biophys Res Commun. 2013;437(1):179–184. https://doi.org/10.1016/j.bbrc.2013.06.065

Sundaramoorthy V, Walker AK, Tan V, Fifita JA, McCann EP, Williams KL, et al. Defects in optineurin- and myosin VI-mediated cellular trafficking in amyotrophic lateral sclerosis. Hum Mol Genet. 2015;24(13):3830–3846. https://doi.org/10.1093/hmg/ddv127

Sun SC, Ganchi PA, Ballard DW, Greene WC. NF-κB controls expression of inhibitor IκBα: evidence for an inducible autoregulatory pathway. Science. 1993;259(5103):1912–1915. https://doi.org/10.1126/science.8096091

Talbott EO, Malek AM, Lacomis D. The epidemiology of amyotrophic lateral sclerosis. Handb Clin Neurol. 2016;138:225–238. https://doi.org/10.1016/B978-0-12-802973-2.00013-6

Takeuchi O, Akira S. Pattern recognition receptors and inflammation. Cell. 2010;140(6):805–820. https://doi.org/10.1016/j.cell.2010.01.022

The Huntington's Disease Collaborative Research Group. A novel gene containing a trinucleotide repeat that is expanded and unstable on Huntington's disease chromosomes. Cell. 1993;72(6):971–983. https://doi.org/10.1016/0092-8674(93)90585-E

Tokunaga F, Iwai K. LUBAC, a novel ubiquitin ligase for linear ubiquitination, is crucial for inflammation and immune responses. Microbes Infect. 2012;14(7–8):563–572. https://doi.org/10.1016/j.micinf.2012.01.001

Trias E, Ibarburu S, Barreto-Núñez R, Varela V, Moura IC, Dubreuil P, et al. Evidence for mast cells contributing to neuromuscular pathology in an inherited model of ALS. Front Cell Neurosci. 2018;12:244. https://doi.org/10.3389/fncel.2018.00244

Trinchieri G. Type I interferon: friend or foe? J Exp Med. 2010;207(10):2053–2063. https://doi.org/10.1084/jem.20101664

Truebestein L, Leonard TA. Coiled-coils: the long and short of it. BioEssays. 2016;38(9):903–916. https://doi.org/10.1002/bies.201600062

Tu D, Zhu Z, Zhou AY, Yun CH, Lee KE, Toms AV, et al. Structure and ubiquitination-dependent activation of TANK-binding kinase 1. Cell Rep. 2013;3(3):747–758. https://doi.org/10.1016/j.celrep.2013.01.033

Tumbarello DA, Waxse BJ, Arden SD, Bright NA, Kendrick-Jones J, Buss F. Autophagy receptors link myosin VI to autophagosomes to mediate Tom1-dependent autophagosome maturation and fusion with the lysosome. Nat Cell Biol. 2012;14(10):1024–1035. https://doi.org/10.1038/ncb2589

Vaibhava V, Nagabhushana A, Chalasani ML, Sudhakar C, Kumari A, Swarup G. Optineurin

mediates negative regulation of Rab8 by the GTPase-activating protein TBC1D17. J Cell Sci. 2012;125(Pt 21):5026–5039. https://doi.org/10.1242/jcs.108969

van Blitterswijk M, van Es MA, Hennekam EA, Dooijes D, van Rheenen W, Medic J, et al. Evidence for an oligogenic basis of amyotrophic lateral sclerosis. Hum Mol Genet. 2012;21(17):3776–3784. https://doi.org/10.1093/hmg/dds199

von Bernhardi R, Eugenín-von Bernhardi J, Eugenín J. Microglial cell dysregulation in brain aging and neurodegeneration. Front Aging Neurosci. 2015;7:124. https://doi.org/10.3389/fnagi.2015.00124

Wagner S, Carpentier I, Rogov V, Kreike M, Ikeda F, Löhr F, et al. Ubiquitin binding mediates the NF-κB inhibitory potential of ABIN proteins. Oncogene. 2008;27(26):3739–3745. https://doi.org/10.1038/sj.onc.1211024

Wang D, Eraslan B, Wieland T, Hallström B, Hopf T, Zolg DP, et al. Quantitative human proteome atlas. Mol Syst Biol. 2019;15(2):e8503. https://doi.org/10.15252/msb.20188503

Wang Y, Colonna M, et al. CSF1R signaling sustains the microglial population in the adult brain. Neuron. 2012;76(6):1035–1045. https://doi.org/10.1016/j.neuron.2012.10.027

Watanabe M, Dykes-Hoberg M, Culotta VC, Price DL, Wong PC, Rothstein JD. Histological evidence of protein aggregation in mutant SOD1 transgenic mice and in amyotrophic lateral sclerosis neural tissues. Neurobiol Dis. 2001;8(6):933–941. https://doi.org/10.1006/nbdi.2001.0434

Weishaupt JH, Waibel S, Birve A, Volk AE, Mayer B, Meyer T, et al. A novel optineurin truncating mutation and three missense variants in patients with familial amyotrophic lateral sclerosis in Germany. Neurobiol Aging. 2013;34(5):1516.e9–1516.e15. https://doi.org/10.1016/j.neurobiolaging.2012.09.023

Wells AL, Lin AW, Chen LQ, Safer D, Cain SM, Hasson T, et al. Myosin VI is an actin-based motor that moves backwards. Nature. 1999;401(6752):505–508. https://doi.org/10.1038/46835

Wild P, Farhan H, McEwan DG, Wagner S, Rogov VV, Brady NR, et al. Phosphorylation of the autophagy receptor optineurin restricts Salmonella growth. Science. 2011;333(6039):228–233. https://doi.org/10.1126/science.1205405

Wilson DM 3rd, et al. Aging as the major risk factor for neurodegeneration: integrating molecular and epidemiological perspectives. Nat Rev Neurosci. 2023.

Wong YC, Holzbaur ELF. Optineurin is an autophagy receptor for damaged mitochondria in Parkin-mediated mitophagy that is disrupted by an ALS-linked mutation. Proc Natl Acad Sci U S A. 2014;111(42):E4439–E4448. https://doi.org/10.1073/pnas.1405752111

Xiao Y, Tan Y, Li C, Wei Q, Jiang Q, Wang S, et al. Genetic and clinical analysis of OPTN in amyotrophic lateral sclerosis. J Med Genet. 2025;62(4):242–248. https://doi.org/10.1136/jmg-2024-109978

Yamakami M, Yoshimori T, Yokosawa H. Tom1, a VHS domain-containing protein, interacts with Tollip, ubiquitin, and clathrin. J Biol Chem. 2003;278(52):52865–52872. https://doi.org/10.1074/jbc.M308903200

Yamanaka K, Boillée S, Roberts EA, Garcia ML, McAlonis-Downes M, Mikse OR, et al. Mutant SOD1 in cell types other than motor neurons and oligodendrocytes accelerates onset of disease in ALS mice. Proc Natl Acad Sci U S A. 2008;105(21):7594–7599. https://doi.org/10.1073/pnas.0802556105

Yamashita S, et al. Optineurin-positive neuronal and glial inclusions in neurodegenerative diseases. Neuropathol Appl Neurobiol. 2014;40(7):867–875. https://doi.org/10.1111/nan.12141

Yu CH, Davidson S, Harapas CR, Hilton JB, Mlodzianoski MJ, Laohamonthonkul P, et al. TDP-43 triggers mitochondrial DNA release via mPTP to activate cGAS/STING in ALS. Cell. 2020;183(3):636–649.e18. https://doi.org/10.1016/j.cell.2020.09.020

Zandi E, Rothwarf DM, Delhase M, Hayakawa M, Karin M. The IκB kinase complex (IKK) contains two kinase subunits, IKKα and IKKβ. Cell. 1997;91(2):243–252. https://doi.org/10.1016/S0092-8674(00)80406-8

Zhang J, Wang J, Zhou Z, Park JE, Wang L, Wu S, et al. Importance of the C terminus of optineurin for its function in autophagy and in neurodegeneration. Nat Commun. 2024;15(1):1142. https://doi.org/10.1038/s41467-024-48163-0

Zhang R, Miller RG, Gascon R, Champion S, Katz J, Lancero M, et al. Evidence for systemic immune activation in patients with amyotrophic lateral sclerosis. J Neuroimmunol. 2005;159(1–2):215–224. https://doi.org/10.1016/j.jneuroim.2004.10.009

Zhao W, Beers DR, Liao B, Henkel JS, Appel SH. TNFα-mediated astrogliosis and neuronal selectivity in ALS involve NF-κB and TDP-43 dysregulation. J Neuroinflammation. 2015;12:39. https://doi.org/10.1186/s12974-015-0243-y

Zhu G, Wu CJ, Zhao Y, Ashwell JD. Optineurin negatively regulates TNFα-induced NF-κB activation by competing with NEMO for ubiquitinated RIP. Curr Biol. 2007;17(16):1438–1443. https://doi.org/10.1016/j.cub.2007.07.041

Zou ZY, Zhou ZR, Che CH, Liu CY, He RL, Huang HP, et al. Genetic epidemiology of amyotrophic lateral sclerosis in China. J Neurol Neurosurg Psychiatry. 2017;88(11):917–925. https://doi.org/10.1136/jnnp-2017-315796

8. LIST OF ABBREVIATIONS

Abbreviation	*Full Term*
aa	Amino acid
ABIN	A20 binding inhibitor of NF-κB
ALS	Amyotrophic lateral sclerosis
AMPA	α-amino-3-hydroxy-5-methyl-4-isoxazolepropionic acid
Arg1	Arginase 1
ATG	Autophagy-related gene
BBB	Blood-brain barrier
BDMC	Bone marrow-derived dendritic cell
BDNF	Brain-derived neurotrophic factor
BMDM	Bone marrow-derived macrophage
C9ORF72	Chromosome 9 open reading frame 72
CC1	Coiled-coil domain 1
CC2	Coiled-coil domain 2
CCL2	C-C motif chemokine ligand 2 (MCP-1)
CCL5	C-C motif chemokine ligand 5 (RANTES)
CCR2	C-C chemokine receptor type 2
CD4	Cluster of differentiation 4
CD8	Cluster of differentiation 8
CD68	Cluster of differentiation 68
CD80	Cluster of differentiation 80 (B7-1)
CD86	Cluster of differentiation 86 (B7-2)
cGAS	Cyclic GMP-AMP synthase

CNS	Central nervous system
CRP	C-reactive protein
CSF1	Colony-stimulating factor 1
CSF1R	Colony-stimulating factor 1 receptor
CXCL1	C-X-C motif chemokine ligand 1
CXCL2	C-X-C motif chemokine ligand 2
CXCL10	C-X-C motif chemokine ligand 10
CYLD	Cylindromatosis (deubiquitinase)
DAM	Disease-associated microglia
DAMP	Damage-associated molecular pattern
DC	Dendritic cell
DISC	Death-inducing signaling complex
DPR	Dipeptide repeat protein
ER	Endoplasmic reticulum
ERK	Extracellular signal-regulated kinase
fALS	Familial amyotrophic lateral sclerosis
FasL	Fas ligand
FIP-2	14.7K-interacting protein 2
FTD	Frontotemporal dementia
FUS	Fused in sarcoma
GFAP	Glial fibrillary acidic protein
GluA2	Glutamate ionotropic receptor AMPA type subunit 2
GRM1	Glutamate metabotropic receptor 1 (mGluR1a)
HACE1	HECT domain and ankyrin repeat containing E3 ubiquitin-protein ligase 1
HD	Huntington's disease
HMGB1	High mobility group box 1

HTT	Huntingtin
IBM	Inclusion body myositis
IFN-β	Interferon beta
IFN-γ	Interferon gamma
IFNAR	Type I interferon receptor (IFNAR1/IFNAR2)
IGF-1	Insulin-like growth factor 1
IKK	IκB kinase
IKKα	IκB kinase alpha
IKKβ	IκB kinase beta
IKKε	IκB kinase epsilon
IKKγ	IκB kinase gamma (NEMO)
IL-1β	Interleukin-1 beta
IL-4	Interleukin-4
IL-6	Interleukin-6
IL-8	Interleukin-8
IL-10	Interleukin-10
IL-12	Interleukin-12
IL-17A	Interleukin-17A
IL-23	Interleukin-23
IL-34	Interleukin-34
iNOS	Inducible nitric oxide synthase
IRF3	Interferon regulatory factor 3
IRF7	Interferon regulatory factor 7
IRF9	Interferon regulatory factor 9
IRFBS	Interferon regulatory factor binding site
ISG	Interferon-stimulated gene
ISGF3	Interferon-stimulated gene factor 3

ISRE	Interferon-stimulated response element
IκBα	Inhibitor of NF-κB alpha
JAK1	Janus kinase 1
JAK/STAT	Janus kinase/signal transducer and activator of transcription
JNK	c-Jun N-terminal kinase
K6	Lysine 6 (ubiquitin linkage)
K11	Lysine 11 (ubiquitin linkage)
K27	Lysine 27 (ubiquitin linkage)
K29	Lysine 29 (ubiquitin linkage)
K33	Lysine 33 (ubiquitin linkage)
K48	Lysine 48 (ubiquitin linkage)
K63	Lysine 63 (ubiquitin linkage)
LC3	Microtubule-associated protein 1 light chain 3
LIR	LC3-interacting region
LPS	Lipopolysaccharide
LUBAC	Linear ubiquitin chain assembly complex
Lys	Lysine
LZ	Leucine zipper
M1	Methionine 1 (linear ubiquitin linkage)
MAP1LC3	Microtubule-associated protein 1 light chain 3
MAPK	Mitogen-activated protein kinase
MCP-1	Monocyte chemoattractant protein-1 (CCL2)
MEF	Mouse embryonic fibroblast
Met	Methionine
mGluR1a	Metabotropic glutamate receptor 1a
Mφ	Macrophage
MGnD	Microglial neurodegenerative phenotype

MHC	Major histocompatibility complex
MHC-II	Major histocompatibility complex class II
MLKL	Mixed lineage kinase domain-like pseudokinase
mRNA	Messenger RNA
mtDNA	Mitochondrial DNA
MYO6	Myosin heavy chain VI (myosin VI)
MYPT1	Myosin phosphatase target subunit 1
NEMO	NF-κB essential modulator (IKKγ)
NF-κB	Nuclear factor kappa B
NFKBIA	NF-κB inhibitor alpha gene
NK	Natural killer (cell)
NLR	NOD-like receptor
NLRP3	NLR family pyrin domain containing 3
NMDA	N-methyl-D-aspartate
NO	Nitric oxide
NOS2	Nitric oxide synthase 2 (iNOS)
NPR	NEMO-related protein
NRP	NEMO-related protein
NTG	Normal-tension glaucoma
OPMD	Oculopharyngeal muscular dystrophy
OPTN	Optineurin (gene)
OXPHOS	Oxidative phosphorylation
p38	p38 mitogen-activated protein kinase
p50	NF-κB subunit p50
p62	Sequestosome 1 (SQSTM1)
p65	NF-κB subunit p65 (RelA)
PAMP	Pathogen-associated molecular pattern

PD	Parkinson's disease
PI3K	Phosphoinositide 3-kinase
POAG	Primary open-angle glaucoma
PRR	Pattern-recognition receptor
pSer172	Phosphorylated serine 172
pSer177	Phosphorylated serine 177
pSer473	Phosphorylated serine 473
pSer513	Phosphorylated serine 513
Rab8	Ras-related protein Rab-8
RANTES	Regulated upon activation, normal T cell expressed and secreted (CCL5)
RelA	v-rel avian reticuloendotheliosis viral oncogene homolog A (p65)
RIG-I	Retinoic acid-inducible gene I
RIPK1	Receptor-interacting serine/threonine-protein kinase 1
RIPK3	Receptor-interacting serine/threonine-protein kinase 3
RNA	Ribonucleic acid
ROS	Reactive oxygen species
sALS	Sporadic amyotrophic lateral sclerosis
SASP	Senescence-associated secretory phenotype
Ser	Serine
SOD1	Superoxide dismutase 1
SPM	Specialized pro-resolving mediator
SQSTM1	Sequestosome 1 (p62)
STAT1	Signal transducer and activator of transcription 1
STAT2	Signal transducer and activator of transcription 2
STING	Stimulator of interferon genes
TAK1	Transforming growth factor-β-activated kinase 1

TARDBP	TAR DNA-binding protein gene
TBK1	TANK-binding kinase 1
TDP-43	TAR DNA-binding protein 43
TFIIIA	Transcription factor IIIA
TGF-β	Transforming growth factor beta
TH1	T helper 1 cell
TH2	T helper 2 cell
TH17	T helper 17 cell
Thr	Threonine
TIR	Toll/interleukin-1 receptor
TLR	Toll-like receptor
TLR2	Toll-like receptor 2
TLR3	Toll-like receptor 3
TLR4	Toll-like receptor 4
TLR9	Toll-like receptor 9
TNF	Tumor necrosis factor
TNFR1	Tumor necrosis factor receptor 1
Tom1	Target of Myb1
TRAF	TNF receptor-associated factor
TRAF3	TNF receptor-associated factor 3
TRAF6	TNF receptor-associated factor 6
TRAM	TRIF-related adaptor molecule
Treg	Regulatory T cell
TRIF	TIR-domain-containing adapter-inducing interferon-β
TYK2	Tyrosine kinase 2
Ub	Ubiquitin
UBAN	Ubiquitin binding in ABIN and NEMO

UBD	Ubiquitin-binding domain
UBQLN2	Ubiquilin 2
UBR	Ubiquitin-binding region
UPR	Unfolded protein response
UPS	Ubiquitin-proteasome system
ZF	Zinc finger
β-TrCP	Beta-transducin repeat containing E3 ubiquitin protein ligase

9. LIST OF FIGURES

10. LIST OF TABLES

11. BIOGRAPHY

Raffaello Cimbro

Nationality: Italian, American Date of birth: 02/12/1982 Gender: Male LinkedIn: Raffaello Cimbro Address: United Kingdom

EDUCATION & TRAINING

Bachelor's degree in Biotechnology

Università degli Studi di Milano Bicocca [01/09/2003 - 31/08/2005]

City: Milan | Country: Italy

Master's degree in Biotechnology

Università degli Studi di Milano Bicocca [01/09/2005 - 18/04/2007]

City: Milan | Country: Italy

PhD student in Biotechnology

University of Rijeka [31/07/2016 - Current]

City: Rijeka | Country: Croatia

WORK EXPERIENCE

National Institutes of Health (NIH) - United States, Bethesda
Visiting Felllow
[19/05/2007 - 31/12/2012]

- Conducted research in immunology/virology, focusing on HIV1 envelope biology and host responses.

Johns Hopkins University - United States, Baltimore
Flow cytometry Lab Manager and Independent Investigator
[01/01/2013 - 31/12/2018]

- Managed a research flow cytometry lab; designed and executed immunology/virology studies; supervised staff; maintained instrumentation; led collaborations.

SmartBridge - United States, Baltimore
Consultant
[01/01/2016 - 31/12/2018]

- Consulted on data analysis and process optimization in life science workflows.

De Novo Software
Consultant and Trainer
[01/06/2017 - 31/12/2018]

- Trained users on flow cytometry analysis platforms and best practices.

AstraZeneca - United States, Gaithersburg
Scientist – Data Scientist, Flow Cytometry Core Research
[01/01/2019 - 31/05/2020]

- Built computational tools and standardized analysis for large scale cytometry datasets.

AstraZeneca - United States, Gaithersburg
Senior Scientist – Data Scientist, Flow Cytometry Core Research
[01/06/2020 - 30/04/2021]

- Managed core operations, project intake, high dimensional analysis workflows, and QC frameworks.

AstraZeneca - United States, Gaithersburg
Associate Principal Scientist – Leader
[01/05/2021 - 30/11/2021]

- Developed automated cytometry data pipelines, clustering/dimensionality reduction, and reporting.

AstraZeneca - United States, Gaithersburg
Associate Director – Global Leader of Flow Cytometry (US/UK)
[01/12/2021 - 30/04/2023]

- Co-led global strategy, harmonized practices, and technology adoption across sites; advanced spectral and imaging flow cytometry capabilities and training.

AstraZeneca - United Kingdom, Cambridge
Director – Global Leader of Flow Cytometry (US/UK)
[01/05/2023 - Current]

- Lead the global Flow Cytometry Centers of Excellence across Gaithersburg (US), Boston (US), and Cambridge (UK).
- Support >650 scientists and ~150 projects annually across discovery and development.
- Project leader and key collaborator for top priority internal and partnered programs.
- Drive innovation in real time imaging/spectral flow sorting and automated analysis pipelines integrating flow cytometry with AI and multiomics to improve reproducibility, efficiency, and cost effectiveness.

PUBLICATIONS

1. Girgis AA, **Cimbro R**, Yang T, Rebman AW, Sewell T, Villegas de Flores D, et al. Aberrant T-cell phenotypes in a cohort of patients with post-treatment Lyme disease. Front Immunol. 2025 Jul;16. doi:10.3389/fimmu.2025.1607619.

2. Irvine A, Moustafa MM, Patel S, Patel A, Hardardottir L, Delvecchio F, et al. Automation of flow cytometry data analysis with elastic image registration. Sci Rep. 2025 May;15(1). doi:10.1038/s41598-025-99118-1.
3. Altshuler RD, Burke MAM, Garcia KT, Class K, **Cimbro R**, Li X. Profiling gene alterations in striatonigral neurons associated with incubation of methamphetamine craving by cholera toxin subunit B-based fluorescence-activated cell sorting. Front Cell Neurosci. 2025 Feb;19. doi:10.3389/fncel.2025.1542508.
4. Taylor JD, Barrett N, Martinez Cuesta S, Cassidy K, Pachl F, Dodgson J, et al. Targeted protein degradation using chimeric human E2 ubiquitin-conjugating enzymes. Commun Biol. 2024 Sep;7(1). doi:10.1038/s42003-024-06803-4.
5. Choudhury FK, Premkumar V, Zecha J, Boyd J, Gaynor AS, Guo Z, et al. Multiomics characterization of a less invasive microfluidic-based cell sorting technique. J Proteome Res. 2024 Feb;23(8):3096–3107. doi:10.1021/acs.jproteome.3c00773.
6. Crawford JD, Wang H, Trejo-Zambrano D, **Cimbro R**, Talbot CC Jr, Thomas MA, et al. The XIST lncRNA is a sex-specific reservoir of TLR7 ligands in SLE. JCI Insight. 2023 Sep;8(20). doi:10.1172/jci.insight.169344.
7. Mohovic N, Peradinovic J, Markovinovic A, **Cimbro R**, Minic Z, Dominovic M, et al. Neuroimmune characterization of optineurin insufficiency mouse model during ageing. Sci Rep. 2023 Jul;13(1). doi:10.1038/s41598-023-38875-3.
8. McGrath-Morrow SA, Venezia J, Ndeh R, Michki N, Perez J, Singer BD, **Cimbro R**, Soloski M, Scott AL. Cellular and molecular dynamics in the lungs of neonatal and juvenile mice in response to E. coli. eLife. 2023 Jun;12. doi:10.7554/eLife.82933.
9. Peradinovic J, Mohovic N, Bulic K, Markovinovic A, **Cimbro R**, Munitic I. Ageing-induced decline in primary myeloid cell phagocytosis is unaffected by optineurin insufficiency. Biology (Basel). 2023 Feb;12(2):240. doi:10.3390/biology12020240.
10. Zhang P, Kwon AL, Guzzo C, Liu Q, Schmeisser H, Miao H, et al. Functional anatomy of the trimer apex reveals key hydrophobic constraints that maintain the HIV-1 envelope spike in a closed state. mBio. 2021 Apr;12(2). doi:10.1128/mbio.00090-21.
11. Cazares LH, Chaerkady R, Weng SHS, Boo CC, **Cimbro R**, Hsu H-E, et al. Development of a parallel reaction monitoring mass spectrometry assay for the detection of SARS-CoV-2 spike glycoprotein and nucleoprotein. Anal Chem. 2020 Sep;92(20):13813–13821. doi:10.1021/acs.analchem.0c02288.
12. Li X, Davis IR, Lofaro OM, Zhang J, **Cimbro R**, Rubio FJ. Distinct gene alterations between Fos-expressing striatal and thalamic neurons after withdrawal from methamphetamine self-administration. Brain Behav. 2019 Jul;9(9). doi:10.1002/brb3.1378.
13. Torchia MLG, **Cimbro R**. Discrimination of seven immune cell subsets by two-fluorochrome flow cytometry. J Vis Exp. 2019 Mar;(145). doi:10.3791/58955.
14. Guzzo C, Zhang P, Liu Q, Kwon AL, Uddin F, Wells AI, et al. Structural constraints at the trimer apex stabilize the HIV-1 envelope in a closed, antibody-protected conformation. mBio. 2018 Dec;9(6). doi:10.1128/mBio.00955-18.
15. Xin W, Schuebel KE, Jair K, **Cimbro R**, De Biase LM, Goldman D, Bonci A. Ventral midbrain astrocytes display unique physiological features and sensitivity to dopamine D2 receptor signaling. Neuropsychopharmacology. 2018 Jul;44(2):344–355. doi:10.1038/s41386-018-0151-4.
16. Zhang P, Gorman J, Geng H, Liu Q, Lin Y, Tsybovsky Y, et al. Interdomain stabilization impairs CD4 binding and improves immunogenicity of the HIV-1 envelope trimer. Cell Host Microbe. 2018 Jun;23(6):832–844.e6. doi:10.1016/j.chom.2018.05.002.
17. Boin F, Giardino Torchia ML, Borrello I, Noonan KA, Neil M, Soloski MJ, **Cimbro R**. Flow cytometric discrimination of seven lineage markers by using two fluorochromes. PLoS One. 2017 Nov;12(11):e0188916. doi:10.1371/journal.pone.0188916.

18. De Biase LM, Schuebel KE, Fusfeld ZH, Jair K, Hawes IA, **Cimbro R**, et al. Local cues establish and maintain region-specific phenotypes of basal ganglia microglia. Neuron. 2017 Jul;95(2):341–356.e6. doi:10.1016/j.neuron.2017.06.020.
19. Birnbaum J, Atri NM, Baer AN, **Cimbro R**, Montagne J, Casciola-Rosen L. Relationship between neuromyelitis optica spectrum disorder and Sjögren's syndrome: Central nervous system extraglandular disease or unrelated, co-occurring autoimmunity? Arthritis Care Res (Hoboken). 2017 Jun;69(7):1069–1075. doi:10.1002/acr.23107.
20. Markovinovic A, **Cimbro R**, Ljutic T, Kriz J, Rogelj B, Munitic I. Optineurin in amyotrophic lateral sclerosis: Multifunctional adaptor protein at the crossroads of different neuroprotective mechanisms. Prog Neurobiol. 2017 Jul;154:1–20. doi:10.1016/j.pneurobio.2017.04.005.
21. Wallace VJ, **Cimbro R**, Rubio FJ, Fortuno LV, Necarsulmer JC, Koivula PP, et al. Neurons internalize functionalized micron-sized silicon dioxide microspheres. Cell Mol Neurobiol. 2017 Mar;37(8):1487–1499. doi:10.1007/s10571-017-0479-z.
22. McMahan ZH, Cottrell TR, Wigley FM, Antiochos B, Zambidis ET, Park TS, et al. Enrichment of scleroderma vascular disease–associated autoantigens in endothelial lineage cells. Arthritis Rheumatol. 2016;68(10):2540–2549.
23. Rubio FJ, Li X, Liu Q-R, **Cimbro R**, Hope BT. Fluorescence activated cell sorting (FACS) and gene expression analysis of fos-expressing neurons from fresh and frozen rat brain tissue. J Vis Exp. 2016;(114).
24. Fava A, **Cimbro R**, Wigley FM, Liu Q-R, Rosen A, Boin F. Frequency of circulating topoisomerase-I-specific CD4 T cells predicts presence and progression of interstitial lung disease in scleroderma. Arthritis Res Ther. 2016;18(1).
25. González-Mariscal I, Krzysik-Walker SM, Doyle ME, Liu Q-R, **Cimbro R**, Santa-Cruz Calvo S, et al. Human CB1 receptor isoforms, present in hepatocytes and β-cells, are involved in regulating metabolism. Sci Rep. 2016;6.
26. Byrareddy SN, Arthos J, Cicala C, Villinger F, Ortiz KT, Little D, et al. Sustained virologic control in SIV+ macaques after antiretroviral and α4β7 antibody therapy. Science. 2016;354(6309):197–202.
27. **Cimbro R**, Peterson FC, Liu Q, Guzzo C, Zhang P, Miao H, et al. Tyrosine-sulfated V2 peptides inhibit HIV-1 infection via coreceptor mimicry. EBioMedicine. 2016.
28. Huang H, Fava A, Guhr T, **Cimbro R**, Rosen A, Boin F, Ellis H. A methodology for exploring biomarker–phenotype associations: Application to flow cytometry data and systemic sclerosis clinical manifestations. BMC Bioinformatics. 2015;16(1).
29. Rubio FA, Liu Q-R, Li X, Cruz FC, Leão RM, Warren BL, et al. Context-induced reinstatement of methamphetamine seeking is associated with unique molecular alterations in Fos-expressing dorsolateral striatum neurons. J Neurosci. 2015;35(14):5625–5639.
30. Li X, Rubio FJ, Zeric T, Bossert JM, Kambhampati S, Cates HM, et al. Incubation of methamphetamine craving is associated with selective increases in expression of Bdnf and Trkb, glutamate receptors, and epigenetic enzymes in cue-activated Fos-expressing dorsal striatal neurons. J Neurosci. 2015;35(21):8232–8244.
31. Sadat MA, Moir S, Chun T-W, Lusso P, Kaplan G, Wolfe L, et al. Glycosylation, hypogammaglobulinemia, and resistance to viral infections. N Engl J Med. 2014;370(17):1615–1625.
32. **Cimbro R**, Gallant TR, Dolan MA, Guzzo C, Zhang P, Lin Y, et al. Tyrosine sulfation in the second variable loop (V2) of HIV-1 gp120 stabilizes V2–V3 interaction and modulates neutralization sensitivity. Proc Natl Acad Sci U S A. 2014;111(8):3152–3157.
33. Varchetta S, Lusso P, Hudspeth K, Mikulak J, Mele D, Paolucci S, et al. Sialic acid-binding Ig-like lectin-7 interacts with HIV-1 gp120 and facilitates infection of CD4+ T cells and macrophages. Retrovirology. 2013;10(1).

34. Guzzo C, Fox J, Lin Y, Miao H, **Cimbro R**, Volkman BF, et al. The CD8-derived chemokine XCL1/Lymphotactin is a conformation-dependent, broad-spectrum inhibitor of HIV-1. PLoS Pathog. 2013;9(12):1–11.
35. Jelicic K, **Cimbro R**, Nawaz F, Huang DW, Zheng X, Yang J, et al. The HIV-1 envelope protein gp120 impairs B cell proliferation by inducing TGF-β1 production and FcRL4 expression. Nat Immunol. 2013;14(12):1256–1265.
36. **Cimbro R**, Vassena L, Arthos J, Cicala C, Kehrl JH, Park C, et al. IL-7 induces expression and activation of integrin α4β7 promoting naive T-cell homing to the intestinal mucosa. Blood. 2012;120(13):2610–2619.
37. Auerbach DJ, Lin Y, Miao H, **Cimbro R**, DiFiore MJ, Gianolini ME, et al. Identification of the platelet-derived chemokine CXCL4/PF-4 as a broad-spectrum HIV-1 inhibitor. Proc Natl Acad Sci U S A. 2012;109(24):9569–9574.
38. Vassena L, Miao H, **Cimbro R**, Malnati MS, Cassina G, Proschan MA, et al. Treatment with IL-7 prevents the decline of circulating CD4+ T cells during the acute phase of SIV infection in rhesus macaques. PLoS Pathog. 2012;8(4).
39. Liu L, **Cimbro R**, Lusso P, Berger EA. Intraprotomer masking of third variable loop (V3) epitopes by the first and second variable loops (V1V2) within the native HIV-1 envelope glycoprotein trimer. Proc Natl Acad Sci U S A. 2011;108(50):20148–20153.
40. Lusso P, Vangelista L, **Cimbro R**, Secchi M, Sironi F, Longhi R, et al. Molecular engineering of RANTES peptide mimetics with potent anti-HIV-1 activity. FASEB J. 2011;25(4):1230–1243.

SKILLS

Flow Cytometry | project management | Team Player/Team Leader | business processes | immunotherapy |
Cell Biology | Data Analysis | data science | Artificial Intelligent

PRESENTATIONS

- ELRIG 2025 — invited speaker: Imaging Flow Cytometry: Innovation from Discovery to the Clinic
- ICCS 2025 — invited speaker: Imaging Flow Cytometry: Innovation from Discovery to the Clinic
- ICCS 2025 — workshop, invited speaker: LUNCH WORKSHOP 8: TROUBLESHOOTING IN SPECTRAL FLOW CYTOMETRY, AN INTERACTIVE SESSION
- CYTO 2025 — invited speaker: Imaging Flow Cytometry: Innovation from Discovery to the Clinic
- CYTO 2024: Accessible Automation in Flow Cytometry to Enhance Reproducibility, Boost Productivity and Reduce Costs

- CYTO 2024 — invited speaker: Post-Clustering Workshop
- CYTO 2024 — invited speaker: Improve and evolve with the first Real-Time Imaging, Spectral Flow Cytometer (RTI-SFC) for previously impossible sorting applications
- CYTO 2023 — invited speaker: Assisted Automation in Flow Cytometry to improve reproducibility, reduce processing time and costs
- CYTO 2022 — workshop, invited speaker: High-dimensionality reduction and clustering
- Webinars: Imaging Flow Cytometry (Dec 2025; ~700 registrants), Enhancing Cell Analysis (Jun 2024; ~300 registrants).

LANGUAGE SKILLS

Mother tongue(s): Italian

English
LISTENING: C2 READING: C2 WRITING: C2
SPOKEN PRODUCTION: C2
SPOKEN INTERACTION: C2